AN ABSTRACT OF THE DISSERATATION OF

Morgan L. Ferguson for the degree of Doctor of Philosophy in Chemistry presented on March 11, 2011.
Title: Preparation and Characterization of Polymer-SiO_2 Hybrids

Abstract approved:

_____

Philip R. Watson

In a search for designed materials that mimic those found in biological systems, combining polymers with inorganic materials in sol-gel chemistry processes has gained momentum in the research world since the 1990's. This work methodically investigated the properties of several related polymer-SiO_2 hybrids prepared by a simple methodology that could be applied to a range of other polymers and organically modified inorganic starting materials. The preparation and drying conditions were varied systematically to provide the best method for combining poly (methyl methacrylate) (PMMA), polystyrene (PS), polystyrene-co-poly (methyl methacrylate) (PS-co-PMMA) and polystyrene-polyisoprene-polystyrene (PS-PI-PS) with pre-hydrolyzed tetraethoxysilane (TEOS).

Thermogravimetric analysis (TGA) provided the weight percent of silica contained in each hybrid and the percentage of retained solvent. The derivative of the TGA curve is useful for illuminating the effect of silica on the degradation pathway of the polymer. Fourier transform infrared spectra (FTIR) probed the chemical interaction between the hybrid constituents. Dynamic mechanical analysis (DMA) provided mechanical data over a range of working frequencies and temperatures. Tapping mode atomic force microscopy (TM-AFM) was used in preference to standard electron microscopies to provide the phase distribution of the constituents as well as a 3D topographical image.

Overall, PMMA interacted with pre-hydrolyzed TEOS to produce more thermally stable hybrids that were stronger at high temperatures. The PS showed

that pre-hydrolyzed TEOS could be added as filler as it did not change the thermal or mechanical properties appreciably. The PS-co-PMMA mixed with the pre-hydrolyzed TEOS showed higher glass transition temperatures with increasing silica content. The PS-PI-PS did not combine well with pre-hydrolyzed TEOS. One of the major findings was that small amounts (a few %) of residual solvent and hydrolysis byproducts (ethanol) act as a plasticizer that significantly reduces mechanical stiffness of the hybrids below that expected.

Preparation and Characterization of Polymer-SiO_2 Hybrids

by

Morgan L. Ferguson

A DISSERTATION

Submitted to

Oregon State University

in partial fulfillment of
the requirements for the
degree of

Doctor of Philosophy

Presented March 11, 2011
Commencement June 2011

Doctor of Philosophy dissertation of Morgan L. Ferguson presented on March 11, 2011

APPROVED:

_____

Major Professor, representing Chemistry

_____

Chair of the Department of Chemistry

_____

Dean of the Graduate School

I understand that my dissertation will become part of the permanent collection of Oregon State University libraries. My signature below authorizes release of my dissertation to any reader upon request.

_____

Morgan L. Ferguson, Author

ACKNOWLEDGEMENTS

First and foremost I would like to thank my husband for supporting me throughout my entire college career and for always offering an encouraging word. My family and family in-law deserve thanks for keeping me on my toes with "when will you be done?" There are many more friends and family to thank also and so I don't forget to include any of them by name I will just throw out an all encompassing THANK YOU! I appreciated all the kind words and support throughout the years I have been here. For all of my editors (Debra, Tanda, and Heather) who took the time to read through my work whether or not they understood it I appreciate your time and critiques. For Emmeline who helped me with instrumentation, thank you. The last big thank you goes out to Dr. Watson for taking me into his group (the most awesome 1 person research group!) and for teaching me so many new things about chemistry and research.

TABLE OF CONTENTS

TABLE OF CONTENTS

TABLE OF CONTENTS

TABLE OF CONTENTS

LIST OF FIGURES

LIST OF FIGURES

LIST OF FIGURES

LIST OF FIGURES

LIST OF TABLES

Preparation and Characterization of Polymer-SiO_2 Hybrids
Chapter 1: General Introduction

Polymer-Inorganic Hybrid Importance

Sol-gel processing of hybrid materials[1-2] formed from a polymer and an inorganic material leads to a diverse class of materials. There are biocomposites which contain an inorganic material reinforcing a polymer matrix. We encounter such biocomposites every day, typically as bones, teeth and shells. Another class of hybrids is flexible ceramics which combine a polymer and ceramic component in a low temperature process. Hybrids can be produced from a tri-block copolymer, which acts as a structure directing agent, and combined with an inorganic material to create an ordered polymer-inorganic hybrid system. Removing the tri-block copolymer component can lead to a highly ordered inorganic material with nanoscale features.

The great diversity of materials available to generate these hybrid materials leads to the variety of applications.[3] Coatings have been created that enhance scratch resistance, prevent corrosion, and permeation of a substance.[4] Soloukhin et al coated polycarbonate with a silica-(meth)acrylate hybrid to enhance the surface mechanical properties.[5] Transparent colored thin gel hybrid layers are used as a coating to provide color to an object.[6] Proton exchange membranes have been formed[7] and Su et al showed that using sulfonated silica nanoparticles in a Nafion® membrane to create a polymer-inorganic hybrid improved its stability in methanol and increased proton conductivity.[8-9] New morphologies, such as the plumbers bi-continuous network, have been found when an inorganic material was introduced into a block copolymer and may have novel properties not seen in traditional nanocomposites.[10] There are many other areas of use and potential uses that have been elucidated.[11-17]

The combination of an inorganic material with a polymer gives the resultant hybrid properties from both constituents – the flexibility of the polymer

with the strength of the inorganic.[18] Depending on the types of interactions that occur between the constituents, better properties than either of the components could emerge. Creating these materials can be as easy as mixing them together in a sol-gel process to produce a homogeneous hybrid. Sol-gel chemistry is a wet chemical process that allows an inorganic oxide to be produced from organically modified pre-cursor materials at lower processing temperature than a traditionally created inorganic oxide.

While polymer-inorganic hybrid creation in principle is simple, selecting which constituents to use can be decidedly more difficult. Polymer constituent choices can be obtained off the shelf from a limited set or synthesized in the laboratory with considerable effort. Many polymers can be chosen or made with a particular functionality in mind. The arrangement of the polymer can be one repeating monomer unit, a copolymer (which has different arrangement of the monomer units used), or a block copolymer (two polymers joined together), all of which are illustrated in Figure 1.1. The organically modified inorganic starting material used in creating the inorganic constituent is generally obtainable from chemical suppliers. These starting materials lead to an inorganic oxide network after hydrolysis and varying hydrolysis conditions can create linear chains, dispersed clusters or nanosized comparatively hard particles. The structure and chemical interactions between the polymer and inorganic species in the hybrid material may give rise to a combination of properties or possibly new properties. The choice of current flexible ceramics is based on the combination of a few ceramic precursors and a seemingly arbitrary choice of polymers and amphiphilic block copolymers. Understanding how the role of the constituent's structure, the chemical interactions and their miscibility in each other relate to the measured properties of the hybrids will allow for better tailoring of the properties of hybrids.

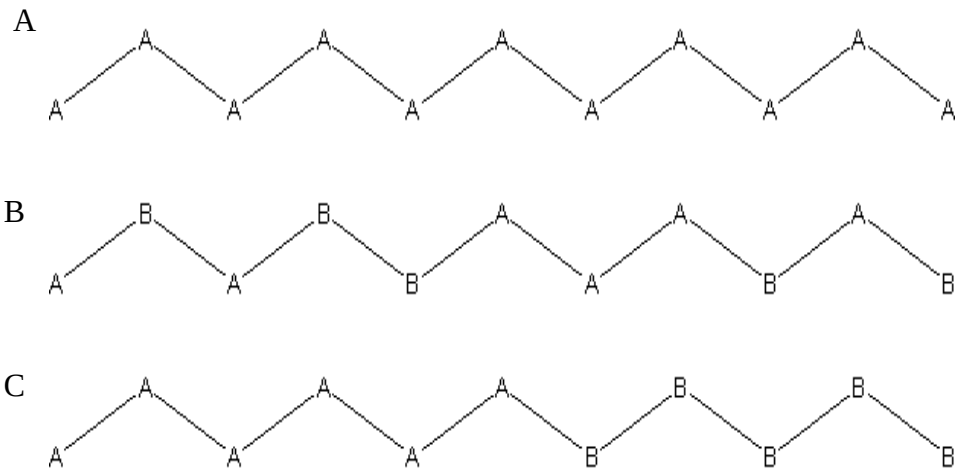

Figure 1.1: Illustrations of polymer types. (A)Polymer (B) random co-polymer and (C) block co-polymer. A co-polymer has a random order to the two monomers employed and a block-polymer has the first monomer units forming a polymer before linking to the second monomer units.

Polymer-inorganic hybrids can be placed into a few general classes and are laid out in Figure 1.2. The first corresponds to a polymer and inorganic components physically mixed together. These hybrids start with a dissolved polymer mixed with an inorganic oxide prepared utilizing sol-gel chemistry before addition or in-situ. The second class corresponds to the organic and inorganic components being connected by covalent bonds. To achieve the covalent bond a molecular precursor is added or the backbone chain of the polymer is modified with groups that will cause the inorganic and organic constituents to be bonded together. A third preparation method involves heating the polymer and inorganic oxide together before applying pressure to create a hybrid. This technique involves no solvents but the components are not always evenly distributed.

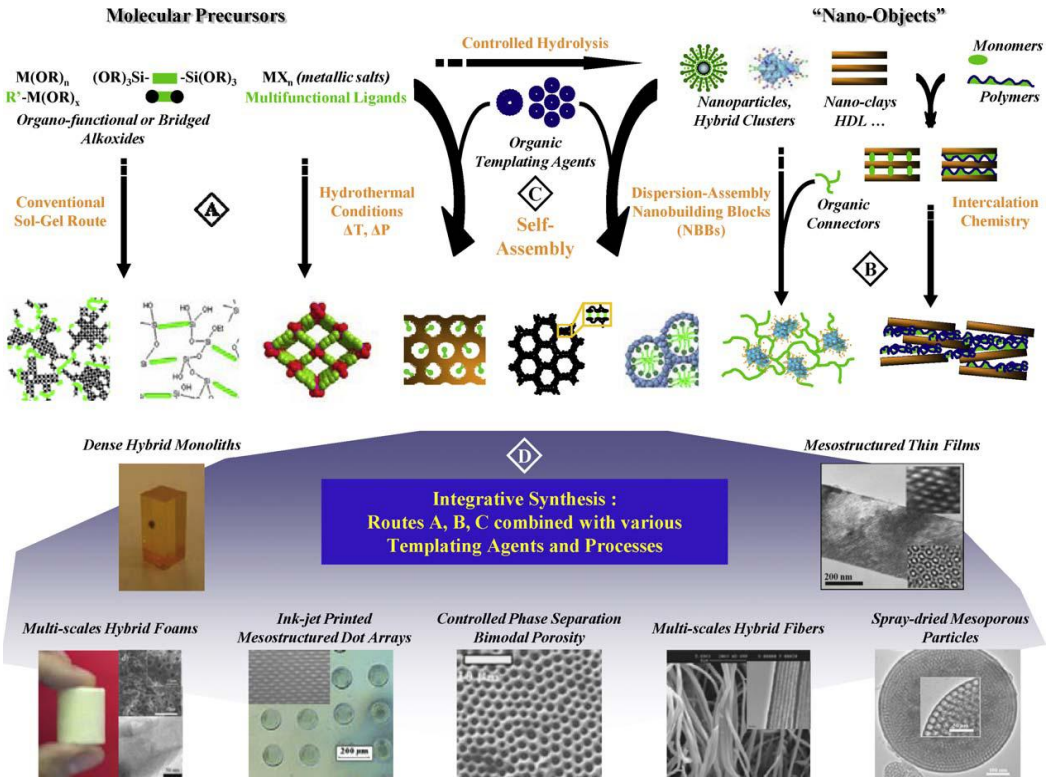

Figure 1.2: Polymer-inorganic flow chart.[19]

To characterize the polymer-inorganic hybrids, there are many techniques available. Modern spectroscopy offers nuclear magnetic resonance (NMR), Raman spectroscopy, and Fourier transform infra-red spectroscopy (FTIR) to determine the chemical interaction of the components. The mechanical properties can be analyzed with dynamic mechanical analysis (DMA) or Tensile tests. The thermal properties are determined by differential scanning calorimetry (DSC), thermogravimetric analysis (TGA), and DMA. There are also numerous other characterization techniques available for a researcher looking into polymer-inorganic hybrids to utilize at their discretion.

The properties resulting from the combination of an inorganic material in a polymer matrix depend on the extent of phase separation. The particle size of the inorganic component and the interfacial interactions between the constituents will determine the amount of phase separation and change the thermal and mechanical response of the hybrid[20]. When the constituents are physically mixed, without a coupling agent, the interactions rely on intermolecular forces and entanglements.

Chemically bonding the constituents will change the morphology/structure of the hybrid and the measured properties will change[21-22]. Without a high degree of dispersion, poor interaction between the constituents the hybrid material will probably lead to poorer mechanical properties and thermal response. To help control interfacial interactions the hydrolysis and polycondensation reaction conditions of the organically modified inorganic can be controlled to achieve a preferred product. The silica hydrolyzed from tetraethoxysilane under acidic conditions grows in a more linear manner than that obtained from basic catalyzed reactions and as a result may allow for a greater number of interactions with the polymer.[23-24] Scanning electron microscopy (SEM) is often used in studies of organic-inorganic hybrids to determine the degree of phase separation. While SEM may show the phase distribution, it is limited in the topographical information obtained and resolution. Transmission electron microscopy (TEM) is also employed to determine phase separation but has poor contrast that makes determining the morphology difficult. The usefulness of atomic force microscopy (AFM) has been shown in morphology studies of several polymer-inorganic hybrids[25-27]. Tapping-mode AFM (TM-AFM) allows for the investigation of the topography and phase separation concurrently. A review of the technique and its use on polymers by Magonov and Reneker explains how elastic inhomogeneity can be observed in great detail[28]. TM-AFM has been used on hybrid fracture and external surfaces of polymer-inorganic hybrids to show how materials with different mechanical properties are dispersed.[29]

Objective

Polymer-inorganic hybrids can be formed through so many different starting material combinations that choosing the constituents needed to achieve a hybrid with specific properties can seem daunting. The combinatorial aspect of the hybrids relies on the physical and chemical interactions between the constituents and the processing conditions. One goal of this project is to determine how the individual properties of the set of polymers combined with the inorganic oxide

transfer to the hybrid combinations. A second goal is to determine how the constituents are interacting (i.e. physical or chemical interactions).

The polymer-inorganic hybrid materials created in this project will fall into class one, where the constituents are physically mixed in a sol-gel process. Each polymer was dissolved in a suitable solvent mix and then pre-hydrolyzed tetraethyl orthosilicate was mixed in to create the hybrid via a sol-gel process. The mixture was cast to achieve a hybrid film. The polymer component choices were made from those available off the shelf. A set of polymers that would exhibit different chemical interactions based on their side groups were picked as well as a co-polymer and block-copolymer. The inorganic alkoxide chosen was tetraethoxysilane (TEOS) due to the substantial literature already available for the hydrolysis conditions and use in other polymer systems.

Polymer-SiO_2 Hybrids

A polymer mixed with a silicon alkoxide in a sol-gel process will yield a polymer-SiO_2 hybrid material. Typical silicon alkoxides are tetramethoxysilane (TMOS) or tetraethoxysilane (TEOS). The measured thermal and mechanical properties will show a combinatorial effect from their constituents if a good interfacial interaction is achieved. Some examples of polymer-inorganic hybrid systems that have been prepared and characterized follow.

Hydroxypropyl cellulose (HPC) was mixed with TEOS to obtain a hybrid.[30] The strength of this hybrid was seen to increase with an increasing TEOS amount up to 40 weight percent. The TEOS was converted to SiO_2 via a sol-gel process during the mixing of the constituents. Above 50 weight percent TEOS the hybrid creation became difficult and the product broke easily.

Poly (N-isopropylacrylamide) (PNIPAM) was combined with TMOS and a cross linker, N, N,-methylenebisacrylamide, to produce a hybrid.[31] The polymer and TMOS were polymerized/hydrolyzed concurrently. The mechanical properties of the hybrid were seen to improve above just the use of PNIPAM.

Dyes dispersed in a polymer matrix give transparent color for use in coatings. Disperse red 1 (DR1) doped PMMA showed increased thermal stability

when SiO_2 was added to create a hybrid.[32] Tetraethoxysilane was used to obtain the SiO_2. This provided a way to increase the properties of a known product rather than synthesize new chemical compounds.

Using block copolymers, such as styrene-butadiene-styrene (SBS), lead to the inorganic component being incorporated in only one of the blocks.[33] SBS and modified SBS chains were mixed with TEOS which was hydrolyzed to form a hybrid. The glass transition temperature of all the hybrids prepared were seen to increase. Depending on the modification to the SBS chain, the SiO_2 was seen to interact with one block over the other.

All of these prepared polymer-SiO_2 hybrids are said to rely on hydrogen bonding in order to prevent phase separation. H-bonding would have the effect of creating a strong hybrid. From the previous studies there is a limit to the amount of TEOS that can be used to improve the mechanical and/or thermal properties of the polymer.

Sol-Gel Chemistry

Inorganic alkoxides are transformed into a three-dimensional inorganic oxide structure via sol-gel chemistry synthesis.[34] The mild processing conditions (low temperature, atmospheric pressure and solvent compatibility) allow for the addition of a polymer with no chain degradation. The sol-gel process also allows for a degree of control over the composition and structure at a molecular level of the inorganic oxide. A commonly studied system in sol-gel chemistry is tetraethyl orthosilicate (TEOS).[35-37] The structure of TEOS is shown in Figure 1.3 and is similar to other inorganic alkoxides.

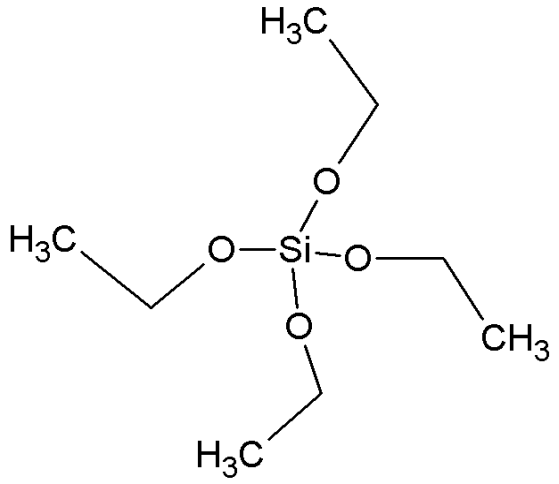

Figure 1.3: Tetraethyl orthosilicate (TEOS) structure. The central Si atom can be changed to another inorganic atom and the ethyl group changed to another alkyl chain to create a wide variety of inorganic alkoxides.

The sol-gel process can be broken down into two steps: hydrolysis and polycondensation, as outlined in Scheme 1.1. The kinetics of the reaction steps are influenced by many factors including the water to TEOS ratio, catalyst presence, and temperature.[38] The hydrolysis and polycondensation reactions generally proceed at the same time with reaction rates that can be controlled by pH. The pH can be used to control the morphology of the resulting oxide.[2-3] The reactivity of the inorganic alkoxide is also influenced by steric effects of leaving group stability from the alkyl group present. A bulkier group corresponds to a slower reaction rate. The sol-gel reaction can be done in an acidic[36, 39] or basic[40-41] environment.

$$\textit{Hydrolysis}: \quad Si(OR)_4 + H_2O \xrightarrow{H^+ or OH^-} (RO)_3SiOH + ROH$$

$$\textit{Condensation}: \quad Y_3SiOH + HOSiY_3 \xrightarrow{H^+ or OH^-} Y_3Si-O-SiY_3 + H_2O$$

$$Y_3SiOH + ROSiY_3 \xrightarrow{H^+ or OH^-} Y_3Si-O-SiY_3 + ROH$$

Scheme 1.1: Hydrolysis and polycondensation reactions that occur during a sol-gel process. Si is used as an example central atom. The Y can be an alcohol or alkoxide group.

Tetraethyl orthosilicate, TEOS, sol-gel chemistry has been studied for many years. The understanding behind the hydrolysis and condensation reactions and the structure of the resultant SiO_2 network makes it a good candidate for an organic-inorganic hybrid. The differences between an acidic or basic catalyzed reaction are reviewed below.

In a basic environment water dissociates to produce a hydroxyl anion which acts as a nucleophile. In the hydrolysis step, this OH^- attacks the silicon atom producing a silanol and alcohol.[41] The condensation involves the attack of a nucelophilic de-protonated silanol on a neutral silicic acid to create the Si-O-Si linkages. This condensation mechanism allows for a more branched, cluster like 3-D structure to emerge.

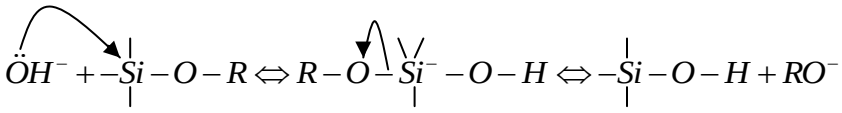

Scheme 1.2: Mechanism for basic catalyzed hydrolysis.

In an acidic environment a proton attaches to an O-R group on the Si atom. This pulls electron density away from the Si atom, allowing water to attack the silicon atom, ultimately producing a silanol and alcohol. The condensation occurs preferentially between a protonated silanol and neutral species to create the Si-O-Si linkages. As the chain grows, the most basic silanols are likely to be protonated, leading to a more linear 3-d structure.

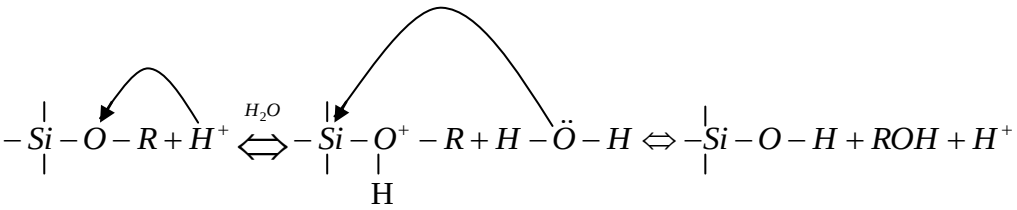

Scheme 1.3: Mechanism for acidic catalyzed hydrolysis

Polymer Background

A large number of small molecules linked together in a repeating manner create a long-chain molecule with a molecular weight in the thousands or larger known as a polymer. A molecular weight high enough to begin entangling with other chains is required for a molecule to be considered a polymer and is illustrated in Figure 1.4. Unique properties, such as mechanical or thermal response, seen in polymers are brought on by this phenomenon. Increasing the chain length and in turn the molecular weight eventually leads to asymptotic behavior of the polymer properties as illustrated in Figure 1.5.

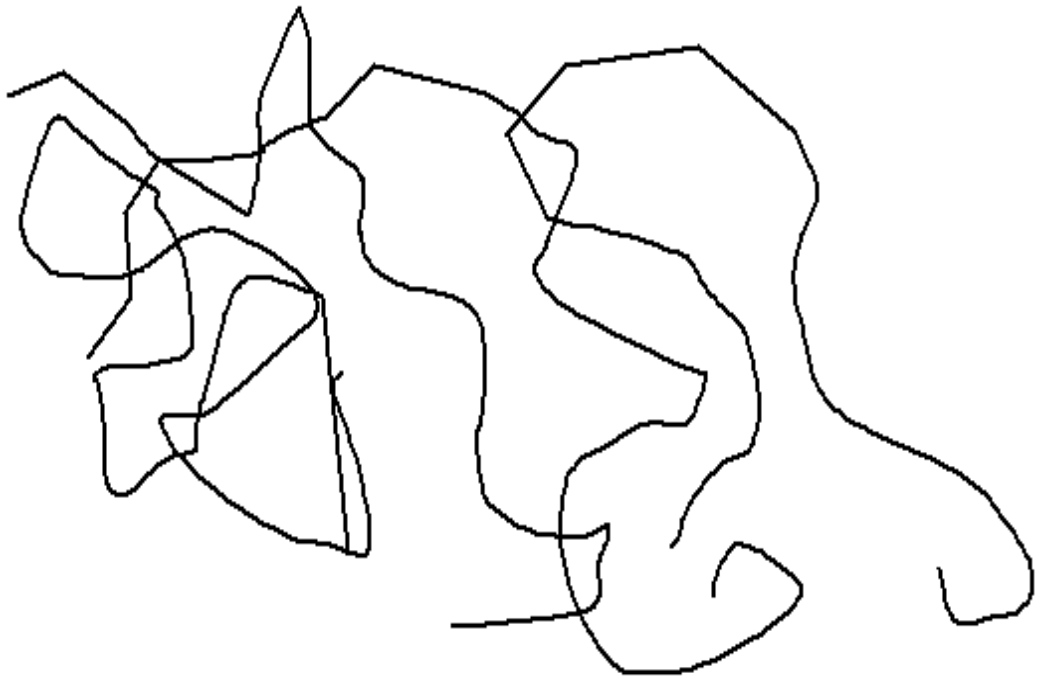

Figure 1.4: Entanglements of Polymer Chains. A high molecular weight is required for this to occur.

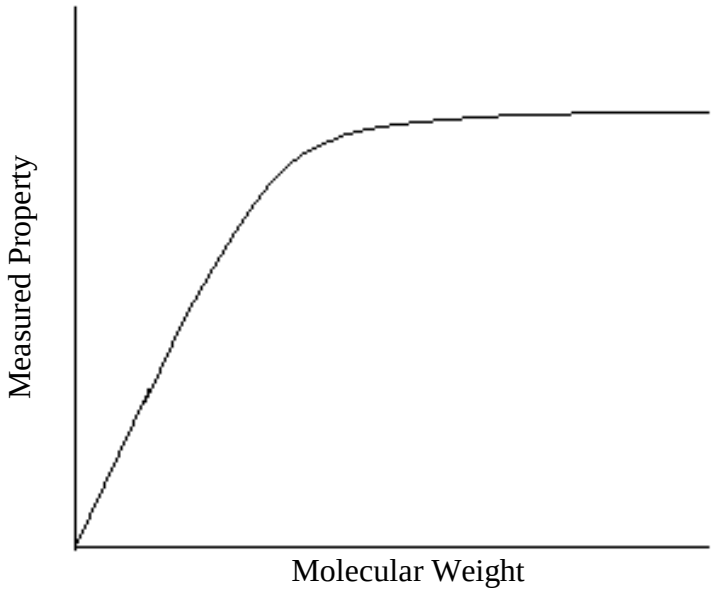

Figure 1.5: Asymptotic behavior of properties of polymers as molecular weight is increased. (melting temperature, mechanical properties)

A polymer's properties can change not only due to the length of the chain but also with the arrangement of a side group around the backbone. A monomer that is chiral leads to a pseudochiral polymer. The starred carbon in the polymer, illustrated in Figure 1.6, is pseudochiral because it shows no optical activity due to the length of the attached carbon chains on either side. The pseudochiral center does lead to different spatial arrangements of the side group along the polymer backbone, known as the tacticity of the polymer chain. Figure 1.7 shows the different tacticities possible in a polymer. When a substituent, R, is ordered randomly along the backbone the structure is atactic. When naming atactic polymers, no prefix is needed. If the substituent is ordered all on the same side, the structure is isotactic and named with a prefix of it- placed before the polymer name. Alternating the substituent on the backbone chain leads to a syndiotactic structure. A prefix of st- is placed before the polymer name when naming syndiotactic polymers.

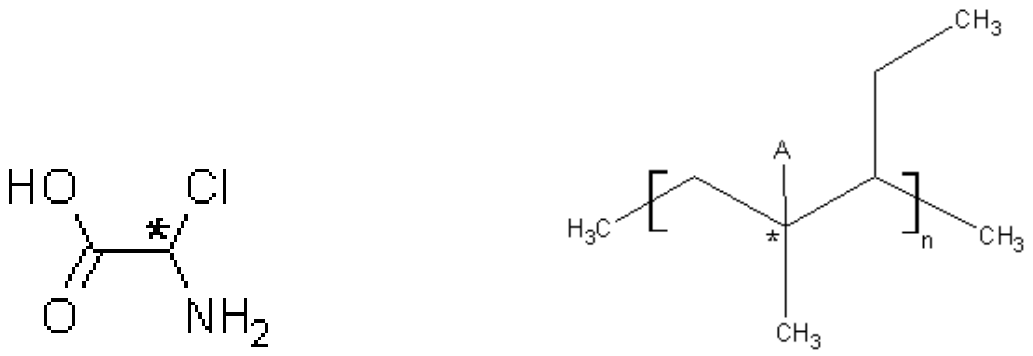

Figure 1.6: Showing a chiral center in a small molecule and a pseudochiral center in a polymer, both marked with a *.

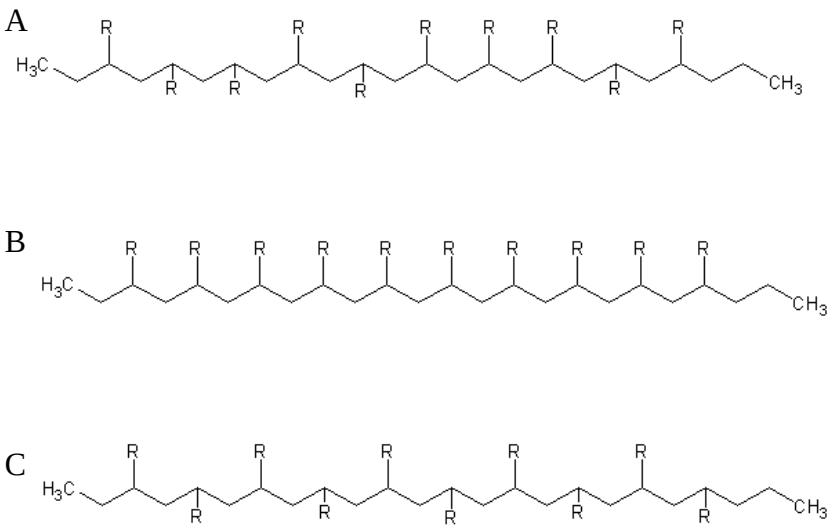

Figure 1.7: Tacticity (spatial arrangement) of polymer chains. A. atactic B. isotactic C. syndiotactic

The spatial arrangement of the polymer can lead to ordering between the chains that will contribute to thermal and mechanical properties in different ways. Ordering causes the polymers to be crystalline in regions of the polymer. Atactic polymers are amorphous and show no ordering between chains. Syndiotactic and

isotactic polymers can both show order and therefore crystallize to various degrees. A polymer will not fully order so it cannot be crystalline like a smaller molecule and is considered semi-crystalline, with different degrees of order based on how efficiently the chains can pack. Figure 1.8 shows how a polymer orders based on its structure with amorphous regions always being present to a certain degree due to the length of the molecules. The degree of crystallinity of a polymer will affect its mechanical properties and in general a semi-crystalline polymer will be stiffer than an amorphous polymer.

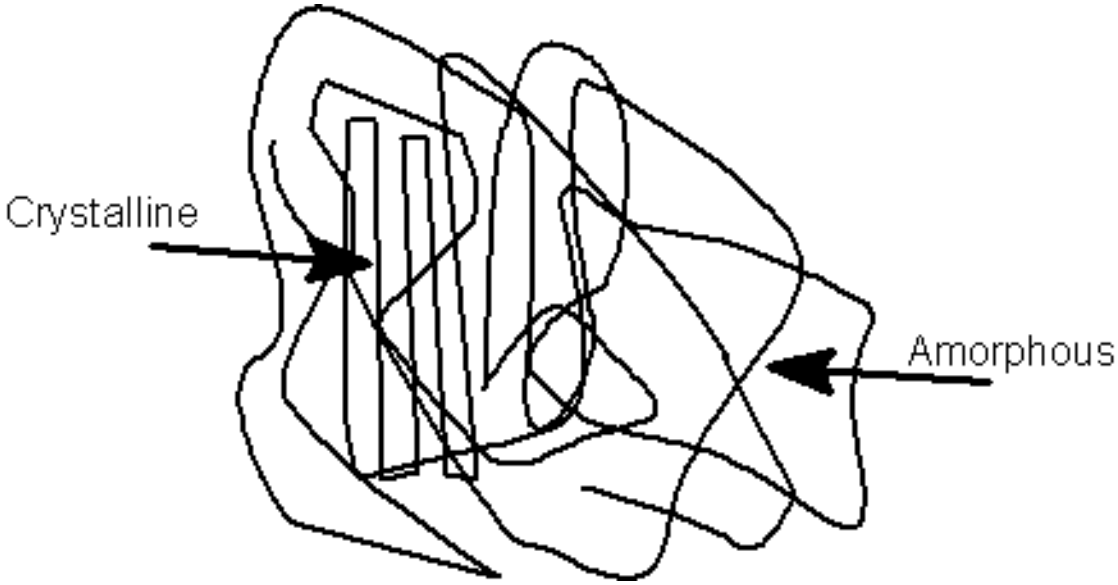

Figure 1.8: A semi-crystalline polymer. Part of the chain is amorphous while part of the chain orders with itself.

Mechanical Properties

The polymer's basic structure and preparation history will affect its mechanical behavior. The measured response of the material to an applied strain gives a stress-strain curve similar to those shown in Figure 1.9. The toughness, modulus, and elongation to break can be determined from this curve. The mechanical response of a polymer over a temperature range can be seen in Figure 1.10. The shape of the curve gives insight into the modulus for a temperature range, where the onset of flow occurs (the vertical portion of the curve) and provides information on the chemical/physical state of the polymer.

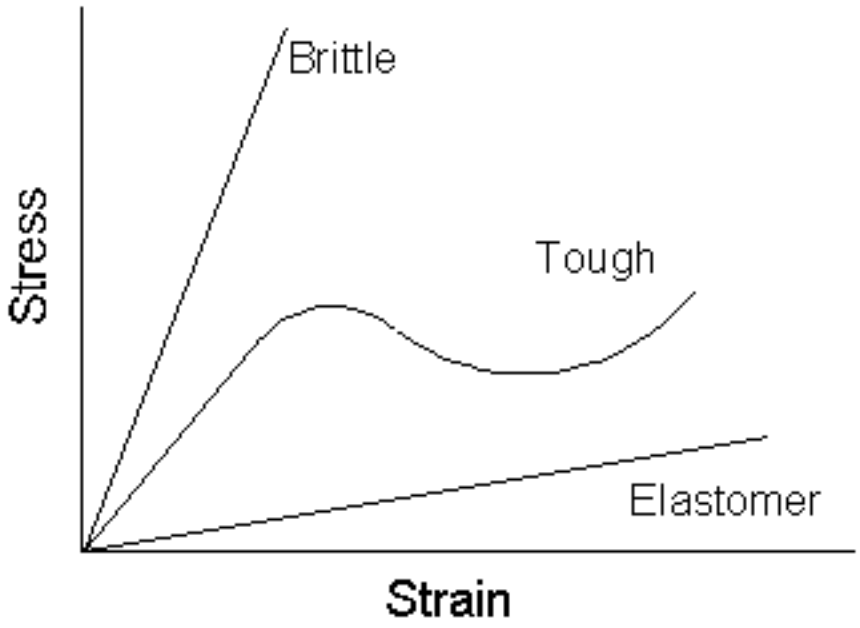

Figure 1.9: Schematic stress-strain curve for polymers. The initial slope yields the Young's modulus.

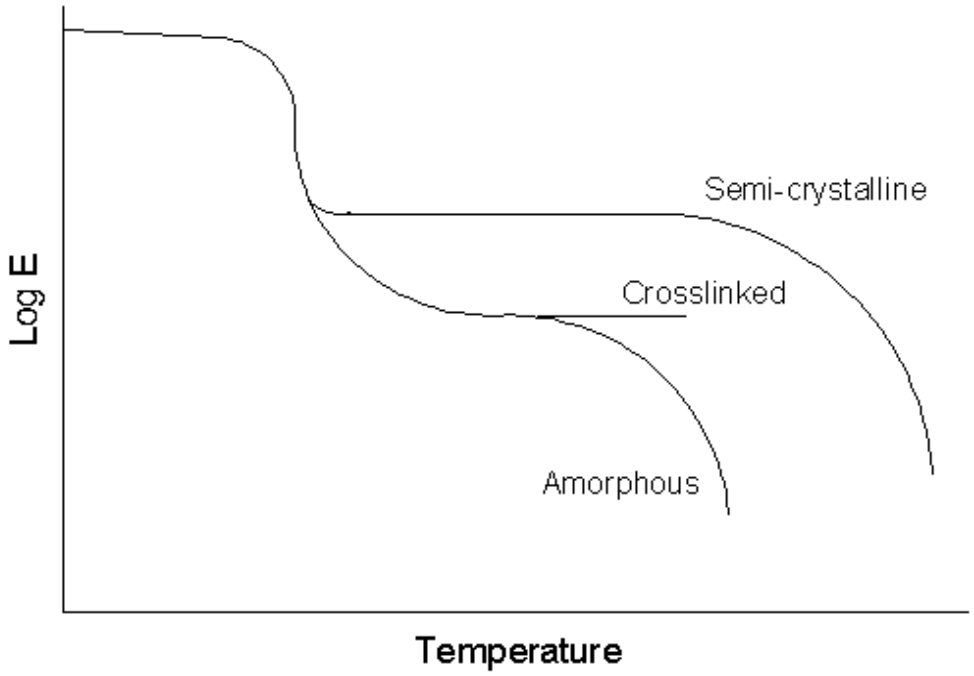

Figure 1.10: Schematic modulus versus temperature curve. Typical curves for amorphous polymers, semi-crystalline and cross linked polymers are shown.

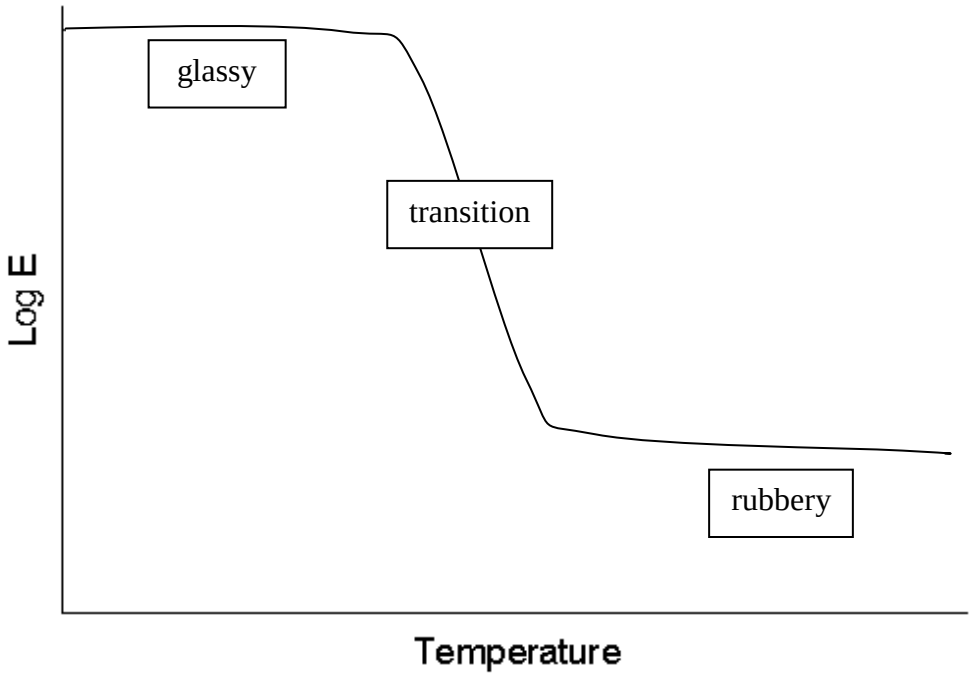

Figure 1.11: Regions of a dynamic mechanical analysis curve.

The curve shown in Figure 1.11 labels the different regions through which a polymer will go with temperature changes. In the glassy region the polymer is stiff and brittle. The modulus will be on the order of gigapascals (GPa). As the temperature is increased and the polymer softens, the polymer chains can flow and move amongst each other. This is the glass transition region and a glass transition temperature is reported by taking the midpoint of the slope change. At high enough temperatures the polymer can become rubbery, becoming very stretchy. After the rubbery region the polymeric material will fail and degrade. The temperatures needed to achieve these behaviors will vary for each polymer. Some polymers, such as polystyrene, are glassy at room temperature while others, like polyisoprene, are rubbery at room temperature.

The modulus of a polymer is simply the degree to which the polymer possesses a property. Three moduli are important to polymers: Young's, Bulk, and Shear. Their differences lie in how they are measured. Young's modulus (E), Figure 1.12, is a measure of the stiffness of a material. The sample is elongated

and the ratio of the stress/strain provides a measurement of how resistant a material is to being stretched. Higher values represent a stiffer material.

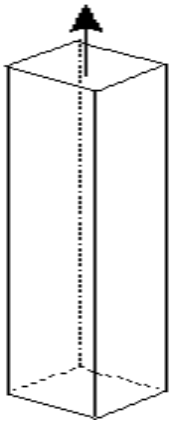

$$E \equiv \frac{\text{tensile stress}}{\text{tensile strain}} = \frac{F / A}{(L - L_o)/ L_o}$$

Figure 1.12: Young modulus. L_o is the initial length, L is the length after the force is applied.

The Shear modulus (G), Figure 1.13, is a measure of how the material responds to shearing or twisting motions. The ratio of shear stress to shear strain gives the shear modulus. The Bulk modulus (B), Figure 1.14, is the response of the material to uniform compression. It is measured as the pressure change needed to cause the volume to decrease.

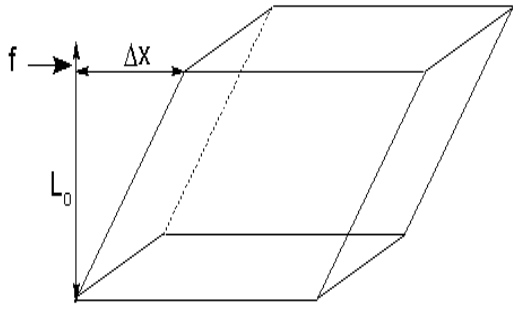

$$G \equiv \frac{\text{shear stress}}{\text{shear strain}} = \frac{F / A}{\Delta X / L_o}$$

Figure 1.13: Shear modulus. L_o is the initial height, ΔX is the change in position after the force is applied.

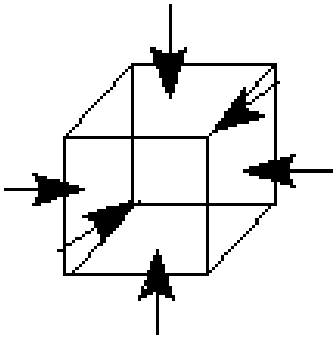

$$B = -V\left(\frac{\delta P}{\delta V}\right)_T$$

Figure 1.14: Bulk modulus. The change in volume when an external pressure is applied.

The moduli can be related to each other by the following equation:

$$E=3B\,(1-2\nu) =2(1+\nu)\,G \qquad (1.1)$$

where ν is the Poisson ratio. The Poisson ratio is a measure of the change in volume for small applied stresses that cause a deformation in the material. When a material has no volume change for a given deformation, ν=0.5. Elastomers come close to having a poisson ratio value of 0.5. For typical polymers, the volume will change upon deformation which gives typical ν values of 0.2-0.4.[42]

Characterization Techniques

The characterization of the polymer-inorganic hybrids was done with the variety of techniques at our disposal. We utilized thermogravimetric analysis, Fourier transform infrared spectroscopy, differential scanning calorimetry, dynamic mechanical analysis, and atomic force microscopy. While there are many other instruments out there that would complement the ones we used, difficulty with sample preparation (contact angle), instrumentation being unavailable (solid

state nuclear magnetic resonance), and time constraints to finish this project ultimately led to our decision on which techniques to include. Details of the instrumentation, running conditions, and programs used are given in the Appendices.

Thermogravimetric Analysis

Thermogravimetric analysis (TGA) is a technique used to monitor the weight changes in a sample as temperature is increased. Figure 1.15 shows the basic set-up of a TGA instrument. The sample is loaded into the pan, which is suspended from a balance arm and when the furnace is closed the temperature is ramped to a final degree setting. The furnace is continuously purged with a gas hooked up to the instrument. Nitrogen and air are the most commonly used. In this study we utilized air as our furnace environment.

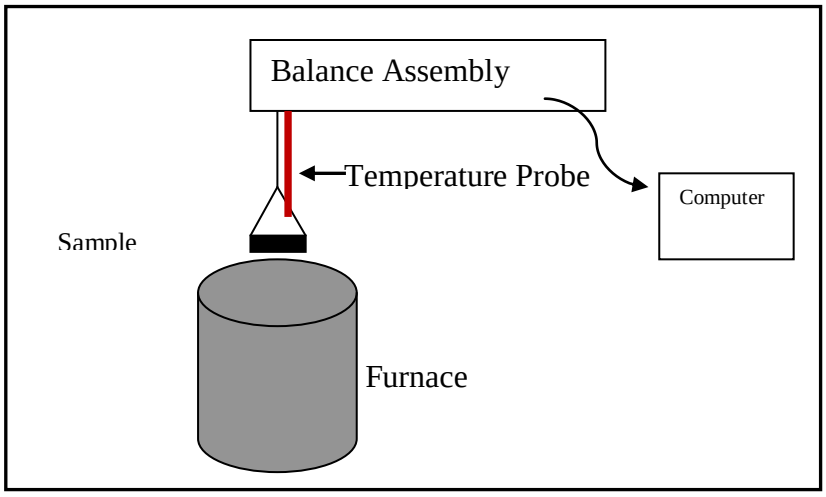

Figure 1.15: Schematic of TGA instrumentation.

The weight loss as the temperature is increased accounts for the release or degradation of the various components in the sample. Figure 1.16 shows a typical TGA curve. The weight loss a low tempertures (A) could be due to volatiles retained in the sample. The next weight loss drop (B) shows a larger weight percent decrease of another component that accounts for the majority of the

sample present. The weight percent left at the end of the temperature run (C) shows a component that is stable at the temperatures used with this particular TGA run.

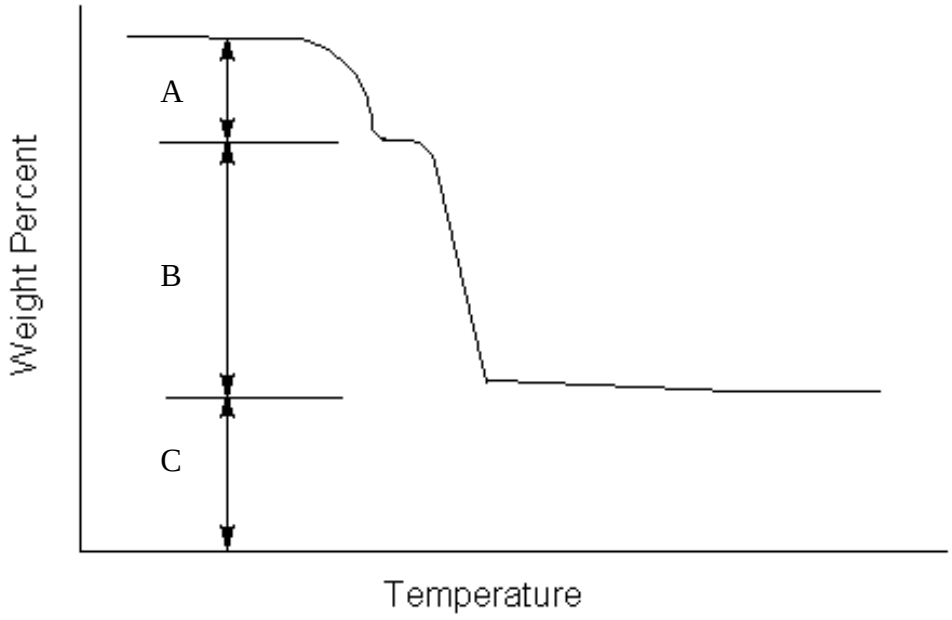

Figure 1.16: A typical TGA trace. The weight loss at different temperatures is indicative of the components burning off.

Fourier-Transform Infra-Red Spectroscopy

Infrared spectroscopy can be used to determine the molecular motions present in the polymer and polymer-inorganic hybrids. The functional groups attached to the polymer backbone will absorb IR energy at specific frequencies that can be used to help identify or confirm a species as being present in a sample. Table 1.1 lists some of the common peaks for molecular motions that will be used to identify components in our samples. Figure 1.17 shows a typical FTIR spectra obtained on a sample of poly(methyl methacrylate), the structure of which is shown in the upper left corner. From the structure of PMMA and the listed frequencies in Table 1.1, we expect to see peaks due to the carbonyl (C=O) and the alkane (C-H) stretching motions. These peaks are easily identifiable in the spectra shown. There are many other stretches and bends that give rise to peaks in the spectra at lower frequencies that are not as easily indentifiable due to their close

proximity to other molecular motions. This lower frequency region is commonly referred to as the fingerprint region and will be unique for each molecule.

Table 1.1: Characteristic IR Absorptions[43]

Group	Frequency range (cm^{-1})
Alkyl C-H stretch	2853-2962
C=C stretch	1620-1600
Aromatic-H stretch	~3030
C=O stretch	1630-1780
Si-O stretch	~1100

*This is not an all inclusive table of the absorptions possible with our systems.

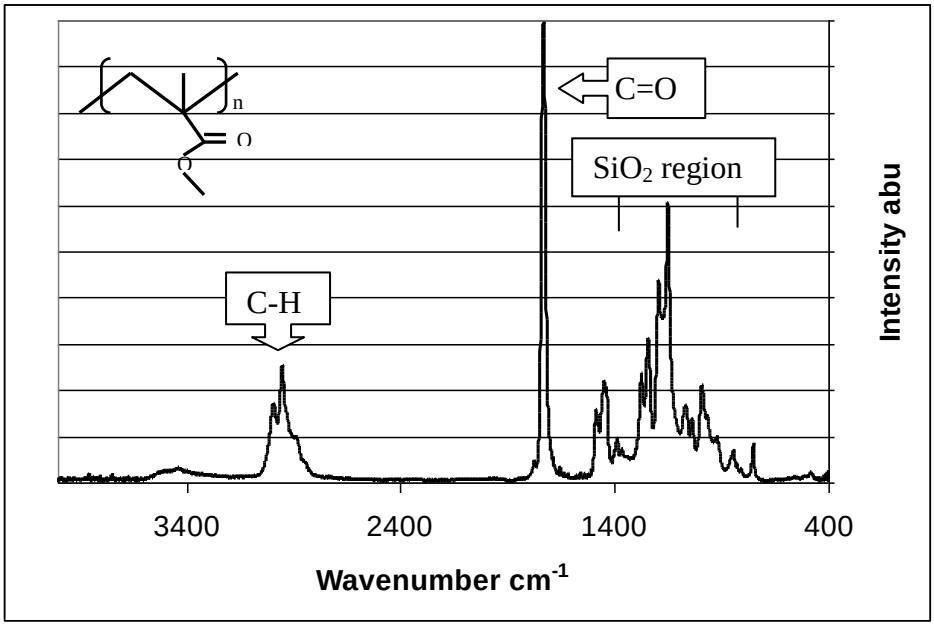

Figure 1.17: FT-IR absorption spectra for PMMA. The carbonyl (C=O) peak is the sharpest.

Since the polymers were bought from Aldrich and not synthesized, no other chemical or structural analyses were run. More characterization testing would be needed to fully determine the structure of the polymer if it were synthesized. The FTIR spectra we obtain for each polymer and their corresponding hybrids will be used to determine that both components, the polymer and inorganic

material, have been incorporated into the hybrid. The SiO_2 will appear as a broad band centered around 1100 cm^{-1} in the spectra and add to the peaks already present from the polymer. SiO_2 is not present in the spectra shown in Figure 1.16 but is labeled to show its general absorption region.

Gel Permeation Chromatography

The molecular weight, size, of a polymer can be determine using gel permeation chromatography (GPC). The technique works using size exclusion principles in which a column is packed with a stationary phase that contains small pores. The polymer, which is contained in the mobile phase, passes through the stationary phase and if the polymer chain is small enough, it will spend more time in the column getting caught up in the pores of the stationary phase. The largest molecules will elute first and show up as a peak in the GPC trace. Figure 1.18 shows a typical GPS trace of a sample. The column and solvent must be calibrated with known polymer standards before any useful data can be obtained.

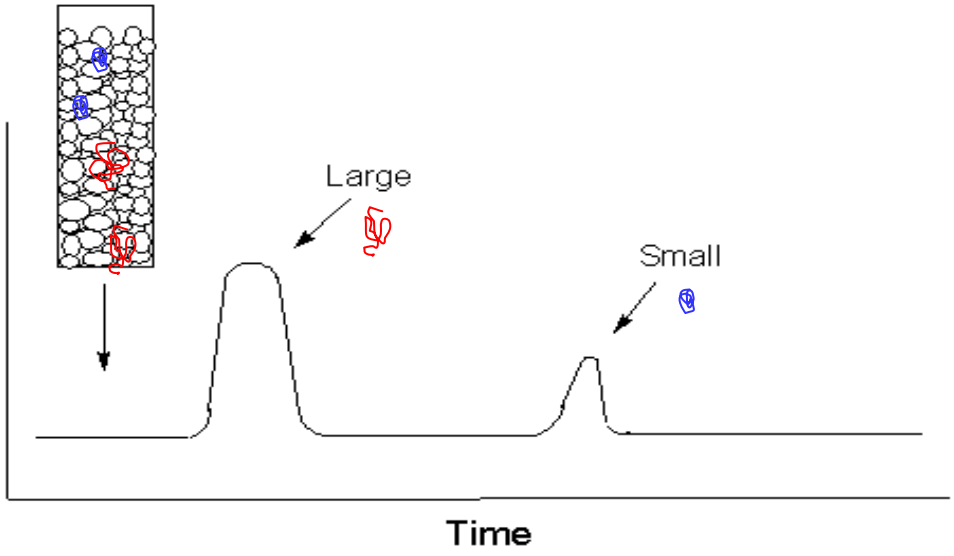

Figure 1.18: GPC schematic. Large molecules are eluted first. The smaller molecules spend more time in the column.

Differential Scanning Calorimetry

Differential scanning calorimetry (DSC) was used to determine the thermal properties and history of the polymers as well as how those properties change upon the introduction of an inorganic material. The schematic in Figure 1.19 shows a typical DSC instrument set-up. The sample and reference pan are maintained at the same temperature, even when the sample is experiencing a thermal event such as melting or crystallization. To maintain a zero temperature differential between the sample and the reference pan requires energy.

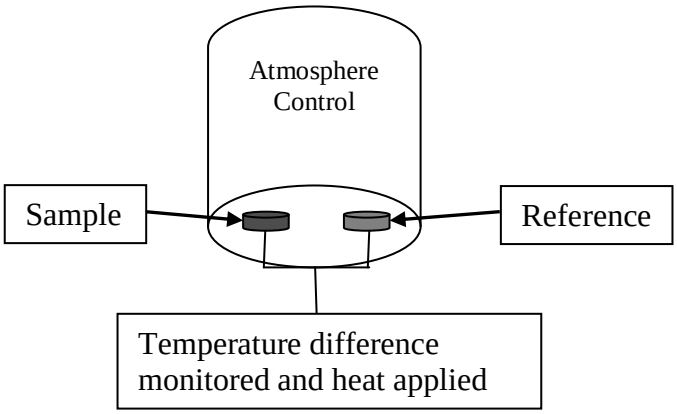

Figure 1.19: Schematic set-up of DSC instrument.

To achieve a DSC trace, the heat capacity (kJ/kg K) is measured as a function of the temperature. A characteristic DSC trace is shown in Figure 1.19. The types of features seen in a DSC trace are dependent on the state of the polymer and the thermal history. There are endothermic effects, which are usually indicative of disordering in the sample, and exothermic effects, which are usually indicative of ordering in the sample. Melting or crystallizing will be an endothermic or exothermic effect, respectively. The curve shown in Figure 1.20 has a slope change along the baseline that is due to the polymer softening as it goes through the glass transition region. The glass transition temperature (T_g) is read as the midpoint of the slope change along the baseline.

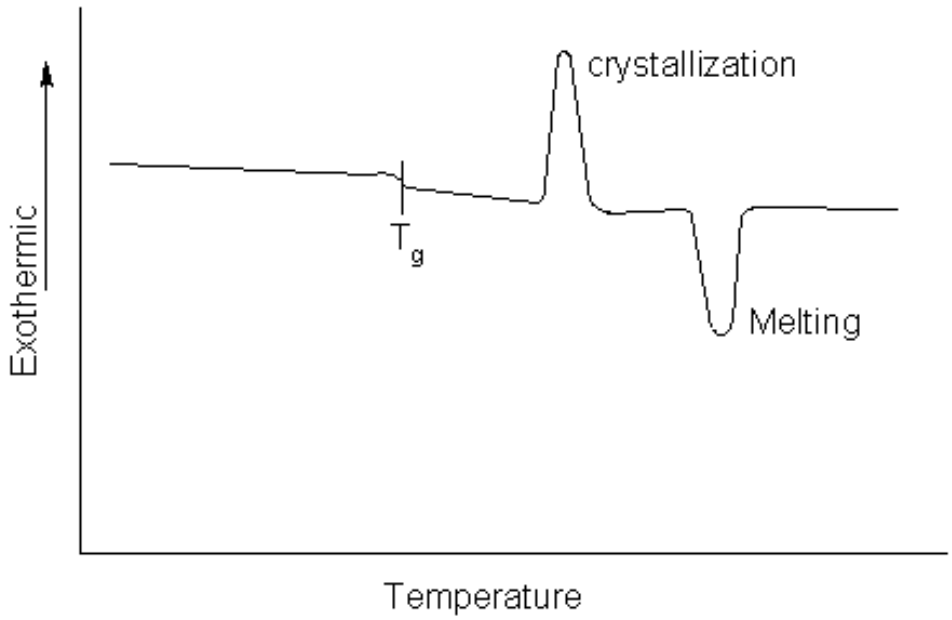

Figure 1.20: Schematic DSC trace with typical features. The T_g is the glass transition temperature.

Dynamic Mechanical Analysis

Dynamic mechanical analysis (DMA) measures the viscoelastic properties of a sample as a function of time, temperature, or frequency. A sinusoidal strain (ε) is applied to a material as a function of time and the stress (σ) from that applied strain is determined. The strain and stress are given by the following equations:

$$\varepsilon = \varepsilon^{\circ}\sin(\omega t) \qquad 1.2$$

$$\sigma = \sigma^{\circ}\sin(\omega t + \delta) \qquad 1.3$$

$$\omega = 2\pi f \qquad 1.4$$

The frequency can be between 0.1 to 110 Hertz, ε° is the amplitude of the applied strain, σ° is the amplitude of the stress response, and δ is the phase angle between the stress and strain. The phase angle is a measure of the amount of viscous response a material has due to the dynamic strain. Because we are dealing with polymers, which are viscoelastic materials, we have two extreme cases to think about, purely elastic or purely viscous.

A purely elastic material is always in phase, giving a phase angle of 0° and will obey Hooke's law. So the strain and stress for an ideal elastic material may be

related by Young's modulus, E, and then applied to our dynamic equations 1.2 and 1.3:

$$\sigma = E\varepsilon \qquad 1.5$$

$$\sigma = \sigma^{\circ}\sin(\omega t) = E\varepsilon^{\circ}\sin(\omega t) \qquad 1.6$$

An ideal viscous fluid will be 90° out of phase so the phase angle, δ, will be π/2. This fluid will obey Newton's law of viscosity where η is the viscosity. The stress written in terms of viscosity and then applied to our dynamic equations 1.2 and 1.3 gives:

$$\sigma = \eta(dE/dt) \qquad 1.7$$

$$dE/dt = \omega\varepsilon^{\circ}\cos(\omega t) \qquad 1.8$$

$$\sigma = \eta\omega\varepsilon^{\circ}\cos(\omega t) = \sigma^{\circ}\sin(\omega t + \pi/2) \qquad 1.9$$

Polymers will behave as a mixture of a Hookian solid and an ideal viscous fluid, which is why they have been termed as a viscoelastic material. When DMA is run a trace similar to Figure 1.21 is obtained. Three curves are obtained and plotted against temperature, log time or log frequency. The curves are of the storage modulus, E', loss modulus, E", and the tan δ. The storage modulus is a measure of the energy that is stored elastically during a deformation. The loss modulus is a measure of energy that is converted to heat during a deformation. The tan δ is the ratio of the loss modulus to the storage modulus and provides information of the damping properties of a material. From the storage modulus curve two plateaus can be seen with a transition region connecting them. The drastic slope change between the plateaus marks the glass transition region. At temperatures below the glass transition region the material will behave more as a Hookian solid at small deformations, at temperatures in the glass transition region the materials are distinctly viscoelastic and at temperatures above the glass transition region the material behaves more as a viscous Newtonian fluid. The reported glass transition temperature is taken from the peak of the tan δ curve.

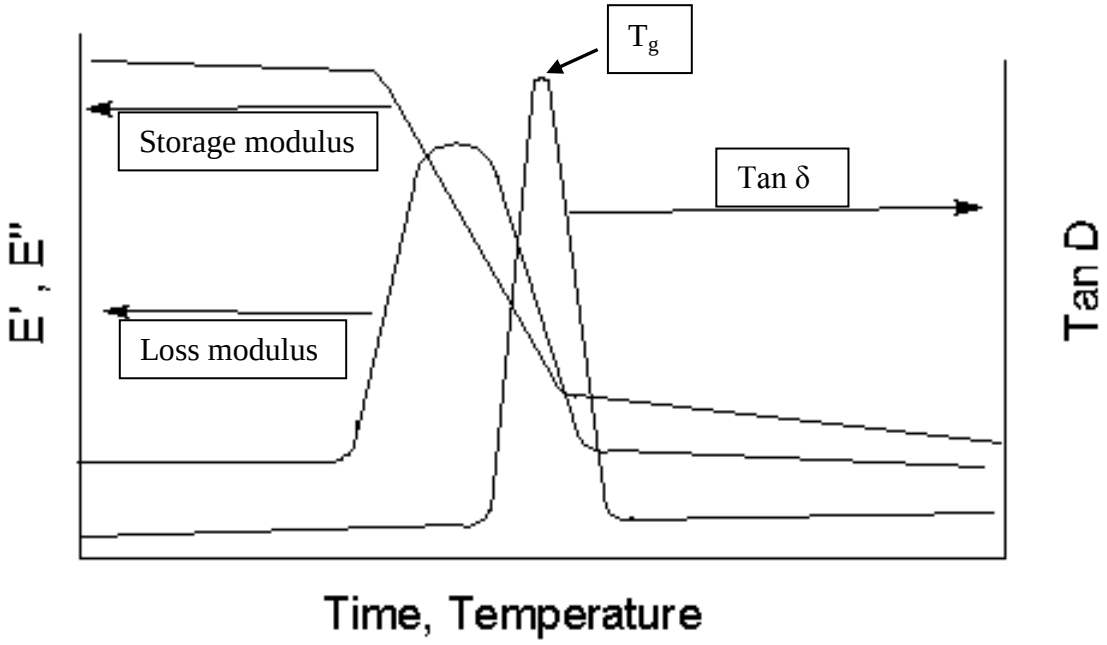

Figure 1.21: DMA trace showing the modulus and tan D response to time or temperature.

A complex modulus for the material can be obtained using complex number notation for the strain and stress giving:

$$\varepsilon^* = \varepsilon^\circ \exp(i\omega t) \qquad 1.10$$

$$\sigma^* = \sigma^\circ \exp\left[i(\omega t + \delta)\right] \qquad 1.11$$

$$E^* = \frac{\sigma^*}{\varepsilon^*} = \frac{\sigma^\circ}{\varepsilon^\circ}\exp(i\delta) \qquad 1.12$$

The complex modulus, E*, can be resolved into two components which give the in phase storage modulus, E', and the out of phase loss modulus, E'', with the applied strain.

$$E^* = \frac{\sigma^\circ}{\varepsilon^\circ}\cos\delta = \frac{\sigma^\circ}{\varepsilon^\circ} i\sin\delta \qquad 1.13$$

$$E^* = E' + iE'' \qquad 1.14$$

The usefulness of defining the complex modulus allows the data to be related to the tensile (Young's, E) modulus under certain conditions by:

$$E = |E^*| = \sqrt{(E')^2 + (iE'')^2} \qquad 1.15$$

Since the Young's modulus is considered the fundamental measure of stiffness of a material obtaining a comparable value from the DMA data is important. When the polymer is at a temperature below the glass transition region the storage modulus, E', is much larger than the loss modulus, E", making the complex modulus rely mostly on the E' value. This in turn makes the E' value approximately equal to the Young's modulus. This will not hold true for other portions of the curve and it is important to remember that while the storage modulus at this point is similar to the Young's modulus, it is not the same value.

Another value of interest that can be obtained from DMA curves taken at different frequencies over the same temperature run is the activation energy of any transitions noted. The activation energy, E_a, of a glass transition will be in the 100's of kilojoules and determining the E_a will help in assigning transitions when they are present in the trace. Figure 1.21 shows multiple tan δ curves obtained for a material run at different frequencies. The temperature from the peaks of the tan δ curve can be obtained for each frequency run and plotted according to an Arrhenius equation:

$$\ln f = \frac{-E_a}{RT} + \ln A \qquad 1.16$$

A plot of ln f versus 1/T will produce a straight line with a slope that is equal to $-E_a/R$, where R is the gas constant. An Arrhenius plot obtained from the data in Figure 1.22 is shown in Figure 1.23.

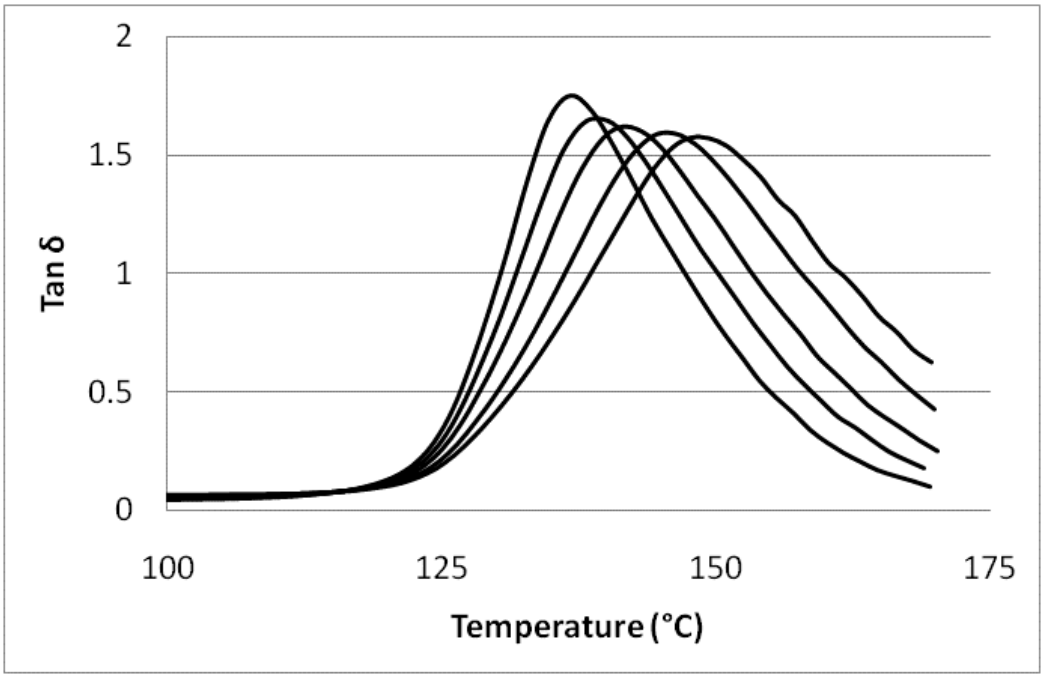

Figure 1.22: Tan δ curves for a PMMA standard. The frequencies run were 0.5, 1.0, 2.0, 5.0 and 10.0 Hertz.

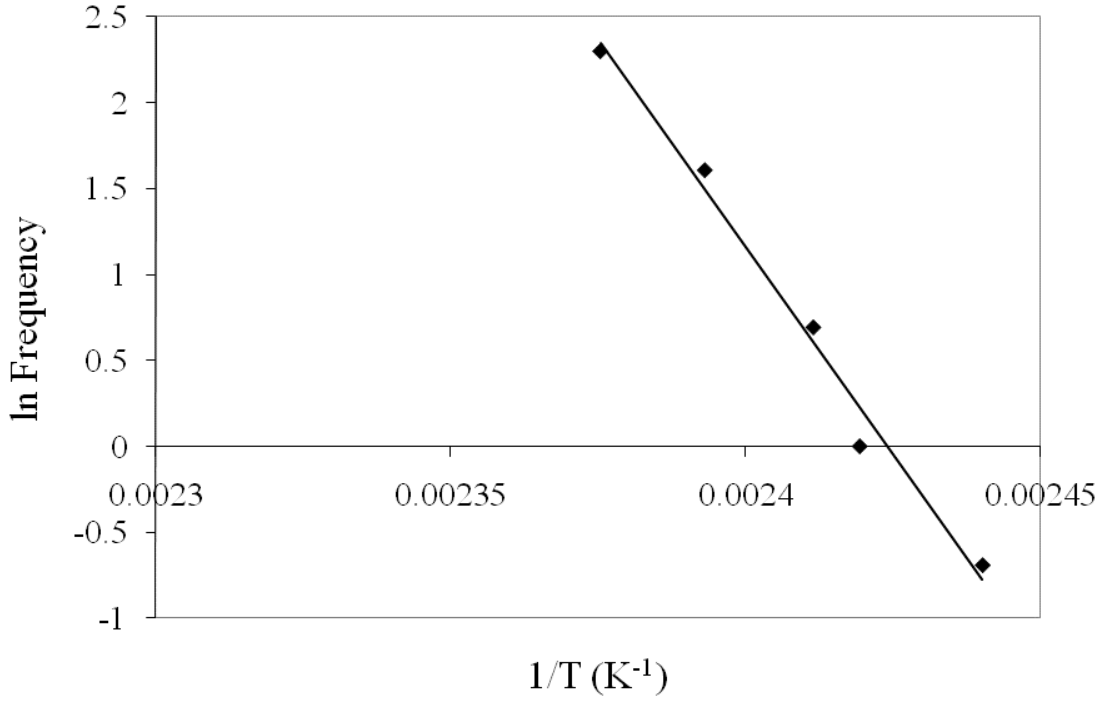

Figure 1.23: Arrhenius plot to determine the activation energy (E_a) of the glass transition. E_a was calculated to be 400 kJ.

Atomic Force Microscopy – Tapping Mode

The topography of a sample as well as its phase image can be obtained using tapping mode atomic force microscopy (TM-AFM). This technique works by approaching an oscillating tip to a surface. The z-piezo is used in a feedback loop to maintain a constant amplitude of the oscillation of the tip as the tip interacts with the surface topography of the sample, thereby generating a 3-d map of the surface. It is also possible to monitor different mechanical compliances in the surface which cause changes in the phase of the oscillation when the tip encounters these regions.[44] Figure 1.24 shows how TM-AFM works. The phase image is obtained concurrently with the height image by determining the lag between the driving oscillator and the oscillating cantilever called the phase difference. Normally this phase difference is 90° but it will change with local surface mechanical properties such as a mixture of polymer and inorganic materials that have different mechanical responses.

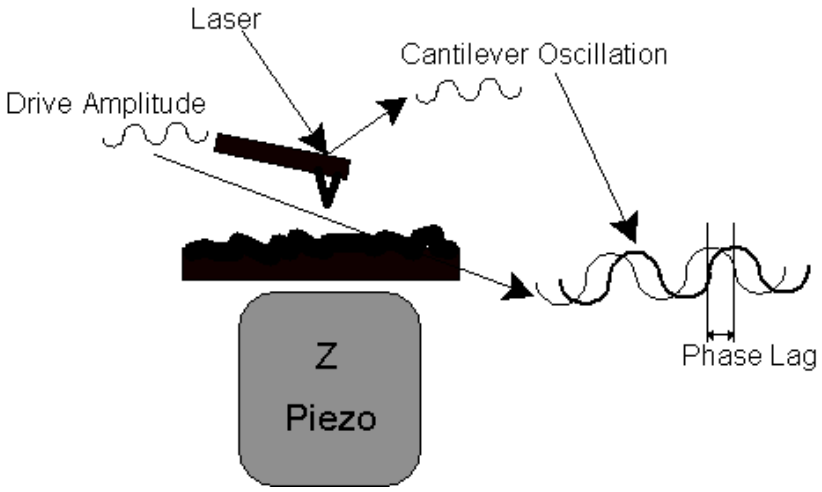

Figure 1.24: TM-AFM instrument set-up showing topographical data collected and phase difference between the driving oscillator and oscillating cantilever.

The set point ratio (R_{sp}) is important when acquiring images in tapping mode and is calculated by

$$R_{sp} = A_{sp} / A_f \qquad (1.2)$$

where A_{sp} is the set point amplitude and A_f is the free-oscillation amplitude. This controls the force applied to the surface by the tip. A ratio close to 1 means the tip is lightly tapping on the surface and as the ratio approaches zero the tapping forces increase. Figure 1.25 shows three images for a Nano Device's grid using light (a), medium (b), and hard (c) tapping R_{sp} values on 10 μm pitch lines that are 20 nm high. The grid is made entirely of one material so no phase changes due to mechanical compliance should be evident. However, the change in z at a grid line seen in the surface image (on the left) can show up as a phase change on the right image. Increasing the tapping force makes the phase image changes less apparent at step changes but with polymers care must be taken to not apply a tapping force great enough to distort the surface topography. When applying this technique to our polymer-SiO_2 hybrids a careful comparison between the topography and phase image must be done so as to not confuse step-induced phase changes with those originating in different constituents.

A)

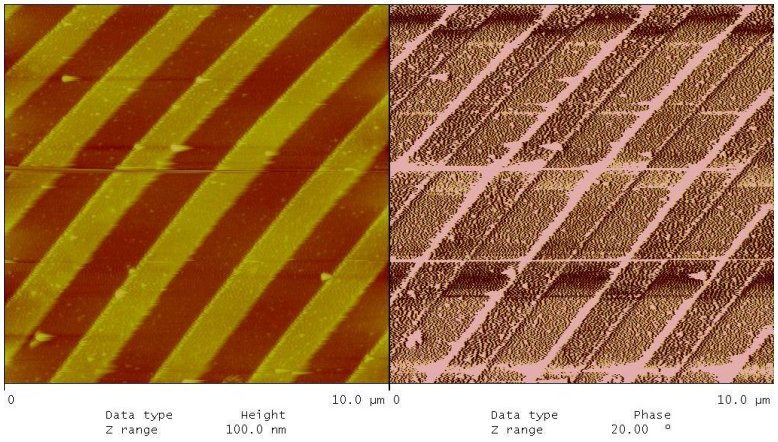

B)

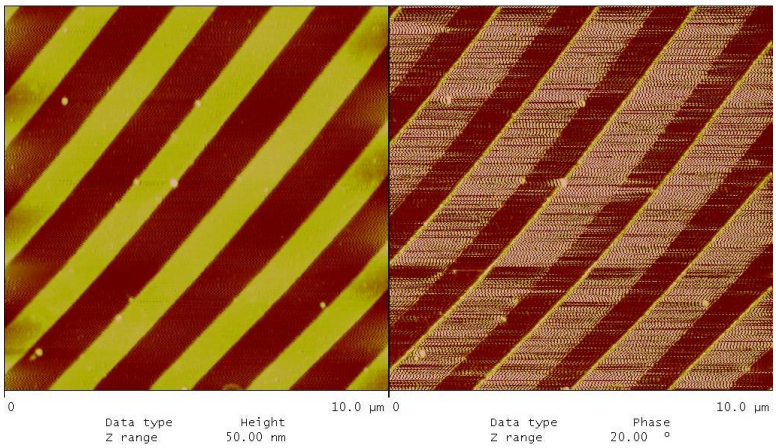

C)

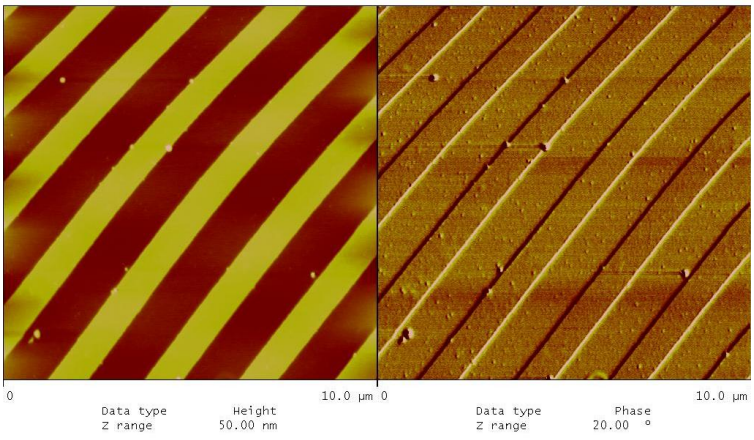

Figure 1.25: Example of typical images acquired in tapping mode. Topography is on the left and phase is on the right. A) light tapping, R_{sp}=0.88, B) medium tapping R_{sp}=0.60, C) hard tapping, R_{sp}=0.40

Dissertation Outline

This project started by obtaining polymers with different pendant groups to achieve a variety of possible interactions between the polymer and inorganic constituents, SiO_2, which is prepared from tetraethoxysilane. Only one ceramic precursor was used to help limit the scope of the project. A random copolymer and tri-block copolymer were also obtained that contained some of the same monomeric units as our polymers.

The properties of the polymers were evaluated as well as the hybrids prepared from them. The preparation and drying conditions for the hybrids and issues encountered are addressed in Chapters 2 and 3. The polymer-inorganic hybrid characterizations follow subsequently in Chapters 4, 5, 6, and 7. The mechanical properties and glass transition temperatures are discussed as to their fit with some literature models in Chapter 8. Finally, in the conclusion, a discussion of how each of the constituents interacted with SiO_2 to create an improved hybrid will follow.

Chapter 2
Polymer-Inorganic hybrid preparation

Introduction

The preparation of the polymer-inorganic hybrids we produced used a sol-gel chemistry process. The hybrids being prepared belong to class one, which relies on physically mixing the constituents. The main focus of this chapter is the constituent preparation and the methodology developed to create the hybrids. This class of hybrid materials provides a unique way to combine the properties of two dissimilar materials as mentioned in chapter 1.

The preparation methodology used for our hybrid preparation shows scalability and allows for the production of more than one hybrid at a time. This method will also apply to many other inorganic alkoxides with some minor adjustments for differences in hydrolysis/polycondensation kinetics (pH, temperature, time). The polymer component can be easily chosen from off the shelf or made in the laboratory and prepared for the inorganic constituent incorporation in the same manner outlined in this chapter. We chose a solvent system that is applicable to many polymers that have a solubility parameter near 9 $(cal/cm^3)^{1/2}$. The preparation of a wide variety of hybrids could come from this methodology and create a class of materials with some very unique uses. The characterization of the materials made for this study will allow for a better understanding of how the properties change due to the interactions between the inorganic and organic constituents and how the properties of the individual components are retained.

Polymer Characterization

The polymers were characterized as received from Aldrich using thermogravimetric analysis (TGA) and differential scanning calorimetry (DSC) to provide their background thermal history and dynamic mechanical analysis

(DMA) to provide their mechanical response. The TGA was employed to see the weight loss in polymers as a function of temperature and to see the pathway for the degradation using the derivative of the TGA curve. The DSC was employed to see the glass transition, melting and crystallization that may be inherent in the polymers. The DMA was employed to see their storage and loss modulus as temperature was changed and to determine the damping properties and glass transition temperature from the tan delta curve. The programs followed for these characterization runs are given in the appendix. The polymers used were poly (methyl methacrylate) (PMMA), polystyrene (PS), polystyrene-co-poly (methyl methacrylate) (PS-co-PMMA) (40 wt% Styrene) and polystyrene-block-polyisoprene-block-polystyrene (PS-PI-PS) (22 wt% Styrene). These polymers give a range of functional groups and arrangements of the monomers which are illustrated in Figure 2.1.

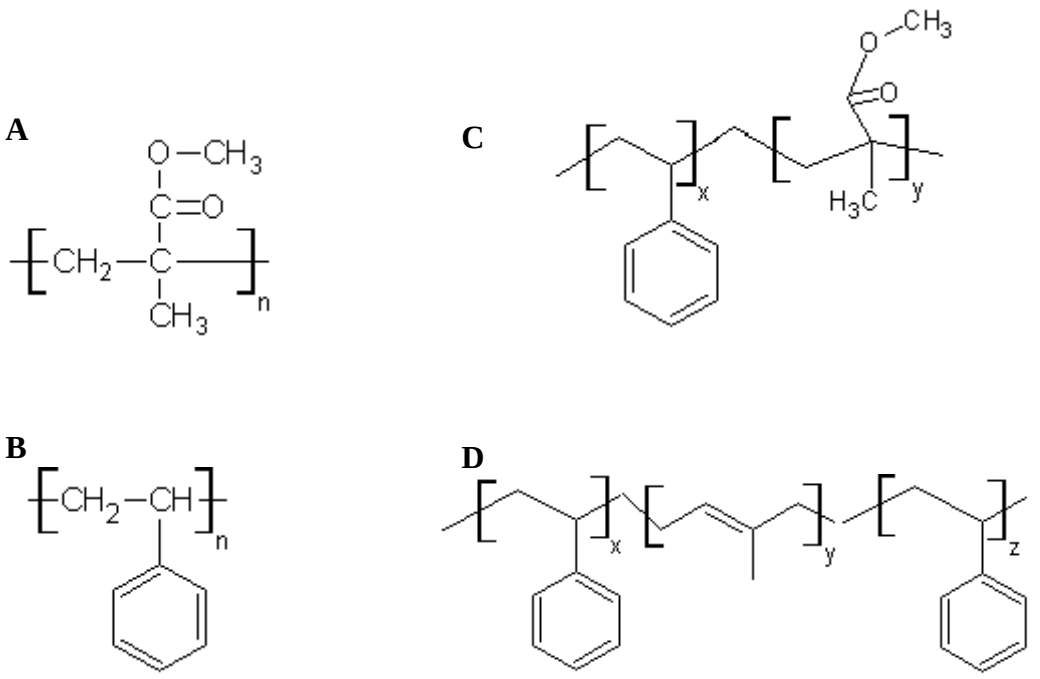

Figure 2.1: Structures of polymers used in hybrid preparation. A) PMMA B) PS C) PS-co-PMMA (monomers are arranged randomly) D) PS-PI-PS (monomers are arranged as blocks)

Thermal Properties of Polymers

The TGA traces are shown in Figure 2.2 for the polymers as received from Aldrich and were run in an air environment. From the traces the onset degradation temperature (taken as the initial downturn in each curve), the temperature at 50 weight percent loss, and the final degradation temperature (taken as the leveling of point of each curve) were determined. These values give the basic thermal behavior to compare with the cast polymers and hybrids.

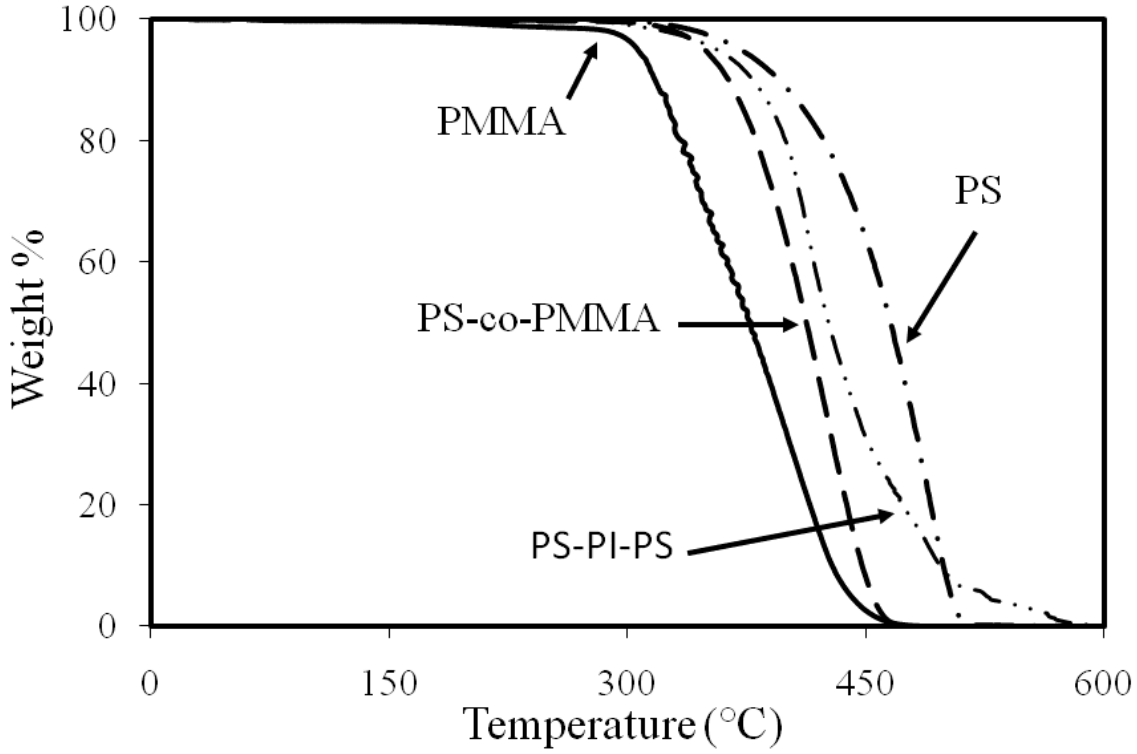

Figure 2.2: TGA traces for the polymers run in air as received from Aldrich.

The derivative curves shown for each TGA trace in Figure 2.3 were prepared by calculating the slope of the initial TGA data set at each point. The derivative plots give insight into the degradation pathway of the polymers and show how the weight loss changes over temperature ranges. By comparing the cast polymers and hybrids with the as received curves we can determine how the solvent and SiO_2 interact with the chain degradation pathway.

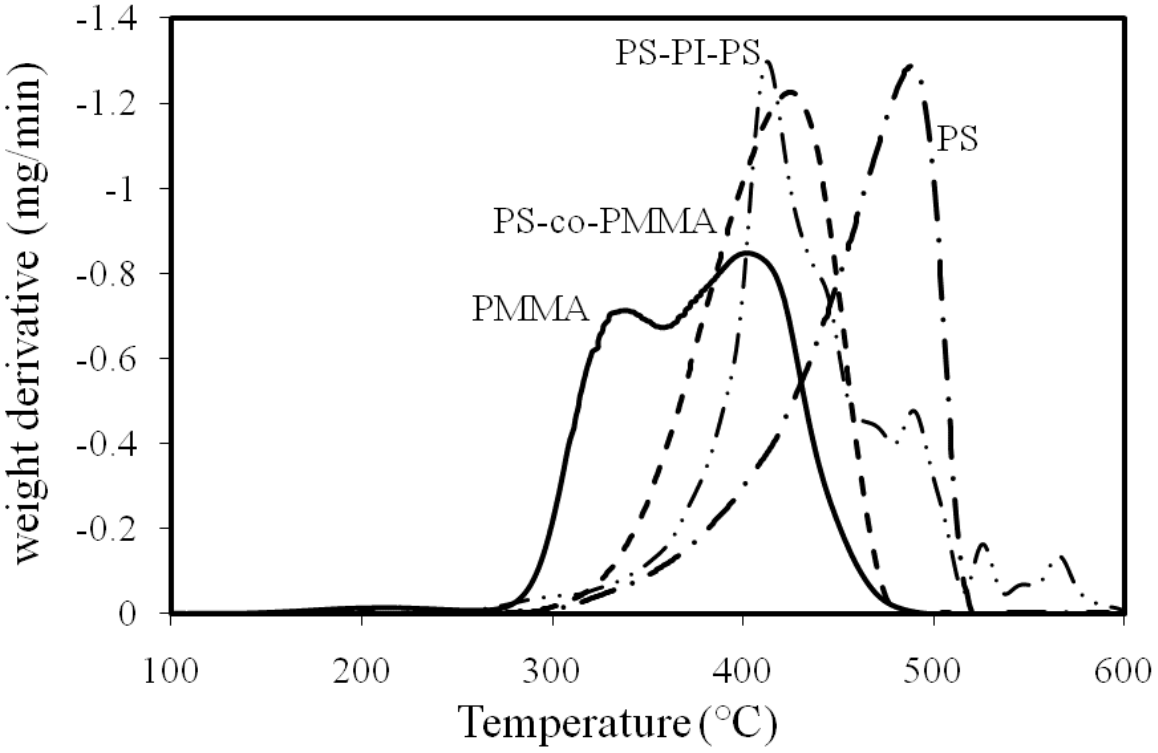

Figure 2.3: Derivative plots of TGA traces for as received from Aldrich polymers.

The polymers were also run on DSC in a nitrogen environment and their traces are shown in Figure 2.4. DSC provides information on thermal changes that do not result in a weight change of the sample. Information on the glass transition temperature, crystallization and melting characteristics of the polymers were determined. The glass transition temperature was taken as the midpoint of the baseline shift.

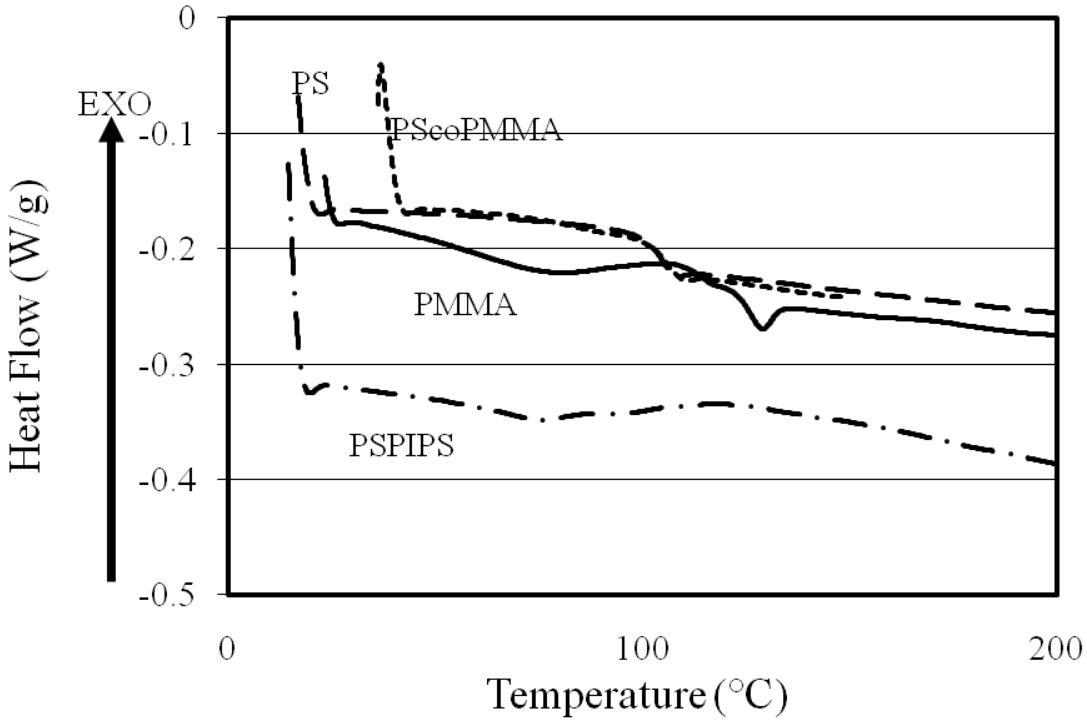

Figure 2.4: DSC traces for as received polymers from Aldrich.

All of the polymers obtained from Aldrich show a clear T_g in the temperature range used for the DSC runs except for the block copolymer. The block copolymer, PS-b-PI-b-PS, should show two glass transition temperatures. One is indicative of the polyisoprene block that occurs at much colder temperatures than those used in this study and a second for polystyrene block, which should appear in the temperature range run. None of the polymers show a melting or crystallization peak that would indicate they are semi-crystalline, leading us to conclude the polymers used are atactic. The PMMA DSC trace does show an endothermic peak at ~120 °C superimposed on the T_g (which occurs between 100-120 °C) due to the stress relief of the polymer chain. The polymers were all stable in air up to about 300 °C when the onset of decomposition was seen. Polystyrene was seen to start decomposition at a higher temperature than the others. The PS-co-PMMA showed a TGA curve that was between the two monomeric polymers PMMA and PS. All of the values reported from Aldrich and the properties we measured for our polymers are listed in Table 2.1.

Table 2.1: Tabulated data for as received polymers measured and reported from Aldrich. Columns with * were measured.

Sample	MW	T_d* (°C)	T_{50}* (°C)	T_f* (°C)	T_g (°C)	T_g*(°C)
PMMA	350000	294	355	474	122	120
PS	140000	343	465	516	104	104
PS-co-PMMA	100000-150000	333	412	474	94	104
PS-PI-PS	Not Given	333	426	583	---	---

Mechanical Properties

To determine DMA running conditions a PMMA calibration sample was obtained from Perkin Elmer and run. The sample dimensions are 50mm x 8mm x 0.2mm, which are comparable to the dimensions of our prepared samples. The molecular weight of the Perkin Elmer sample determined from GPC (630,000), the trace is shown in Figure 2.5, is higher than the PMMA used in our experiment as seen from the shorter retention time. This will cause the DMA curve to shift to higher temperatures so this calibration sample will not be comparable to any of our samples. It is also extruded which means there is no residual solvent to interfere with short or long range molecular motions. A DMA trace for this sample run at 0.5, 1.0, 2.0, 5.0 and 10.0 Hertz is shown in Figure 2.6. The modulus (E') value near room temperature is comparable to the Young's modulus acquired through tensile tests. The tan δ curve is the ratio between E" and E' and the peak is taken as the glass transition temperature. For the PMMA calibration sample the plateau at low temperatures is the glassy region and at high temperatures is the rubbery region. The noise seen at the end of the DMA trace is due to the instrument reaching the end of its movement range and/or the failure of the polymer. The running conditions for our samples are given in the Appendix. All of the polymers that are glassy at room temperature (PMMA, PS, and PS-co-PMMA) followed the conditions used for the Perkin Elmer sample while the block copolymer had a few minor changes noted in its program due to its extreme flexibility from the polyisoprene block.

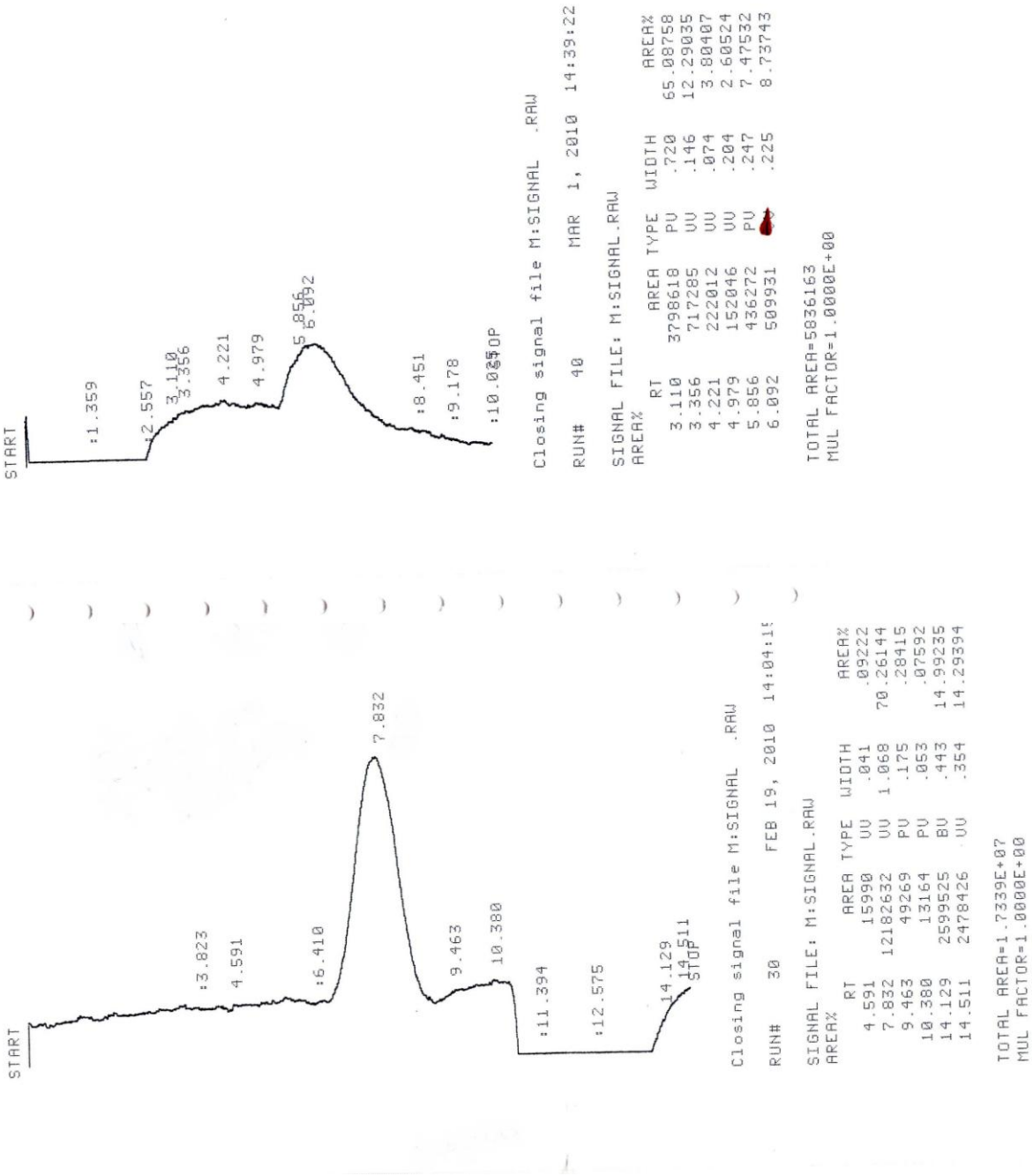

Figure 2.5: GPC trace for Perkin Elmer standard DMA sample. The Perkin Elmer standard is shown on the top and the PMMA used from Aldrich is shown on the bottom.

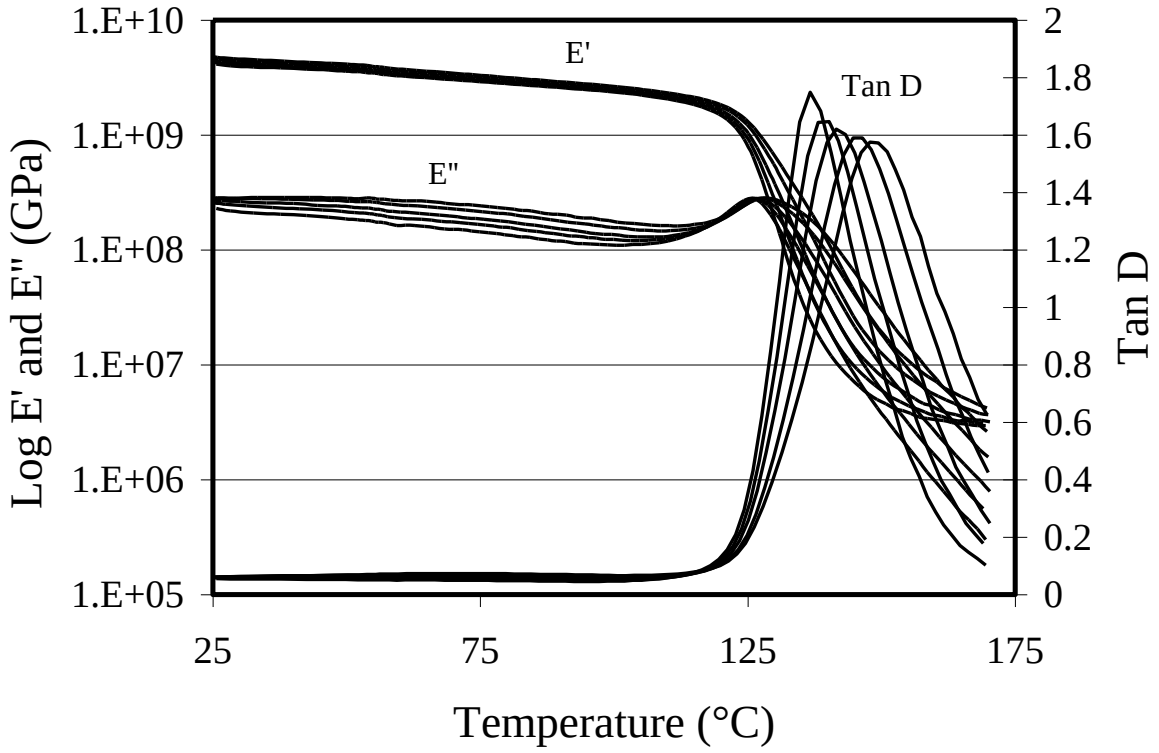

Figure 2.6: DMA traces for Perkin Elmer PMMA sample. Run at 0.5, 1.0, 2.0, 5.0 and 10.0 Hz The curves shift to slightly higher values with increasing frequency.

Methodology

The polymer-inorganic hybrids were all prepared using a sol-gel process, in which the polymers were fully dissolved before a pre-hydrolyzed tetraethoxysilane (TEOS) precursor solution was added. The resultant mixture was stirred and then cast in an aluminum weigh dish. Hybrids with different weight percents of SiO_2 were obtained through this method by varying the amount of pre-hydrolyzed TEOS precursor solution added. The polymers and TEOS were obtained from Aldrich and used as received. Tetrahydrofuran (THF) was obtained from Omnisolv and chloroform ($CHCl_3$) from Fischer. A 50/50 w/w mixture of tetrahydrofuran and chloroform was used due to their applicability to many polymers and compatibility with the typical inorganic alkoxides used to create the inorganic component. [45]

Solvent Cast Polymers

The sol-gel process involved in creating our polymer-inorganic hybrids has mild reaction conditions that will not degrade the polymer chain when incorporating an inorganic moiety but allows for solvent and hydrolysis products to become trapped. These trapped molecules could be detrimental to the hybrids thermal and mechanical properties. While studies on the effect of plasticizers on polymers are quite common, detailed investigations of the role of low volume fractions of small solvent molecules on polymers are rare. Studies on the effect of solvents on polymers[46-47] show a decrease in the mechanical properties causing a decrease in the glassy plateau and a shift in the glass transition temperature to a lower value. [48-50]

There are several models available that can potentially be used to predict the modulus of a plasticized film, but all have limited applicability. Simon and Ploehn[49] used a tube junction model to calculate the modulus of diglycidyl ether of bisphenyl epoxy cured with triethylene tetramine. Unfortunately, the general utility of this model is low because it involves many variables whose values need to be calculated or estimated for the particular system being studied. Zhang et al[48] investigated the disruption of H-bonding in nylon when a solvent is introduced to the system. This approach, however, is specific to polymers that have side groups capable of hydrogen bonding as efficiently as nylon. Flory-Rehner theory[51] describes how to calculate the modulus of a polymer that is swollen to equilibrium with a solvent by determining the number of crosslinks in the polymer network. This relies on having a crosslinked polymer and enough solvent remaining in the system to cause swelling.

Wong[46] shows how to predict the modulus value of a polymer-inorganic hybrid made by solvent free mixing of the components using various theories, but these models do not account for the effects of any residual solvent. Incorporating the solvent as a third component into these methods is not possible as solvent molecules possess no sensible modulus value. In order to quantitatively account for the effect of residual solvent on the modulus and other viscoelastic properties

of a hybrid material, it is necessary first to discover the effects of the retained solvent on a simple cast polymer sample.

Here we have studied the thermal and mechanical properties of several cast samples of poly (methyl methacrylate) (PMMA) which were dried for various times in an air furnace or vacuum furnace and also prepared containing ethanol to simulate hydrolysis byproduct retention. PMMA was chosen due to the studies of plasticizer effects on PMMA already done. Bistac and Schultz[47] studied the effect of unquantified residual amounts of several solvents, THF, $CHCl_3$, acetone and toluene, on the loss factor (tan D) of PMMA films. The results showed that the alpha peak seen in a tan delta trace always decreased and the beta peak decreased for chloroform but increased for all the other solvents. Scott et al[52] studied the effect of large amounts (30 weight percent) of diethylhexylphthalate and imidazolium ionic liquids on the storage and loss modulus on cast PMMA samples.

Heating Conditions

The atactic PMMA was first run as received from Aldrich to determine the heating environments effects on the stability of the PMMA chain with no added solvents. The TGA and DSC traces are shown in Figures 2.7 and 2.8 for PMMA heated for 3 hours at 120 °C. The TGA trace shows no deviations from the PMMA that was run with no heat treatment (solid black line). The oven furnace or vacuum furnace caused no chain degradation that affected the PMMA's decomposition. The DSC trace shows a glass transition temperature for both heating environments that coincide with the non-heat treated sample.

There are no new thermal effects that appear showing that our heating method does not cause the PMMA chain to reorder or degrade, we moved on to preparing and drying solvent cast PMMA samples in both heating environments. For other atactic PMMA systems reported grass transition temperatures varied. A value of 108 °C was reported by Bistac and Schultz[47] for a sample with a molecular weight of 120 kg/mol measured by dielectric spectroscopy. Ute et al[53] reported 123 °C for lower molecular weight material while Scott et al[52] gave a

value of 120 °C for an unspecified PMMA both determined by differential scanning calorimetry. The glass transition temperature of bulk PMMA varies with molecular weight, tacticity, and the measurement method employed. The T_g determined for the PMMA as received from Aldrich sample was 120 °C by DSC which is in the range of the other studies for atactic PMMA.

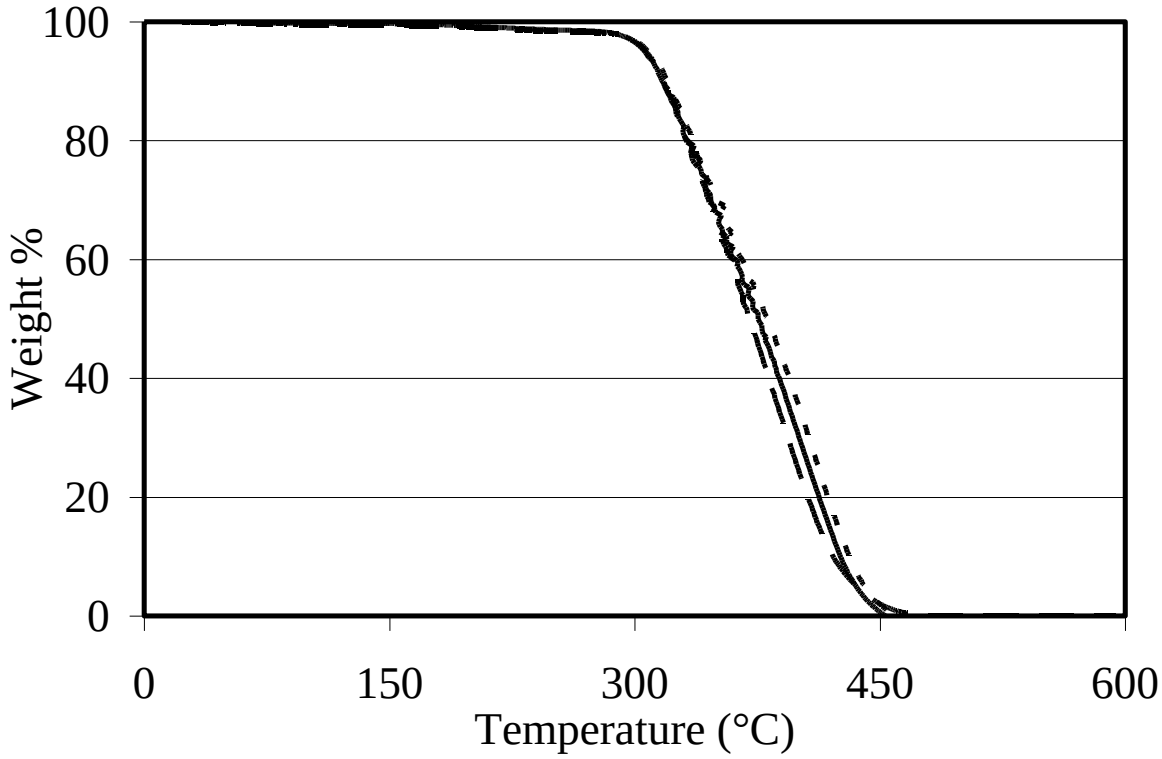

Figure 2.7: TGA trace for PMMA as received from Aldrich heated in a vacuum and oven.

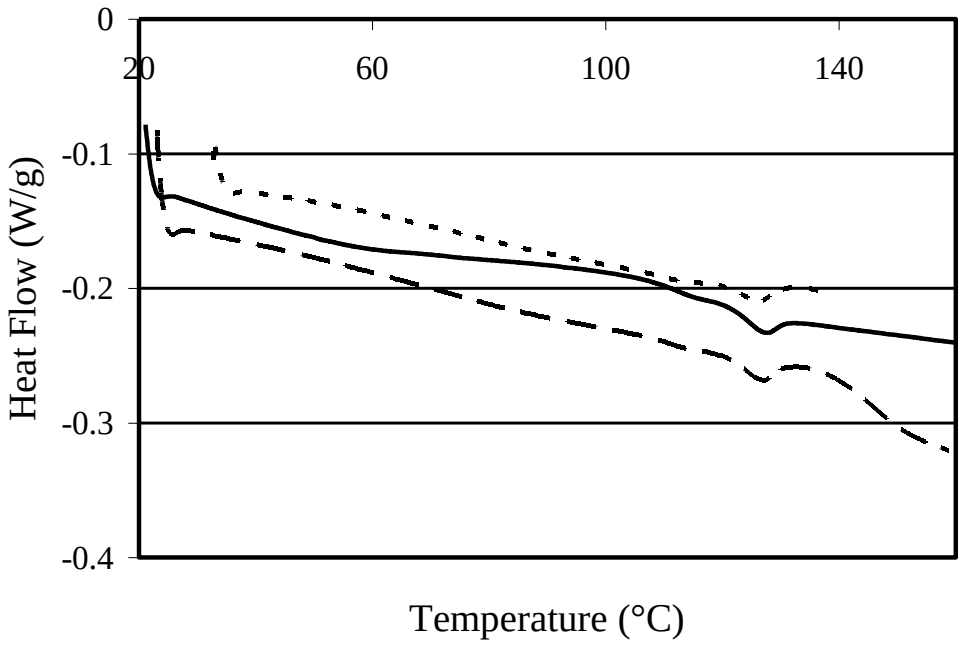

Figure 2.8: DSC trace for PMMA as received from Aldrich heated in a vacuum and oven.

Solvent Cast PMMA

PMMA solvent cast samples were prepared by dissolving 1.0g of PMMA in 5.0g each of THF and $CHCl_3$. The mixture was stirred at room temperature until the polymer had fully dissolved, replacing solvent as necessary due to evaporation. After full dissolution of the PMMA excess solvent was allowed to evaporate while continuing stirring to create a thick solution. The resultant solution was poured into an aluminum weighing dish, covered, and allowed to solidify at room temperature. This step could take 1-3 days depending on the amount of residual solvent and ambient temperature.

Additional films were made as above with 0.34 mL ethanol and 0.30 mL water to account for excess water and ethanol produced in a typical hydrolysis reaction of TEOS. This assumes a 4:1 ratio of water to inorganic.

A set of samples prepared above were placed in both ovens starting at 120 °C, the glass transition temperature of PMMA. This produced bubbling in the samples and rendered them unusable for future characterization tests. The next

samples were placed in both ovens closer to the boiling point temperatures of the solvent at 65 °C (66 °C for THF and 63 °C for $CHCl_3$). This produced fewer bubbles and left sections of the sample intact for our other characterizations.

Looking to improve the overall sample quality, another step was added to the drying test. Following literature[53] procedures, samples were left covered upon initial introduction into the oven to help control the rate of solvent evolution that leads to bubble formation. It was found that after heating the samples covered for 3 hours, removal of the cover did not adversely affect the films as the solvent content had already decreased by up to 5 weight percent. The vacuum was seen to remove about the same amount of solvent as the air oven for same time periods as seen in Figure 2.9 but the samples always showed some surface defect that affected the mechanical integrity of the sample. Figure 2.10 shows the mechanical response of the oven dried versus vacuum dried solvent cast PMMA samples. The DSC trace shown in Figure 2.11 shows that for both heating environments the glass transition temperatures were depressed the same amount and probably rely more on the solvents retained than the drying conditions. For these reasons, the air oven was chosen for drying the samples.

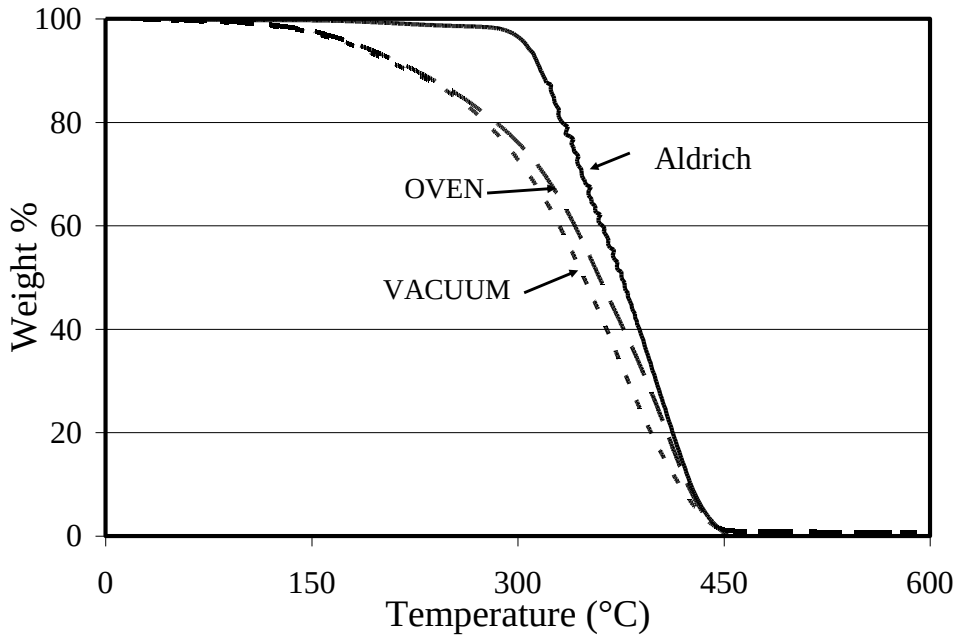

Figure 2.9: TGA traces of an oven and vacuum cured PMMA film covered for 3 hours in the heating environment.

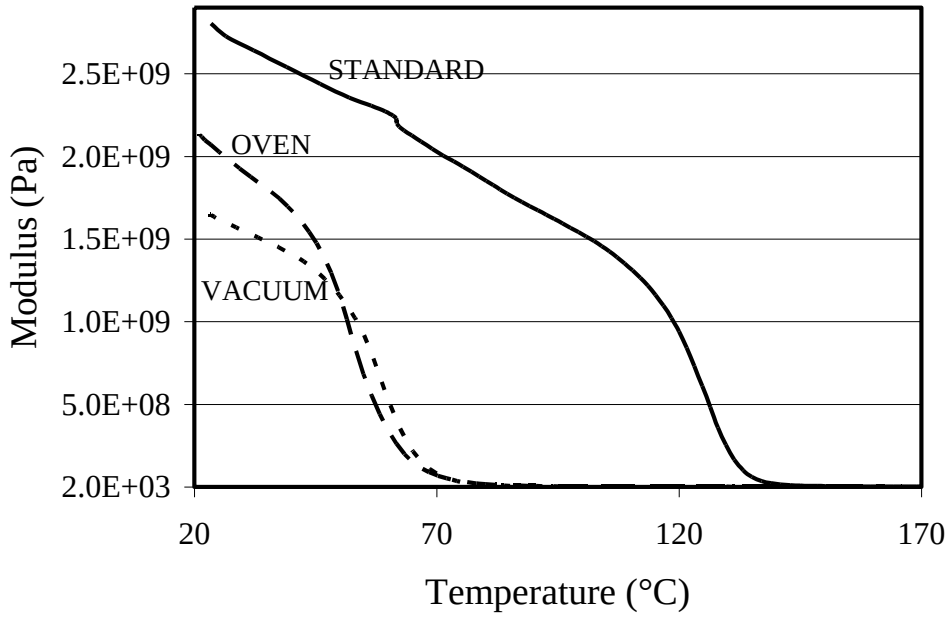

Figure 2.10: DMA traces for PMMA cast samples dried in oven or vacuum compared with Perkin Elmer standard covered for 3 hours in the heating environment.

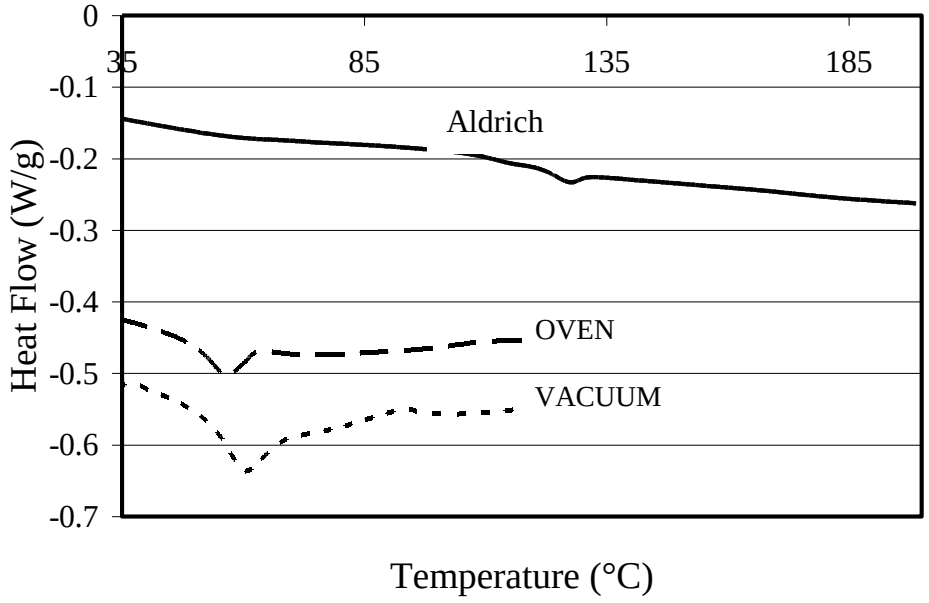

Figure 2.11: DSC traces showing shift in T_g due to curing environment covered for 3 hours in the heating environment.

A set of samples dried for 3 days at room temperature were then placed in an air oven at 65 °C and left to dry for times ranging from 3 to 180 hours. The first three hours of drying in the oven the samples were covered. Immediately following removal from the oven, 10 mm x 40 mm x ~0.3 mm samples were run on DMA with smaller pieces being run on TGA and DSC. The heights of the samples for DMA were measured using an optical scope and calibration grid.

DSC was run on the cast PMMA samples dried for 3 to 180 hours. Some of the curves do not show a clear T_g and the samples off-gassed in the system causing the pan lids to burst on some runs. Figure 2.12 illustrates a trace where the data is hard to interpret. Since the T_g can be obtained through other methods (DMA) and the polymers were determined to be amorphous, DSC was not run on all of our hybrids or cast polymer samples.

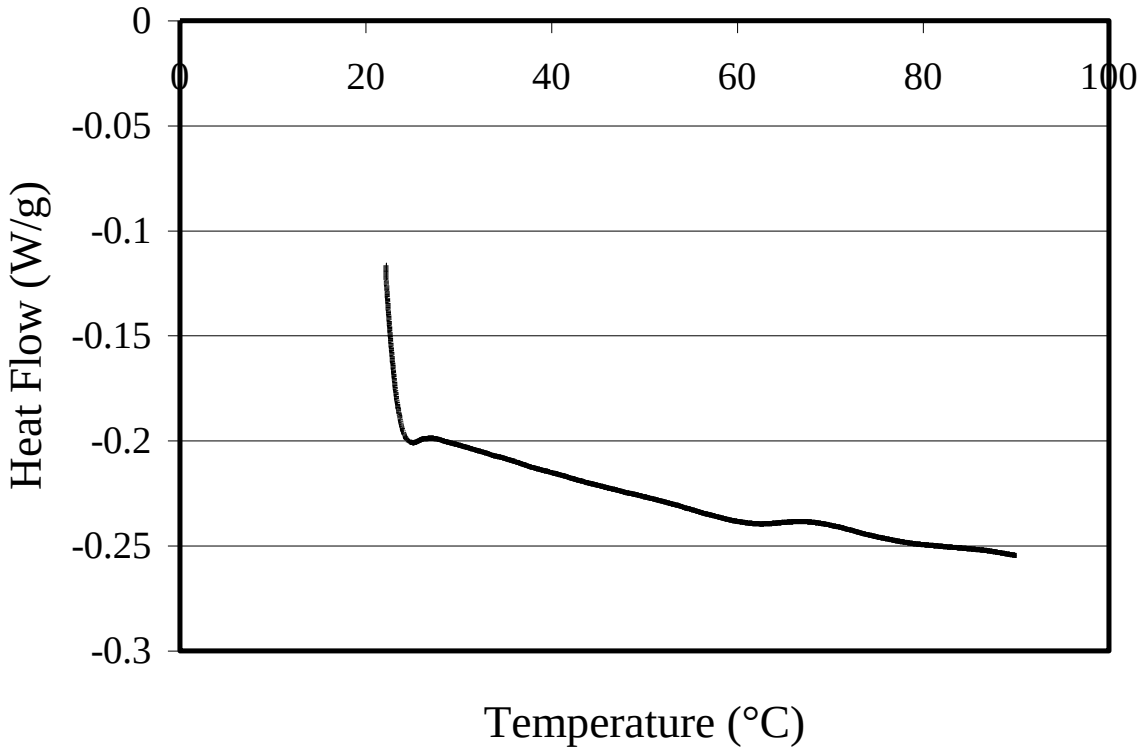

Figure 2.12: DSC of cast PMMA dried in an air oven. The glass transition point is not clearly defined.

A representative TGA curve is shown in Figure 2.13, in this case for a THF/$CHCl_3$ sample that had been cured at room temperature for 3 days. A slow drop in weight occurs before the onset of PMMA's decomposition, which presumably indicates the presence of retained solvent. A TGA trace of pure PMMA does not show this initial drop. In order to remove all of the residual solvent without decomposing the polymer (at about 250 °C), the TGA ramp was paused at 150 °C. The flatness of the curves after the isothermal halt indicates that the residual solvent had been removed by this treatment. The weight fraction (W1) of retained solvent in the sample is therefore given by the mass loss during the isothermal hold (marked as a in Figure 1) and the further mass loss (b) is simply the weight fraction of the polymer in the sample.

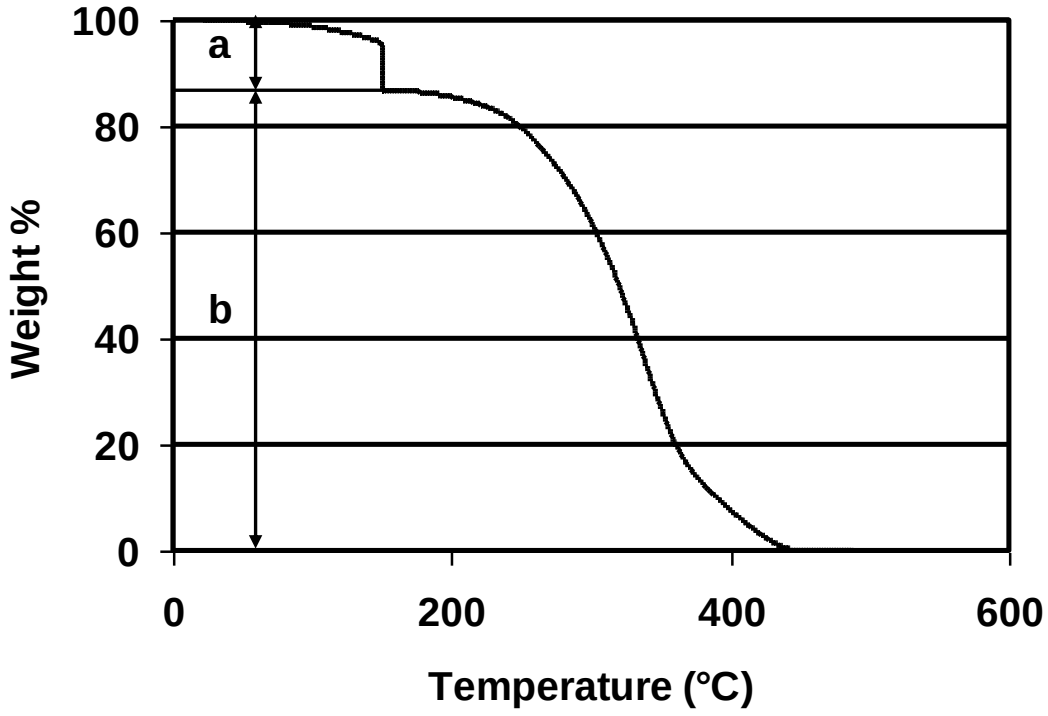

Figure 2.13: TGA trace of PMMA cast from THF/$CHCl_3$ dried at room temperature for three days. A) solvent weight percent B) polymer weight percent

The weight loss of solvent is shown in Figure 2.14 for our PMMA samples cured over 3 hours to 8 days at 60 °C following thickening at room temperature for 3 days. In order to completely remove all of the residual solvent without decomposing the polymer (at about 250 °) the TGA ramp was paused at 150 °C for 45 minutes. The drying times increase along the arrow in Figure 2.15. The samples dried for six days and eight days overlay each other on the TGA's and show that it is not apparently possible to remove all of the solvent. The sample dried for eight days appeared yellow so a drying time of six days is recommended.

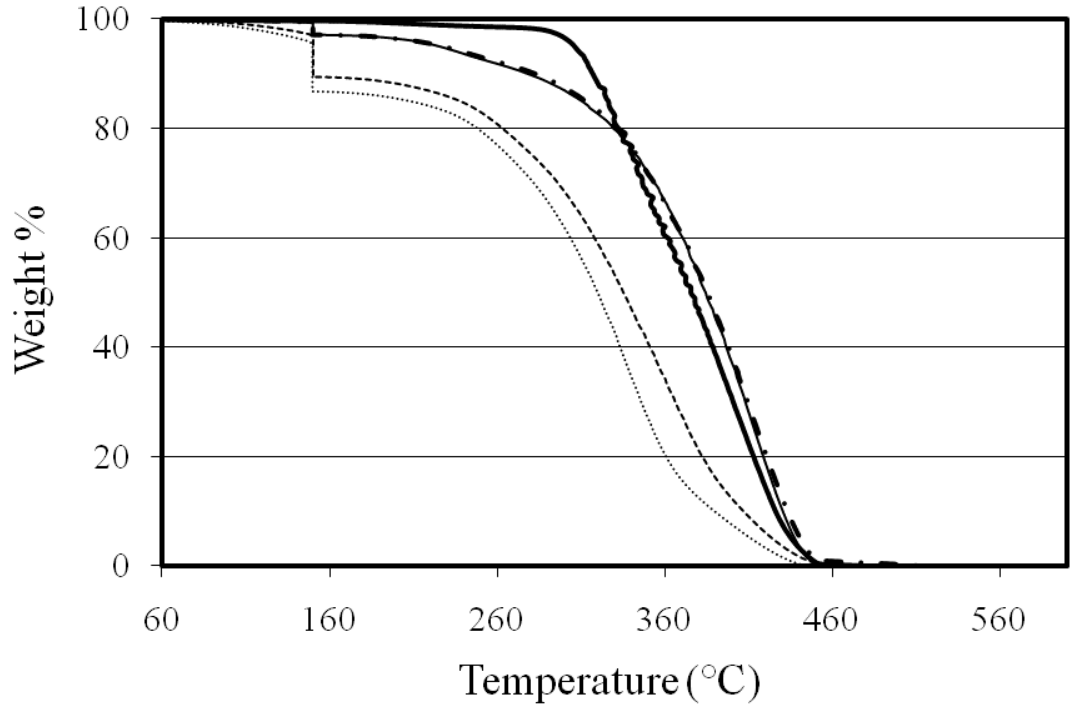

Figure 2.14: TGA traces for PMMA cast samples. The drying times were 3 days at room temperature (…), 4 hours (---), 6 days (thin solid), and 8 days (-·-·). Solid line represents PMMA run as received from Aldrich.

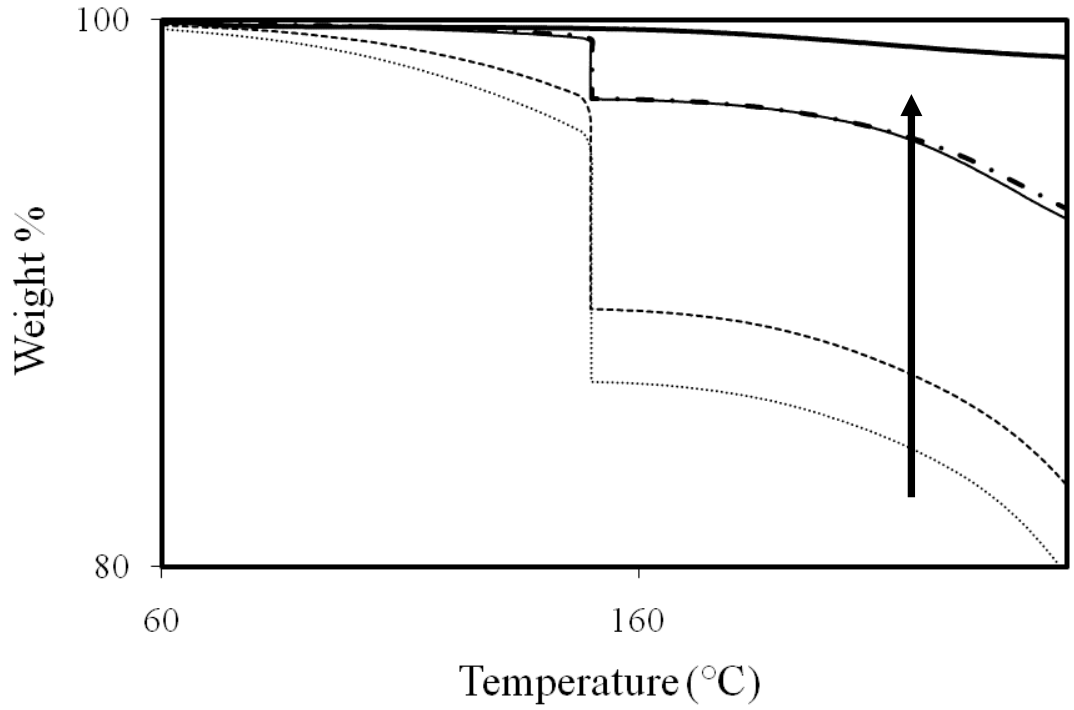

Figure 2.15: Blow up of TGA traces for PMMA cast samples. Increasing drying time follows arrow. Day 6 and Day 8 appear as the same line. The drying times were 3 days at room temperature (…), 4 hours (---), 6 days (thin solid), and 8 days (-·-·). Solid line represents PMMA run as received from Aldrich.

From the weight percents obtained from the TGA curves, the volume fraction of solvent in each sample can be found using the following relation:[46]

$$\nu_1 = \frac{W_1}{W_1 + (1 - W_1)\frac{\rho_f}{\rho_m}} \qquad (1)$$

Here ρ_f is the density of the solvent and ρ_m is the density of the polymer matrix. The average density of THF and $CHCl_3$ is very close to the density of PMMA effectively making $\nu_1 = W_1$. The corresponding volume fraction of PMMA can be taken as $\nu_2 = (1-\nu_1)$. The volume fraction is commonly used to express the relative amounts of molecules in a mixture when the molecules in question differ

greatly in size. Some assumptions are built into this calculation, one being that we have an ideal solution and no expansion or contraction occurs upon mixing.

The cast samples run on DMA shown in Figure 2.16 show how the retention of the solvents used in the sol-gel process affect the mechanical properties. The decrease in modulus at the glassy plateau drops by a factor of two or more over the range of volume fractions of solvents explored here. Figure 2.17 shows the corresponding tan δ curves which show the decrease experienced in the glass transition temperature clearly which follows the results reported from Bistac and Schultz. Values obtained from the TGA and DMA runs are given in Table 2.2.

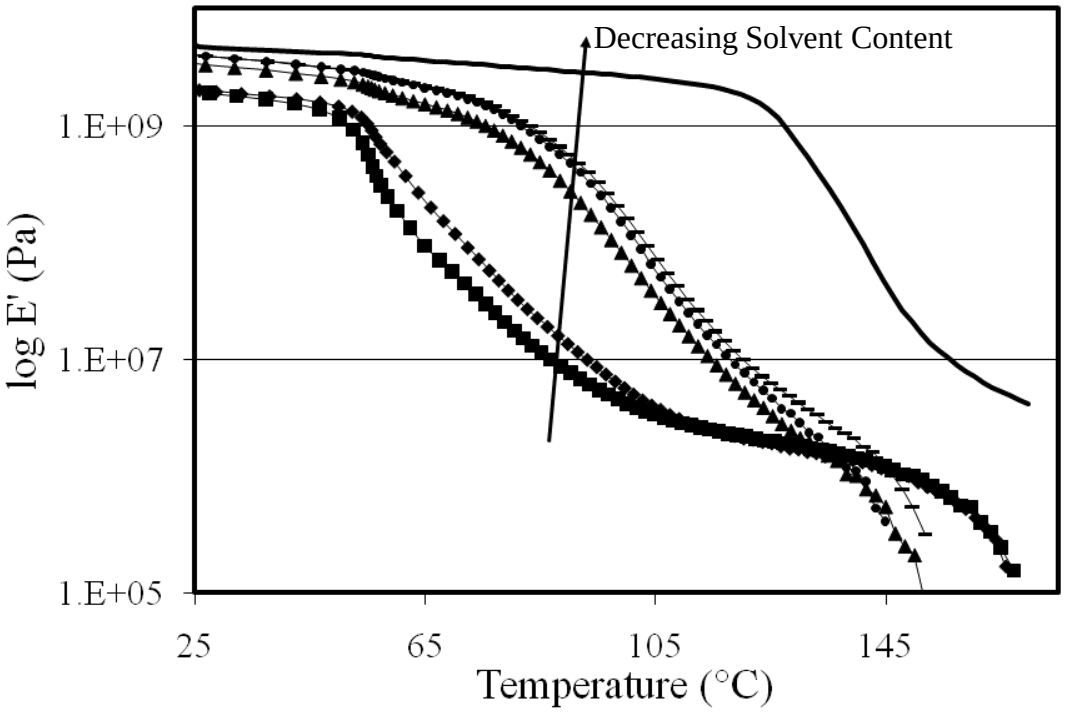

Figure 2.16: DMA curves for PMMA cast samples dried for varying times in an air oven. Increasing drying time along arrow. Samples are defined in Table 2.2.

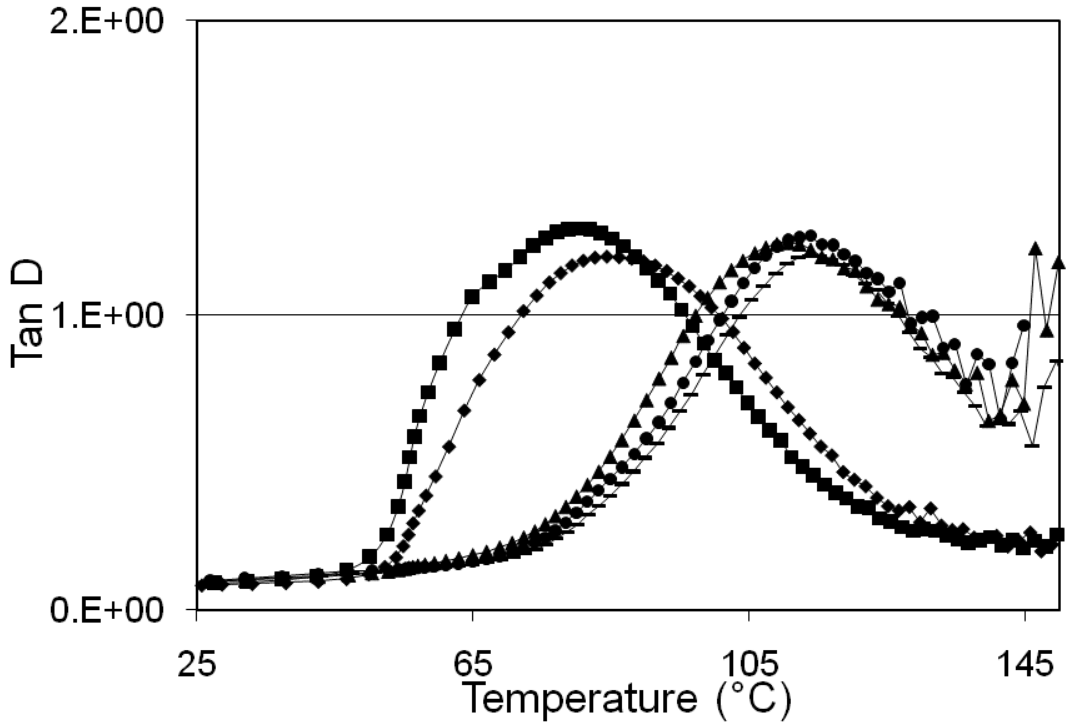

Figure 2.17: Corresponding tan D curves for the DMA data above. The T_g is taken as the peak of the curve. Samples are defined in Table 2.2.

Table 2.2: PMMA films solvent content and measured mechanical properties. Dried 3 days at room temperature and then placed in 65 °C oven for varying drying times.

Sample	Symbol	Drying time 65 °C	Weight Fraction	Solvent fraction	E' at 25 °C	T_g (°C)
3TC	■	0	14.3	0.14	1.98	80.43
4TC	♦	4	11.2	0.12	2.04	84.38
72TC	▲	72	4.4	0.044	3.41	98.25
144TC	●	144	4.1	0.041	4.08	110.67
192TC	▬	192	3.6	0.036	4.00	113.73
3ETC	◊	132	6.1	0.061	2.64	95.45
4ETC	○	156	4.5	0.045	2.77	99.40
Perkin		---	---	---	4.79	147.8

Solvent Content Modeling

Trying to determine how the amount of solvent affects the glass transition temperature led us to try and fit the data. Scott et al[52] found that 10 % volume of diethylhexylphthalate caused a similar drop of 40 °C in the T_g of a PMMA sample. Of more interest in the context of our work are the results of Bistac and Schultz[47] who measured changes in the T_g of PMMA containing residual amounts of both of the solvents used here but not in combination. They found that choloform produced a drop of 33 °C and tetrahydrofuran a drop of 26 °C. They attributed the larger effect of chloroform to strong acid-base interactions between the acidic solvent and basic sites of PMMA. These interactions limit the self-association of PMMA chains and allow the acrylate groups to move more freely, thereby dropping the T_g. They also argue that tetrahydrofuran is a basic solvent that interacts weakly with the PMMA chains and so does not affect the T_g as much as chloroform. Their results are difficult to compare directly with our own since their samples were of much lower molecular weight and were simply air dried for two days. They also did not quantify the amount of residual solvent remaining.

The changes in T_g, shown in Figure 2.18, seen without solvent mix showed an overall drop of 40 °C from the PMMA as received measurement (from DSC) and the PMMA cast sample containing 15 wt% solvent. Most models available rely on the additive having a glass transition value, such as the Fox[54] equation. Since neither of our solvents are a large enough molecule to have a glass transition, we relied upon a phenomenological fit. The data shows a reasonable linear fit through the solvent weight percents prepared here. Based on the amount of solvent retained in the hybrids we now have an idea of what the T_g value would be.

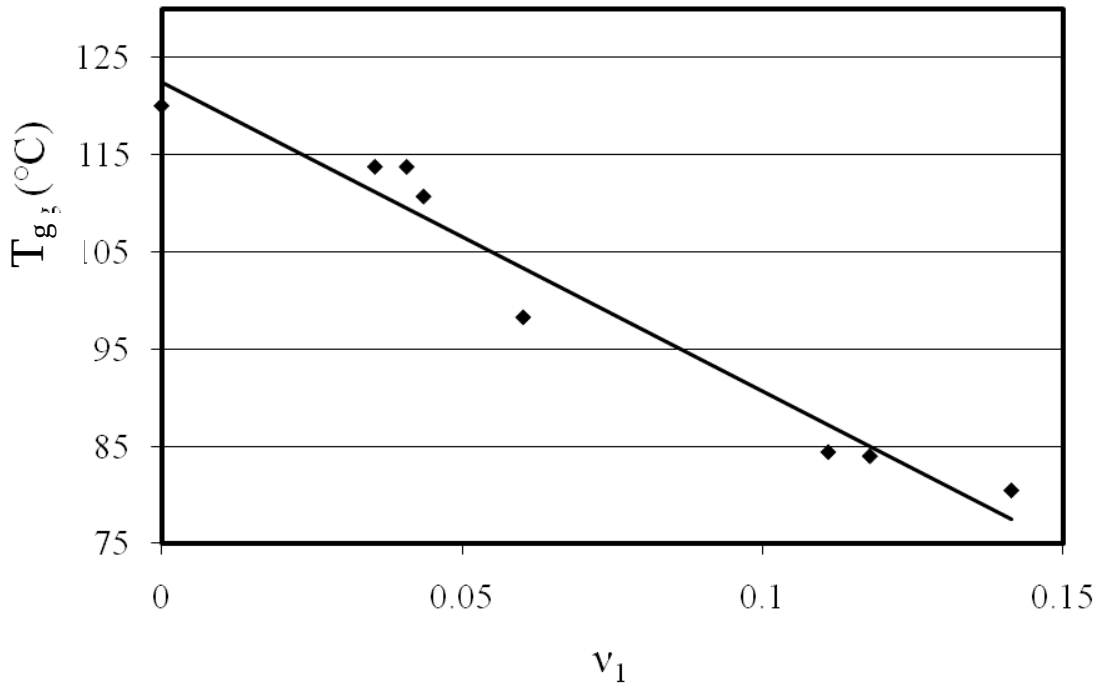

Figure 2.18: Change in T_g over the solvent volume fraction range for PMMA.

The changes in the modulus show the glassy plateau remaining of the same order of magnitude for all of the solvent volume fractions studied here but the values still drop by a factor of two. For the rubbery plateau, the modulus is seen to change by orders of magnitude between the solvent cast samples and the extruded Perkin Elmer standard. This large change could be due to defects left in the PMMA matrix as the solvent molecules leave or the lower molecular weight of our PMMA.

We looked at a number of models to determine the relationship between solvent content and modulus response. Most of these models are not ideal for our system. The rubber elasticity free volume model is based upon calculating the modulus from the derivative of the stress response when a strain is applied. This would work only if the polymer in question was rubbery and crosslinked. While our polymer goes through a rubbery plateau, the PMMA was not crosslinked. Work done by Takayanagi[55] gave a parallel and series models to provide an upper and lower bound for the modulus.[42, 56] In this model a value for the modulus of the

diluent is needed. Unlike a polymeric plasticizer, THF and $CHCl_3$ have no moduli. We also investigated straightforward phenomenological fits of the experimental data shown in Figure 2.19.

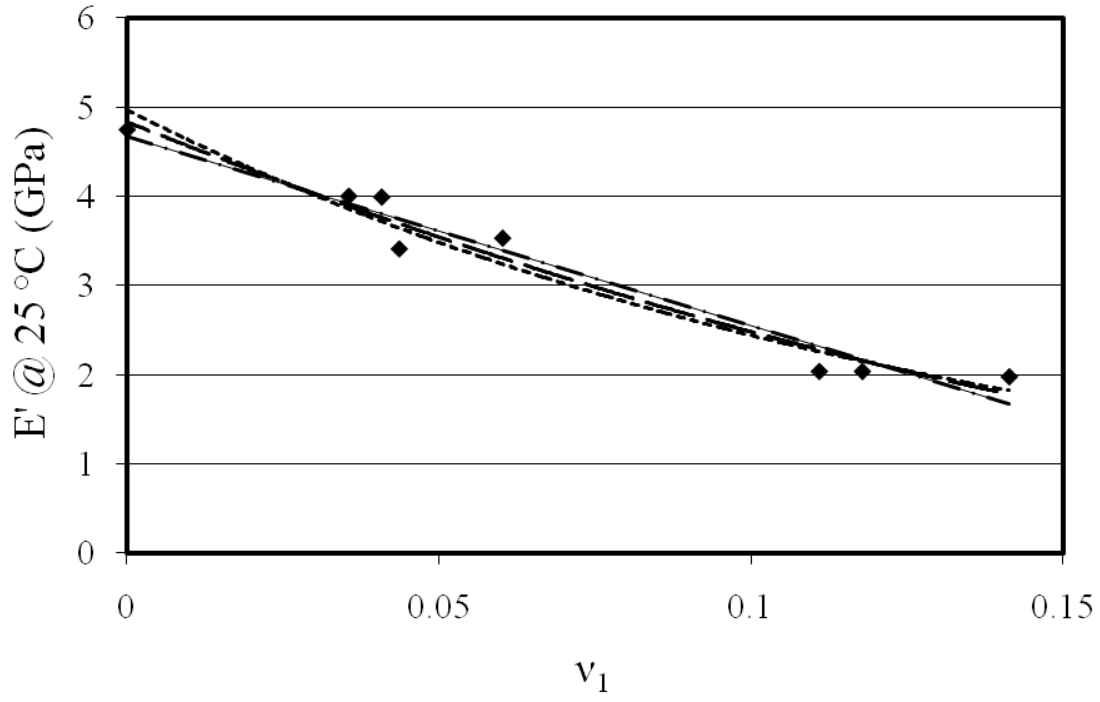

Figure 2.19: Glassy modulus for PMMA solvent cast samples. Perkin Elmer standard used for 0 solvent volume fraction. Linear (— ▪), Exponential (- -) or 2nd order polynomial (— —).

While a decrease in the modulus is apparent the change due to the solvent content does not follow an easily discernable pattern. All phenomenological fits applied (linear, exponention, 2nd order polynomial) produced results that were difficult to tell apart. Given the scatter in the data and the similar quality of the fits there is little reason to choose one over another. Using any of the fits a value of the glassy modulus could be determined for a hybrid based upon its solvent content.

For the THF/$CHCl_3$ samples, simply drying in air for 3 days leaves a fraction of about 0.15 solvent. The amount of solvent retained in the PMMA films drop quite sharply on heating at 65 °C and then starts to plateau at about 0.04 weight fraction after 72 hours drying in the oven. The PMMA films started to yellow on day 8 in the oven, so a drying time of less than 8 days is recommended.

Apparently it is not possible to remove all traces of solvent from the THF/$CHCl_3$ PMMA films.

The films prepared with a THF/$CHCl_3$/EtOH mixture showed a higher solvent weight fraction for comparable drying times as the THF/$CHCl_3$ films. The day 6 sample containing ethanol and day 3 sample containing only the solvent mixture showed similar weight percents retentions of unwanted molecules. This illustrated that longer drying times are necessary when ethanol is introduced into the system to achieve a correspondingly low solvent weight percent.

Figure 2.20 shows the DMA curves obtained for the ethanol (EtOH) prepared samples. A PMMA sample cast from THF/$CHCl_3$ with a comparable amount of solvent is also shown. For the ethanol cast films a steady increase in modulus is seen with decreasing solvent content, shown along the arrow in Figure 2.20. Compared to the THF/$CHCl_3$ cast film with 0.044 weight fraction the ethanol containing film with 0.045 weight fraction of THF/$CHCl_3$/EtOH shows a decreased transition region and a slightly lowered glassy modulus values. The glassy moduli for the ethanol containing samples are of the same order of magnitude as the THF/$CHCl_3$ samples, 10^9 Pa. The ethanol containing films required a greater drying time to achieve the same solvent weight fractions as the THF/$CHCl_3$ films. The rubbery plateaus drop off quickly around 140 °C. The moduli values for the ethanol containing films are reported in Table 2.2.

The tan delta curves are shown in Figure 2.21. The glass transition temperature was taken as the peak of the curve. As the solvent weight fraction decreases, the tan delta curves shift to higher temperatures for each solvent system.

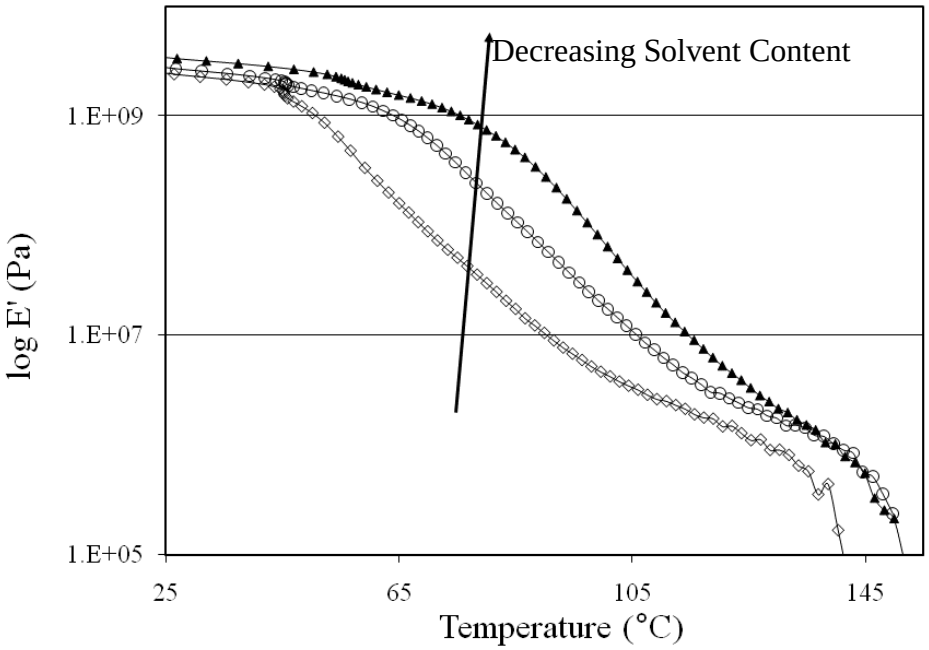

Figure 2.20: DMA traces for PMMA films with ethanol. Decreasing solvent content along arrow. The closed symbols were used for THF/$CHCl_3$ cast film (v_1= 0.044) and open symbols for THF/$CHCl_3$/EtOH cast films (◊ v_1=0.061, ○ v_1=0.045) .

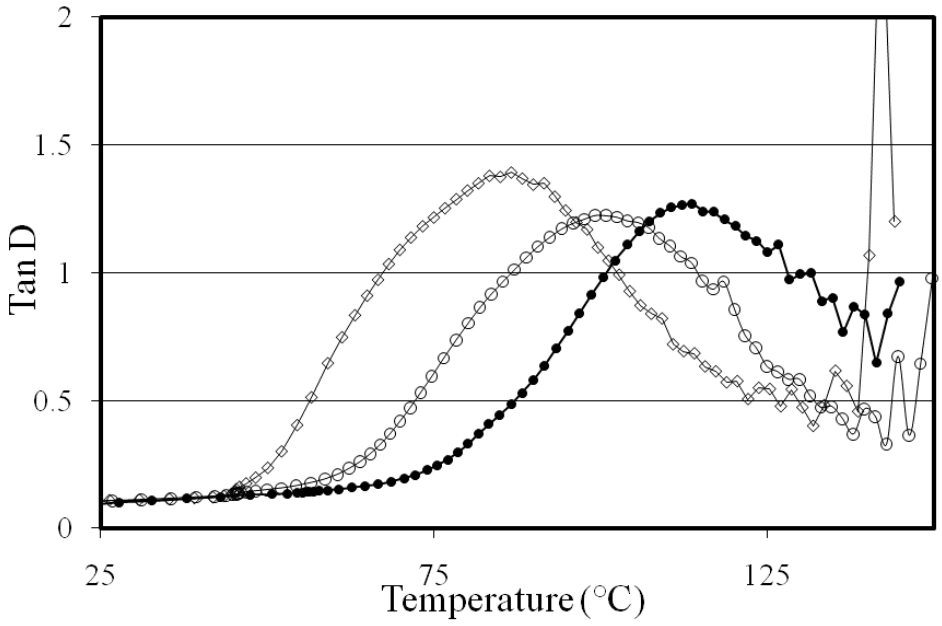

Figure 2.21: Tan delta traces for PMMA films. Tg is read as the peak of the curve. Values reported in Table 2.2.

The glass transition trends seen with the solvent content do not seem to depend on the solvent identity as much as the room temperature modulus does. Since the Tg is where long chain polymer motion is allowed, solvent molecules may escape easier. The T_g is also above the boiling points of the THF and $CHCl_3$ being retained.

The hydrolysis products produced in sol-gel film synthesis of polymer-inorganic hybrids cause a greater decrease in the mechanical properties than just the solvent system generally employed. The glass transition temperatures vary from each other over a range of 30 degrees. The glass transition temperatures changed due to solvent weight fraction and did not seem to depend on the solvent mix used. When predicting the properties of a polymer-inorganic hybrid, accounting for the solvent and hydrolysis products effects on the film become important. The added ethanol in the solvent mixture depressed the glassy modulus and transition region to lower values than comparable THF/$CHCl_3$ weight fraction films. The glass transition temperature of ethanol containing films showed relatively steady values for the 6.1-4.5 solvent weight percent films at around 99 °C. Ethanol is known to hydrogen bond with methyl methacrylate (MMA)[57] and has a higher boiling point, both of which may allow it to act as a better plasticizer for the PMMA film causing lowered mechanical properties.

Preparation of SiO_2 precursor

The SiO_2 needed as the inorganic componenet in our polymer-inorganic hybrids were prepared by pre-hydrolyzing TEOS under acidic conditions. The water to TEOS ratio, which was set at 4:1 (double the stoichiometric ratio), and the catalyst, chosen as HCl, were picked to help achieve a more linear SiO_2 product. A higher water to TEOS ratios or a basic catalyst would have caused the SiO_2 to form a more cluster like formation.[58] The overall reaction is shown below in Scheme 2.1. The hydrolysis and condensation steps are also included in the scheme.

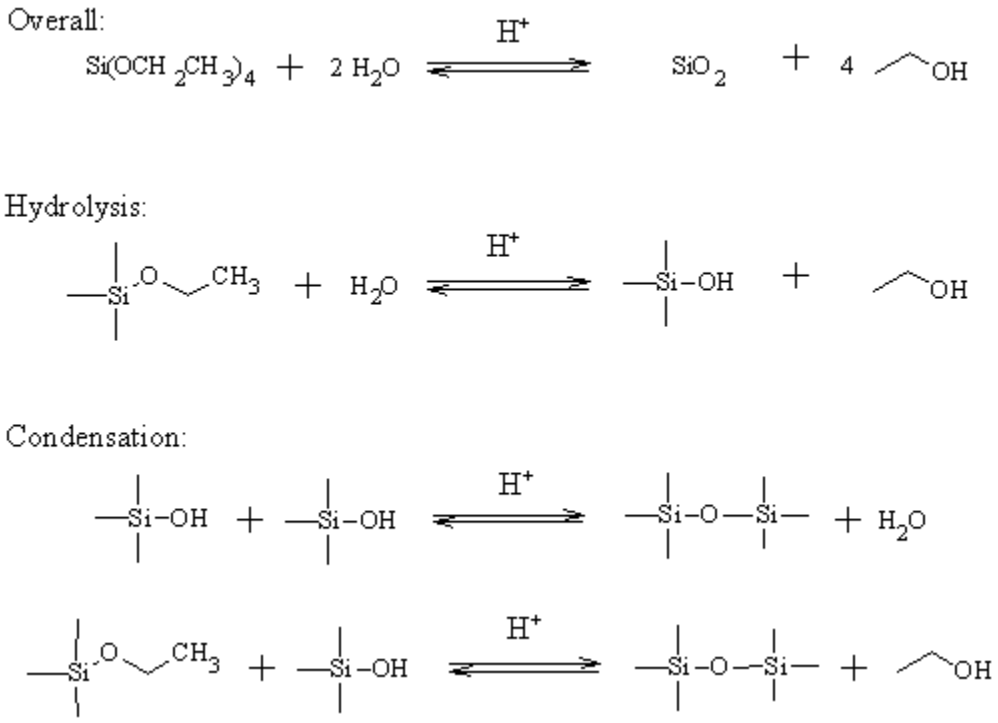

Scheme 2.1: Hydrolysis of TEOS by water and polycondensation reactions that produce SiO_2 and water and/or ethanol.

Procedures for TEOS and other similar inorganic alkoxides hydrolyses preparations varied in the literature and a few trials were performed to determine a preparation method that suited our hybrids. The hydrolysis of inorganic alkoxides will proceed more quickly with higher water amounts but, as mentioned above, a ratio greater than two times the stoichiometric amount of the reactants in the case of TEOS was found by Sakka to cause the hydrolysis under acidic conditions to proceed following the basic mechanism. Preparing the SiO_2 from TEOS being hydrolyzed in-situ in the polymer solution was attempted but led to much lower amounts of SiO_2 than calculated from the balanced reaction. This was attributed to the presence of the polymer and solvent molecules not allowing the reactants to find each other. The next attempt involved preparing the SiO_2 by pre-hydrolyzing the TEOS and then adding to the dissolved polymer solution.

We started by hydrolyzing the TEOS to achieve a specific weight percent of SiO_2 in a 1.0 g sample of polymer. The TEOS to SiO_2 ratio was taken as 1:1 as

seen in the balanced reaction. The amounts of TEOS and 0.01M HCl used to achieve 5-25 weight percent SiO_2 are given in Table 2.3. A trial run of TEOS hydrolysis showed that reaction times greater than one hour could lead to the precursor solution starting to gel and make incorporation into the polymer solution difficult. The TEOS and water were measured out at room temperature and stirred for one hour before addition to the polymer solution. As suggested in the literature, a filter was employed when adding the inorganic precursor solution to help eliminate formation of any large inorganic oxide particles that may have formed during the pre-hydrolysis.[45] A 0.2 micron filter was used to add the pre-hydrolyzed TEOS precursor solution to the dissolved polymer.

Table 2.3: Amounts of TEOS and 0.01M HCl measured to produce SiO_2 for a given weight percent. 1.0g of polymer assumed.

Theory SiO_2 wt %	SiO_2 needed (mol)	TEOS (mL)	0.01M HCl (mL)
5	8.32E-4	0.1858	0.05998
10	1.66E-3	0.3716	0.1199
15	2.49E-3	0.5574	0.1799
20	3.32E-3	0.7433	0.2399
25	4.16E-3	0.9291	0.2999

A ratio of 1:1 SiO_2: TEOS and 4:1 H_2O: TEOS was used in the calculations. The 0.01M HCl was added as the water amount.

The product obtained from the pre-hydrolyzed TEOS reaction was characterized by X-ray diffraction and FTIR to ensure that SiO_2 was formed. The XRD trace is shown in Figure 2.22 and the FTIR in Figure 2.23. The XRD peaks present were matched with software on the instrument to the formation of quartz. The FTIR spectra showed peaks centered on 1100 cm^{-1} that arise from the Si-O-Si stretch. The appearance of peaks indicative of ethanol can be seen in the red line at 3400 cm^{-1} and 2900 cm^{-1}.

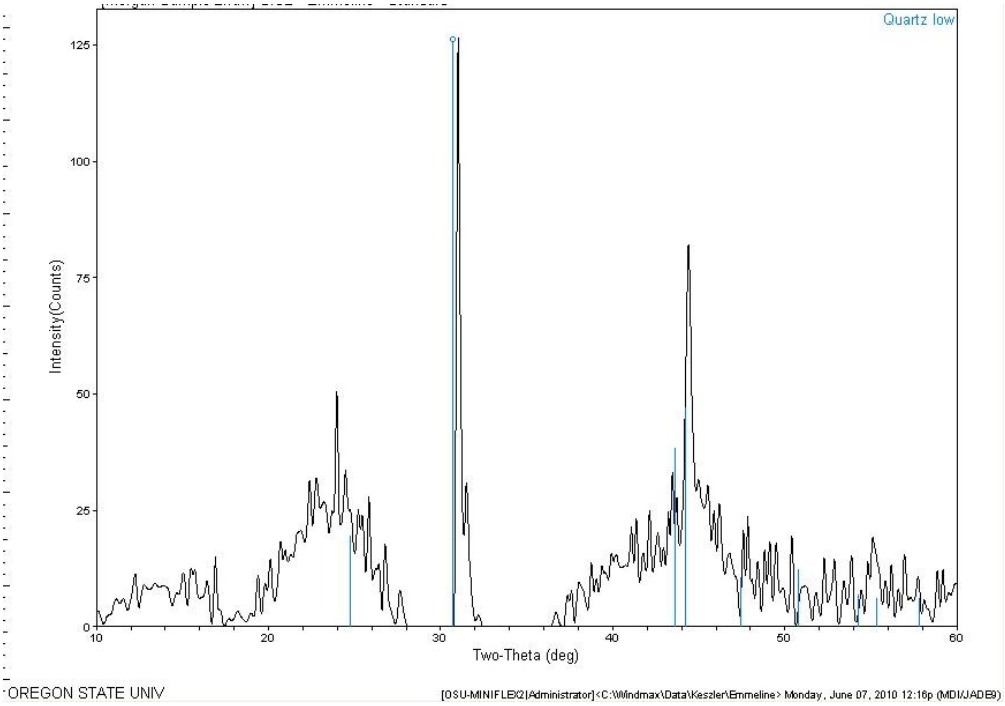

Figure 2.22: XRD trace of SiO_2 prepared from the hydrolysis/polycondensation of TEOS under acidic conditions.

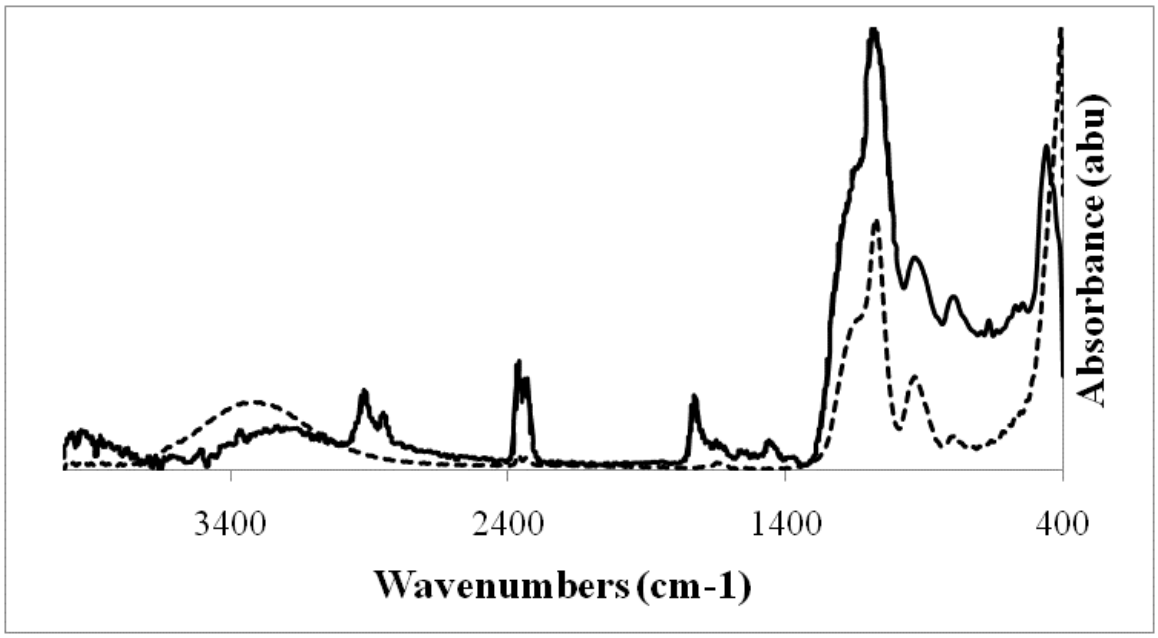

Figure 2.23: FTIR spectra of the hydrolysis of TEOS. Dashed line shows TEOS hydrolysis at 1 hour (still liquid). Solid line shows TEOS after forming a solid.

This process of preparing the precursor solution for each individual hybrid allowed for easy calculation of reagent amounts and addition to the polymer. The difference in the physical amounts of the reagents in the reaction flask led to

differences in the completion of the hydrolysis after addition to the polymer which affected the amount of SiO_2 produced. To help control the SiO_2 amount and allow for the preparation of more than one hybrid at a time a batch hydrolysis of TEOS was devised.

In order to prepare hybrids with 5, 10, 15, 20, and 25 weight percent SiO_2 15.0mL of TEOS was hydrolyzed. The TEOS was stirred with 4.85 mL of 0.01M HCl for 60 minutes. To determine the amount of SiO_2 produced, the solution was then passed through a 0.2 micron filter and into an alumina weigh dish. This was allowed to dry and weighed. The ratio of SiO_2 to TEOS was determined to be 1:2. From this the amount of precursor solution was determined to achieve varying theoretical SiO_2 weight percents. These values are given in Table 2.4.

Table 2.4: Batch hydrolyzed/condensed TEOS precursor solution prepared from 15.0mL of TEOS with 4.84mL of H_2O. Amount of precursor needed to prepare hybrids with given SiO_2 weight percent.

Theory SiO_2 wt %	g precursor solution added
5	0.4596
10	0.9193
15	1.379
20	1.839
25	2.298

A ratio of 1:2 SiO_2: TEOS and 4:1 H_2O: TEOS was used in the calculations. The 0.01M HCl was added as the water amount.

The actual weight percent of SiO_2 was determined using TGA. The precursor solution was continuously stirred while removing aliquots for addition to the polymer. This method allowed for hydrolysis of the SiO_2 that would appear in all the samples to occur under the same conditions (amount, pH) until removal for addition to the polymer. Both preparation methods gave varying agreement between the theoretical and actual amount of SiO_2 in the hybrids. Since the batch method allowed for the preparation of multiple hybrids concurrently, it was chosen for hybrid preparation.

Hybrid Preparation

The polymer-inorganic hybrids were prepared as follows: five samples of 1.0 grams of the polymer was weighed out and dissolved in 10.0g of the 50/50 w/w THF/$CHCl_3$ mixture. This was stirred and more solvent was added as needed due to evaporation. Once the polymer was fully dissolved, a batch hydrolysis of TEOS was prepared. The TEOS mixture was added in amounts according to table 2 through a 0.2 micron filter. The hybrid mixture was then stirred for up to an hour uncovered to allow for solvent evaporation and thickening of the mixture. This was then cast in a 57mm aluminum weigh dish. This dish was covered for up to three days to form a more solid product (i.e. sample did not move when dish was tilted, could still appear soft to the touch). The dish was then placed into an air oven and dried at 65 °C for 3 hours covered and then uncovered for 6 days. This produced samples with solvent content around 5 weight percent.

Comparisons of the hybrids DMA trace with a cast polymer sample containing an equivalent amount of solvent led to some questions. The addition of the silica did not improve the mechanical properties of the polymer. This led me to look back over the chemistry involved. Originally, we did not feel that the ethanol byproduct from the hydrolysis of TEOS would cause a problem but the mechanical results seemed to show otherwise. For this reason, polymer samples were prepared with the solvent mix and ethanol to get an appropriate baseline of properties to compare the hybrids too.

Ethanol added Polymer Film Preparation

To account for the effect of the hydrolysis product ethanol on the solvent cast polymers a set of samples were prepared by dissolving 1.0g in 10.0g of a 50/50 w/w THF/$CHCl_3$ mixture and adding ethanol. The amount of ethanol used was 0.27g to give 20 weight percent ethanol in the sample before drying. The water amount was calculated based on the ethanol amount and the hydrolysis reaction shown in Scheme 1. The actual amount of water used was calculated from 4:1 water to TEOS (or ethanol) ratio and then subtracting the amount required to

react stoichiometrically with TEOS. This gives 0.30 mL of water added to the sample. These were dried as above and compared with the solvent cast samples to determine how ethanol interacts and effects the thermal and mechanical properties of the polymer used. The PMMA-ethanol samples are described in more detail below and the other polymer-ethanol samples are mentioned in their respective polymer-SiO_2 chapters as the base property sample.

CHAPTER 3

PMMA-SiO_2 Sol-Gel Prepared Inorganic-Organic Hybrids

Introduction

Polymeric materials have a wide variety of uses and adding a functional filler, for example an inorganic oxide, can lead to an even more diverse class of materials with applications in areas such as optics[59], electronics[46], biology[60], and creating inorganic mesostructures[10]. These polymer-inorganic hybrids show combinatorial properties from the constituents[45-46] and may exhibit interesting new properties. Creating polymer-inorganic hybrids can be performed by mixing the constituents in a heated press[61] or in a sol-gel process[37, 39].

Hybrid materials made from poly (methyl methacrylate) (PMMA) and SiO_2 are a commonly studied system[59, 61-67]. They have been created by various avenues with a variety of silica precursors. Silicic acid[68] was used to obtain thin hybrids. Tetraethoxysilane was hydrolyzed concurrently with the polymerization of methyl methacrylate to PMMA in the presence of a coupling agent in an attempt to increase the interactions between the constituents[64]. Another study hydrolyzed TEOS in-situ to create PMMA-SiO_2 hybrids[59]. Previous work however does not always provide a wide range of samples or techniques to determine how the SiO_2 changes the PMMA base properties. Sun et al[59] only looked at three samples for their optics study. Another study only used thermal lens spectroscopy and depth sensing indentation and Vickers microhardness[64]. Our study looks at a way to combine pre-hydrolyzed TEOS into a PMMA network to create hybrids with differing SiO_2 content. This process relies on physical interactions between the constituents to bring about changes in the thermal and mechanical properties. The properties were determined using thermogravimetric analysis, dynamic mechanical analysis, FTIR spectroscopy and atomic force microscopy.

The PMMA-SiO_2 hybrids were prepared by pre-hydrolyzing TEOS before addition to PMMA dissolved in a good solvent mix. The amount of pre-hydrolyzed TEOS added was varied to give hybrids with a range of SiO_2 up to 30 wt %. The results of investigations of the thermal stability, mechanical properties and chemical make-up of the hybrids has increased our understanding of how organically modified inorganic starting materials can be used in the preparation and control of the properties of a polymer-inorganic hybrid.

Experimental

PMMA (350,000 g/mol) and tetraethylorthosilicate (TEOS) were purchased from Aldrich. Tetrahydrofuran (THF) was obtained from Omnisolv and chloroform ($CHCl_3$) from Fischer. All chemicals were used as received.

Hybrid samples were prepared by dissolving 1.0 g of PMMA in 10 g of a 50/50 w/w THF/$CHCl_3$ mix and stirring. A pre-hydrolyzed sol-gel solution was prepared by combining 15 mL of TEOS and 4.85 mL of 0.01M HCl and stirring for 40 minutes. In order to create hybrids with different SiO_2 content, varying amounts of the pre-hydrolyzed TEOS batch were added to the PMMA. The actual SiO_2 content was determined by thermogravimetric analysis.

The combined solution was stirred an additional hour then poured into an aluminum weighing dish. The dish was allowed to sit covered for up to 3 days at room temperature to allow the reaction to finish and the sample to start to solidify. Subsequent heating in the oven at 65 °C for 2 days covered, and then 3 days uncovered, allowed excess solvent to leave.

An additional sample was made to establish the PMMA baseline properties. PMMA with the solvent mix and ethanol added in an amount comparable to that produced in a typical hydrolysis reaction was prepared and dried in the same manner as the hybrids.

Following removal from the oven, 10 mm × 40 mm × ~0.3 mm samples were obtained and subjected to thermogravimetric (TGA) analysis (TA Instruments) and dynamic mechanical (DMA) analysis (Perkin Elmer Inc.). The

TGA experiment was run in air with a ramp rate of 10 °C/min to 150 °C, held isothermally for 45 min, then ramped to 600 °C. The DMA instrument used a ramp rate of 2 °C/min from room temperature to 170 °C at 10 Hz. Fresh fracture pieces were made before AFM imaging on a Nanoscope III. Images were modified using Nanoscope software and were formatted using SPIP.

PMMA Solvent Cast Sample

From Chapter 2 we saw that the inclusion of ethanol produced by the hydrolysis and polycondensation of TEOS had a profound impact on the thermal and mechancial properties of PMMA. As the solvents and ethanol will be present in our hybrids, the PMMA cast sample was prepared with them added. The properties of our solvent cast PMMA is compared with the PMMA as received from Aldirch to obtain a fundamental understanding of how the solvent/ethanol mix affects the properties.

The TGA trace for as-received (bulk) PMMA, shown in Figure 3.1, shows no obvious weight loss until about 265 °C. The onset of degradation of PMMA in an oxygen-containing atmosphere is delayed relative to that in an inert atmosphere to around or above 220 °C, dependent upon the initiator used[69]. The weight loss seen in bulk PMMA occurs by the initiation of weak linkages followed by random scission of the PMMA chain[69-70].

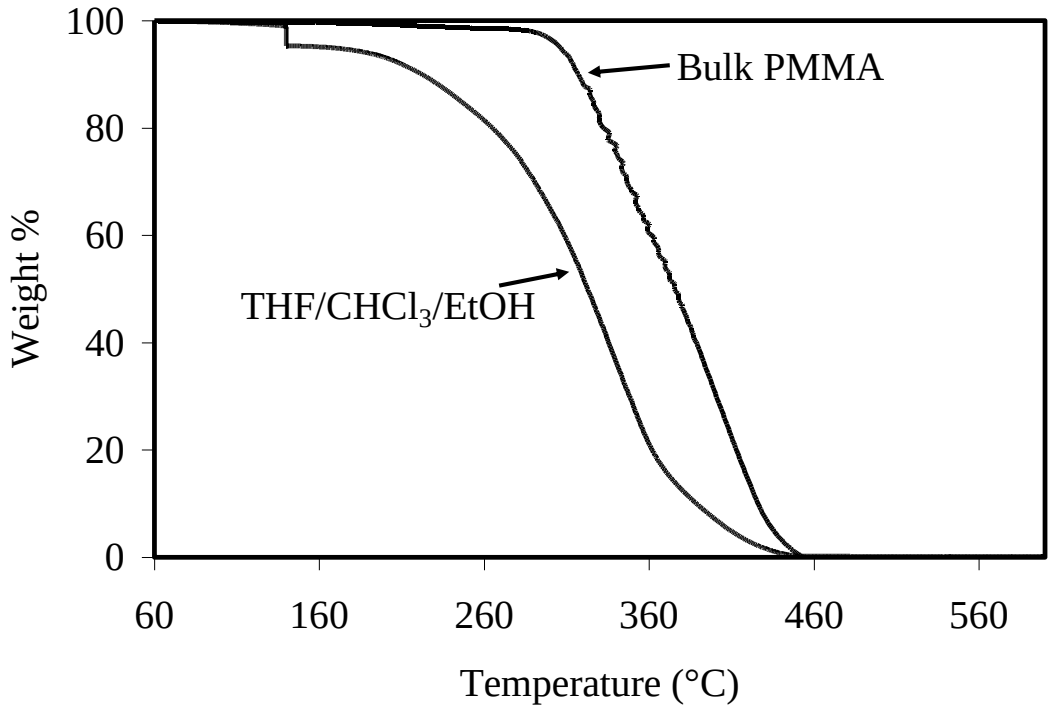

Figure 3.1: TGA traces for cast PMMA and PMMA received from Aldrich.

The effects of the solvent mix on the baseline properties was already shown in Chapter 2 and here we go over sample that more closely models the baseline properties for our hybrids. The PMMA cast from solution was characterized on TGA and DMA. The TGA data in Figure 3.1 for this sample does indeed show that it contained some retained solvent as evidenced by the weight loss at temperatures well below that of the bulk PMMA curve. To more easily quantify the amount of solvent mix retained in the sample, the TGA run was adjusted to have an isothermal hold at 140-150 °C for 45 minutes. This temperature is above the boiling point of the solvents ($CHCl_3$ 63 °C, THF 66 °C, and EtOH 78 °C).

In making the hybrids, the hydrolysis of TEOS produces four moles of ethanol per mole of SiO_2 present in the final material. Hence, our hybrids before drying will contain certain amounts of ethanol in addition to the usual solvent pair. The PMMA cast sample was prepared to contain a comparable amount of ethanol. During the isothermal hold (above the 78 °C boiling point

of EtOH) this sample lost 4.5% of its weight. The drop in weight during this hold translates into 4.5 wt. % of retained solvent for the film.

The solvent cast samples both showed a much less well-defined decomposition onset than that of bulk PMMA. The ethanol-containing sample shows a depressed thermal response in which the onset of decomposition appears to start near 200 °C. Ethanol is the only solvent of the three that can effectively hydrogen bond to itself or the PMMA[57], so the unusually low onset of decomposition of the sample presumably reflects the influence of ethanol that is still bound to the PMMA after the isothermal hold.

The ethanol contained in the sample could inhibit the oxygen stabilization process which initially pushes PMMA's degradation to higher temperatures than other atmospheres. Oxygen creates a radical species that is thermally stable and suppresses unzipping of the polymer[70]. If this process is impeded by the presence of ethanol H-bonded to the polymer, the degradation onset would be moved to a lower temperature.

Figure 3.2 shows the DMA traces (modulus and tan D) for the solvent cast sample and the calibration piece received from Perkin Elmer. From the GPC in Chapter 2 run on the Aldrich PMMA and the Perking Elmer sample we know that the molecular weight of the Perkin Elmer sample is higher. So we expect that the mechanical properties measured by the DMA will be slighly lower for the Aldrich PMMA. The marked decrease in mechanical properties of the ethanol sample presumably also reflects the interaction between the ethanol and PMMA.

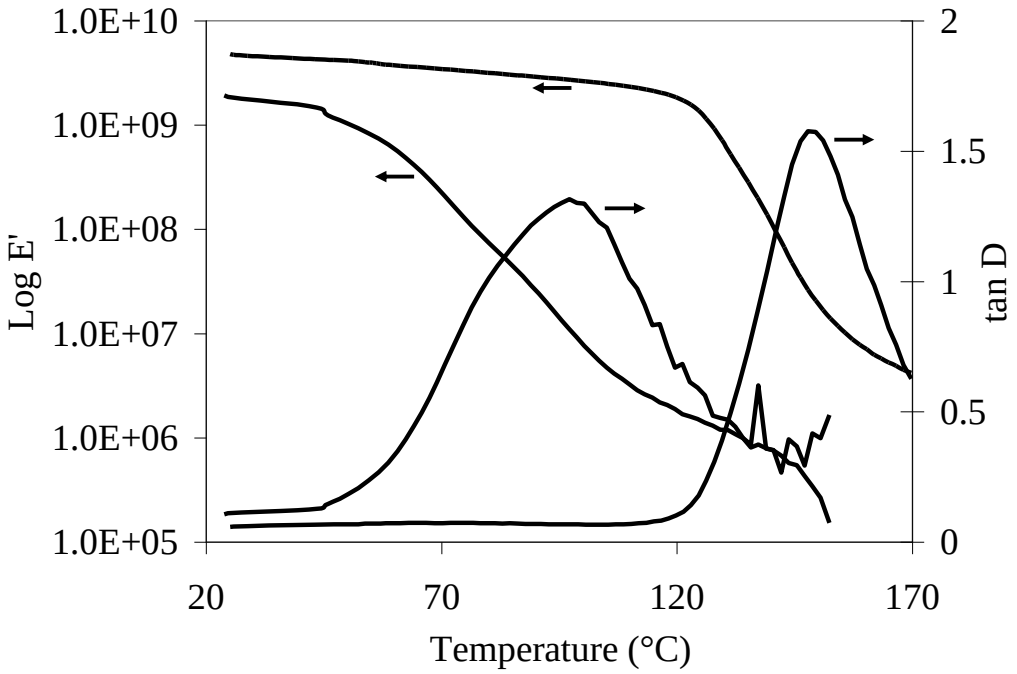

Figure 3.2: PMMA solvent cast sample mechanical response. THF/$CHCl_3$/EtOH (- -) shows a lower modulus and T_g than the perkin elmer calibration.

From the data presented in Figure 3.1 and 3.2 for the two types of solvent-cast sample, it is apparent that ethanol has a marked effect on the thermal and mechanical properties of PMMA. The retention of the solvents in these SiO_2 free samples strongly suggests that the SiO_2 hybrids prepared will also retain ethanol produced by the condensation reaction of TEOS as well as the initial solvent mix. The appropriate baseline material to use for comparison with the hybrids is the S2, THF/$CHCl_3$/EtOH, sample.

PMMA Hybrids

Appearance

The prepared hybrids appear transparent to opaque with increasing silica content. Figure 3.3 shows the PMMA hybrids containing increasing amounts of silica. The hybrids appearance can be related to the interaction between the silica and PMMA. When phase separation between the constituents occurs the hybrids reflect more light and appear whiter. The samples at 0 and 13 weight percent SiO_2

were the most transparent with 5 weight percent running slightly opaque. The 28 weight percent SiO_2 hybrid completely blocks out the colored line behind the sample.

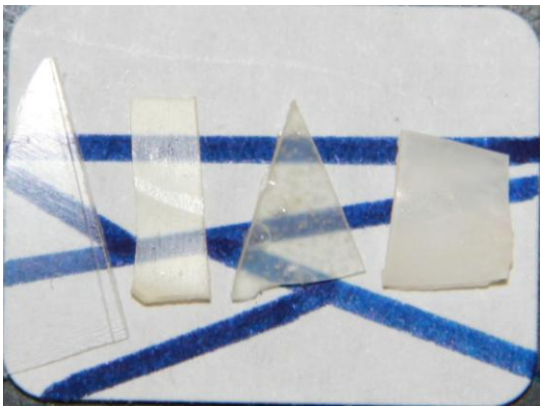

Figure 3.3: Appearance of PMMA-SiO_2 hybrids. The silica content increases from left to right: 0% silica, 5% silica, 13 % silica, and 28 % silica.

Fourier Transform Infrared Spectroscopy

Figure 3.4 shows the FTIR spectra of hybrid materials spin cast onto KBr windows. The spectra are shifted arbitrarily for comparison. These samples were dried in an air oven to remove solvent and keep water from adsorbing to the surface of the samples. The spectra shows no evidence that $CHCl_3$ or THF were retained. Presumably, it is much easier for these solvents to escape from very thin samples on KBr than from the thicker ones used for the TGA and DMA experiments.

The cast PMMA sample showed no O-H stretch at 3400 cm^{-1} indicating that ethanol was removed from our cast sample with our IR sample preparation method. The peak at 1730 cm^{-1} is from the C=O stretch of the ester side group on PMMA. This peak is easily identifiable as it is generally free from interfering bands. The peaks centered around 2950 cm^{-1} are from the symmetric and asymmetric stretching of methyl groups. The peak at 1480 cm^{-1} is due to the asymmetric deformation of the alkyl group. At 1450 cm^{-1} the dermation of the methyl group attached to the ester is seen. The peaks between 1100 cm^{-1}

and 1300 cm^{-1} are from the methyl group and the C-O stretch of the ester. These peaks are seen in all of the spectra of the hybrids proving that the PMMA was not degraded in any manner using our preparation and drying methodology.

The hybrids prepared from pre-hydrolyzed TEOS and PMMA in Figure 3.4 have additional peaks not seen in the PMMA spectrum. The peaks at 1040 cm^{-1}, 1070 cm^{-1} and 1120 cm^{-1} arise from the Si-O stretch. The peak seen at 857 cm^{-1} is indicative of silanol, Si-OH. We also see an O-H stretch at 3400 cm^{-1} The appearance of these two peaks show that the hydrolysis/polycondensation reaction of TEOS did no go to completion. No shift was seen in the C=O peak for PMMA indicating that if there is hydrogen bonding occuring it is not on a very large scale. The 13 weight percent and 28 weight percent SiO_2 hybrids do show that largest O-H peak at 3400 cm^{-1} and a broadening of the C=O peak at 1730 cm^{-1} which may mean some hydrogen bonding is occuring.

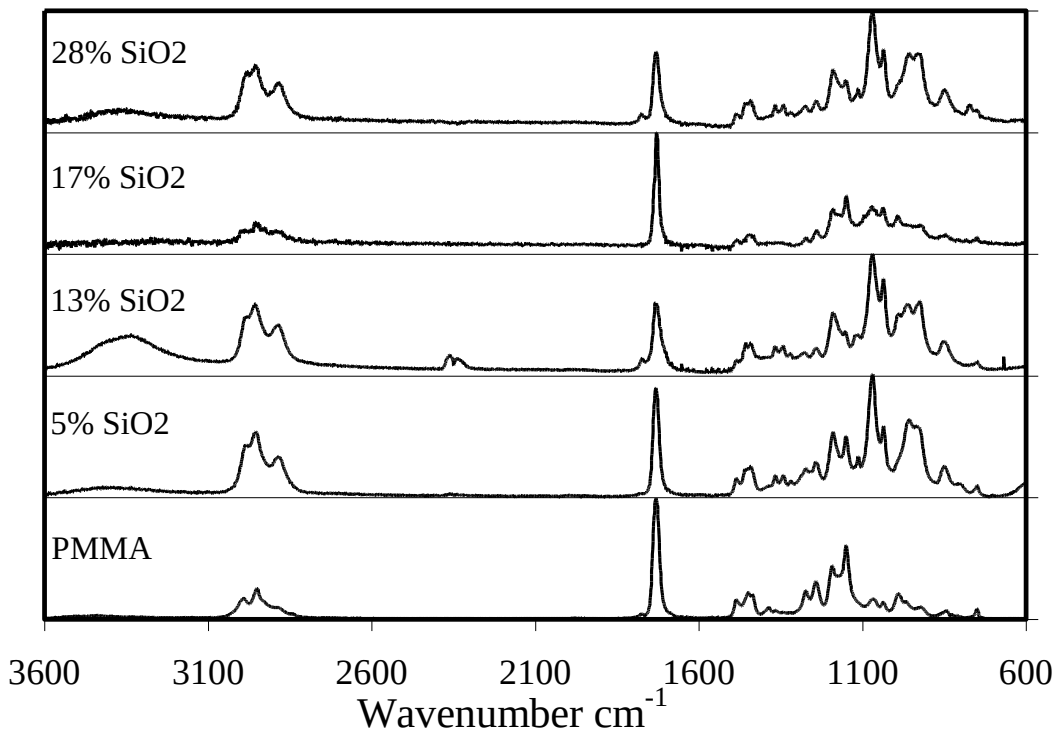

Figure 3.4: IR spectra for PMMA-SiO_2 hybrids.

Tapping Mode-Atomic Force Microscopy

Height and phase images of the fresh fracture surfaces of PMMA-SiO_2 hybrids were obtained using tapping mode AFM and are shown in Figure 3.5. At a low SiO_2 content (5%, a) the topography appears random. With increasing SiO_2 content (b,c) the hybrids exhibit a more granular aspect. This is similar to AFM data from other polymer-inorganic hybrids[25]. The average roughnesses of the samples, given in Table 3.1, show no trend with SiO_2 content. These were averaged from many images.

While the height images give us a clear view of the topography of the fracture surfaces, they do not differentiate between the polymer and ceramic components. The phase image shows the chemical composition of the hybrid fracture surfaces due to the difference in the stiffness of the components. The light areas correspond to the SiO_2. While the phase image for the S5 sample shows a change in shading along a height boundary, the phase difference is slight (20°). The unevenness of the fracture is believed to cause this slight change in the phase.

With increasing SiO_2 content (b, c) more differences in phase are apparent with at least some of silica being present in particles. The phase range is 50° or greater. In the 13% sample (b) these particles appear lumped together along the fracture. As the SiO_2 increases to 27 % (c) a better dispersion of particles is seen. The SiO_2 areas do not seem to correspond to any particular topographical feature. Thus in (b) the light areas occur in regions of different topography and in (c) they do not match the granular features. The coverage of the light phase areas are 4.75% and 6.65% for b and c respectively. Overall this data indicates that most of the silica is well-dispersed in the poymer matrix.

a)

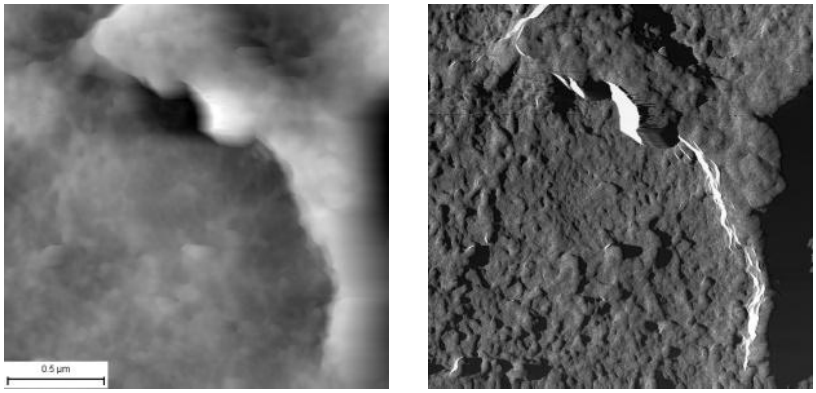

b)

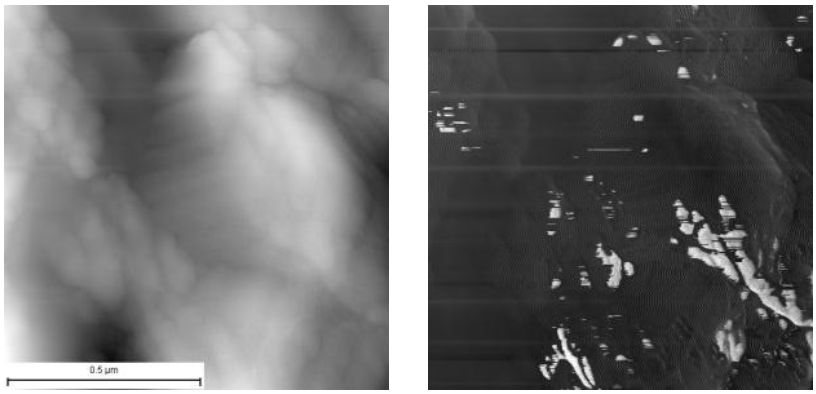

c)

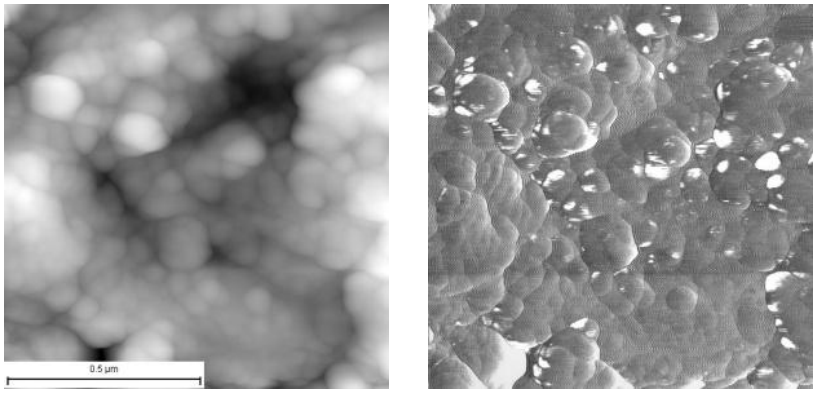

Figure 3.5: Height and Phase images acquired in tapping mode AFM. Shown for a). S5 (z=407nm; 20 °), b). S13 (z=213nm; 125 °), c). S28 (z=116nm; 58 °). Height images on the left with corresponding phase images on the right.

Table 3.1: TM-AFM tabulated data for PMMA-SiO_2 hybrids .

Sample	% SiO_2	R_a (nm)	SiO_2 Phase Coverage %
S2	0	--	--
S5	5.4	16.3	0
S13	12.5	26.9	4.75
S28	27.8	14.2	6.65

Thermogravimetric Analysis

The TGA traces for the PMMA-SiO_2 hybrids are shown in Figure 3.6. The SiO_2 content was determined from the weight percent remaining at 600 °C. The initial weight loss seen during the isothermal hold is due to the loss of solvent mix and condensation products that are retained in the hybrid. No weight loss was seen from a pure PMMA sample run with an isothermal hold at 140 °C. The temperatures at 50 percent weight loss (T_{50}) given in Table 3.2 shows an increasing temperature with SiO_2 content. The thermal stability increased from 338 °C to 388 °C over a 30 weight percent SiO_2 range.

The derivative plots for the TGA traces are shown in Figure 3.7. The pure PMMA curve (run on the Aldrich sample) shows two stages of degradation in air. The first temperature weight loss around 325 °C is brought on by end group initiation and the higher temperature process around 410 °C involves random chain scission[71-72]. The PMMA cast samples show more weight loss occurring at lower temperatures, possibly due to the increased motion of the PMMA chains from the presence of the solvent molecules which exposes more end groups. As SiO_2 is added, the main weight loss process shifts to higher temperatures, indicating less end group initiation and more random scission processes. The SiO_2 restricts the movement of the PMMA chains and contributes to this improvement in thermal stability of the hybrids.

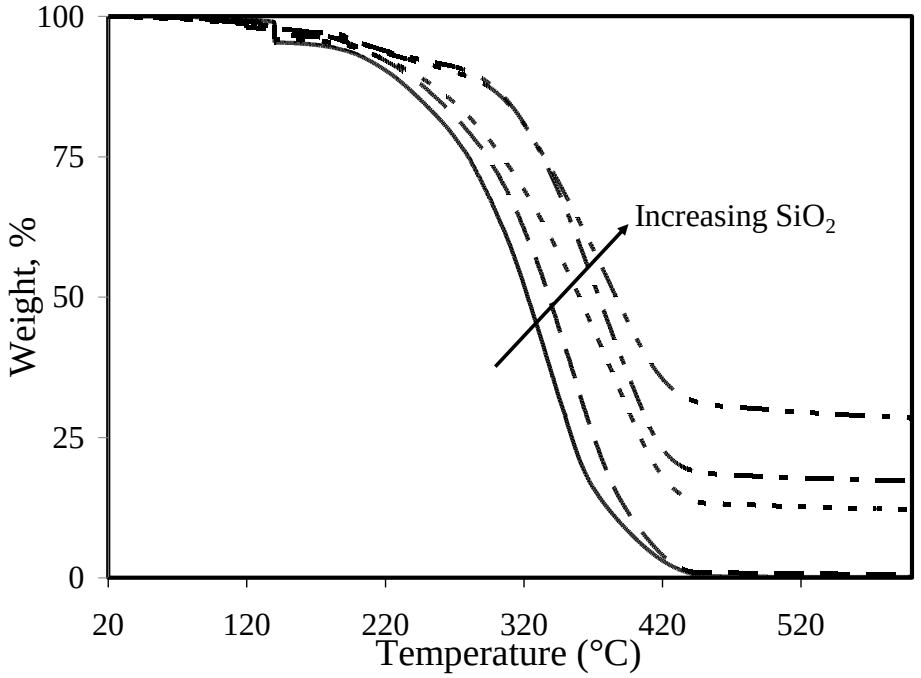

Figure 3.6: TGA traces for PMMA-Silica hybrids. The hybrids are shown along the arrow S5, S13, S17, and S28. Solid line is PMMA cast THF/$CHCl_3$/EtOH.

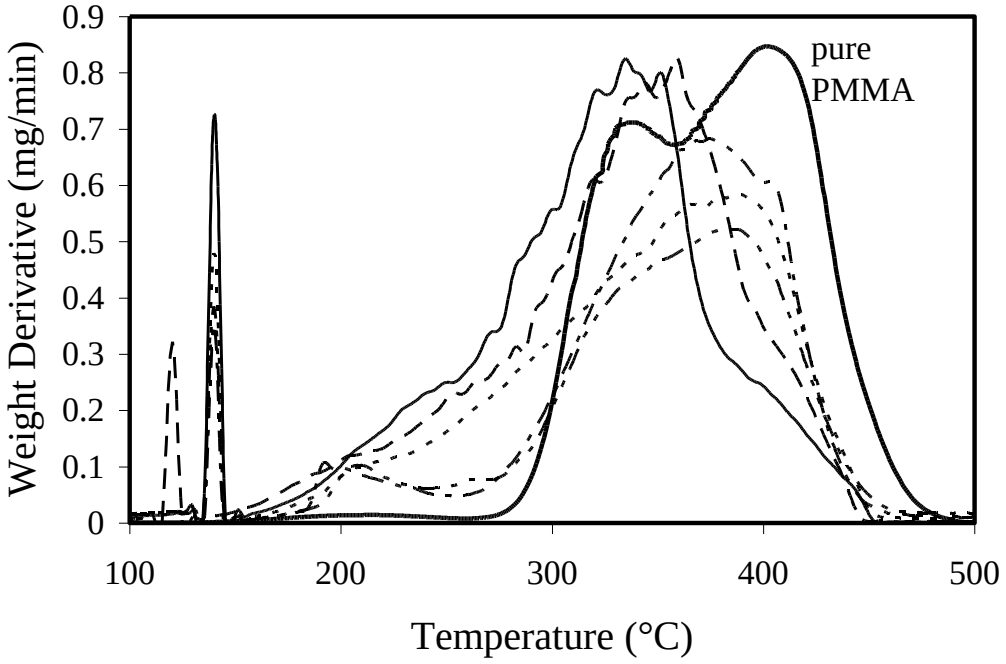

Figure 3.7: Corresponding derivative plots for the data in Figure 4.5. The hybrids are shown along the arrow S5, S13, S17, and S28. Solid line is PMMA cast THF/$CHCl_3$/EtOH. Pure PMMA shown as a reference.

Dynamic Mechanical Analysis

The change in mechanical properties as a result of silica content was investigated with DMA over a temperature range of 20 °C to 170 °C (or until material failure). The viscoelastic response is shown in Figure 3.8. The storage modulus (E´) shows a glassy plateau at low temperatures. The order of magnitude is the same for all amounts of silica. This is consistent with the lack of chemical interaction between the PMMA and silica as seen in the IR spectra. The PMMA in the hybrids still has the same short chain motions as pure PMMA and thus similar modulus values.

The rubbery modulus plateau increases by orders of magnitude with silica content. Apparently, the silica particles are able to interact with the PMMA chains sufficiently to inhibit their flow characteristics. The mechanical response of the hybrid materials were all higher than that of the ethanol-containing S2 sample, while the S1 sample fell amongst the curves. This behavior reinforces our belief that ethanol is being retained in the samples, even after extensive curing.

The glass transition (T_g) temperature was taken as the tan delta peak at 10 Hz. They are shown in Figure 3.9 and listed in Table 3.2. The value of T_g is seen to increase with silica content. We attribute this trend in a similar manner to the changes in the rubbery modulus values. The physical interaction of the silica with the PMMA inhibits the polymer's ability to flow and shifts the T_g of the hybrids to higher temperatures. The increase in T_g levels off at the higher SiO_2 weight fractions. The 17 wt. % sample curve split into two peaks. Careful examination of this sample revealed that it was not as homogenous as the other samples. The first peak was taken as the glass transition temperature.

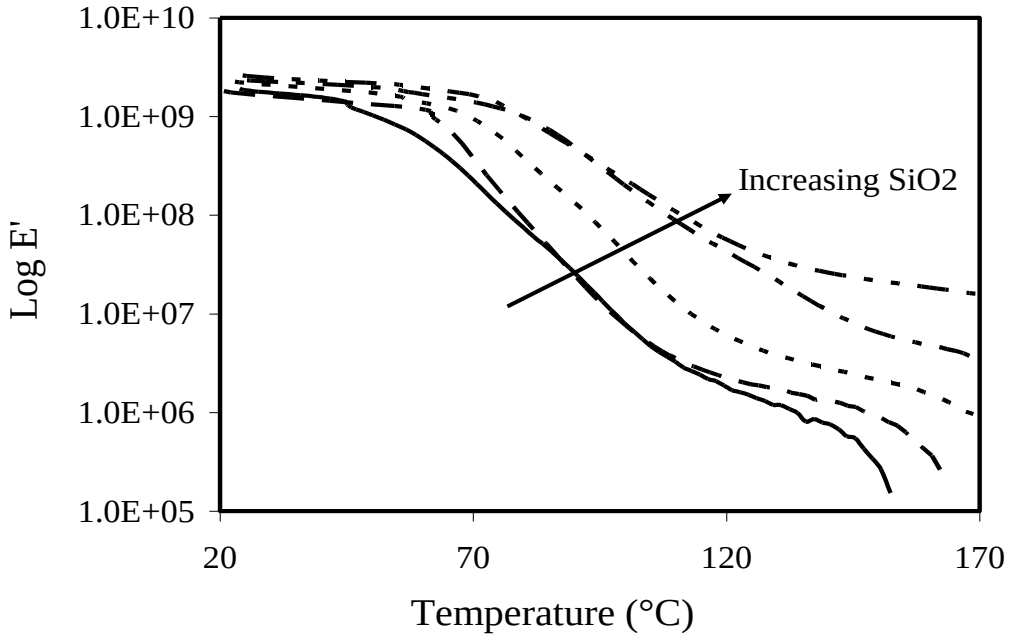

Figure 3.8: DMA traces of hybrids at 10 Hz. The hybrids are shown along the arrow S5, S13, S17, and S28. Solid line is PMMA cast THF/$CHCl_3$/EtOH.

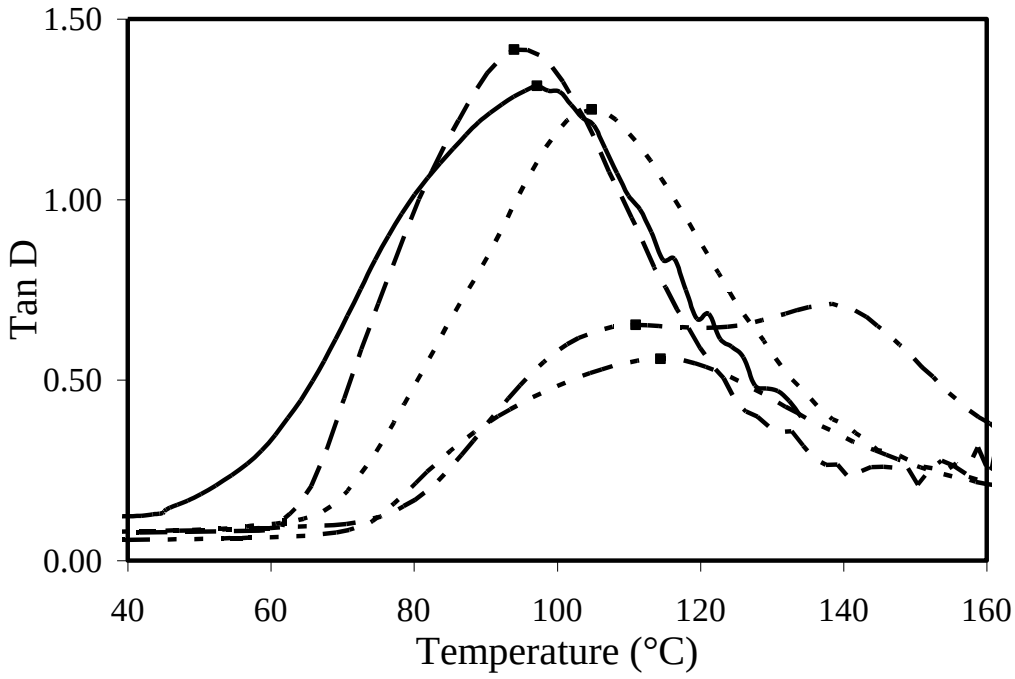

Figure 3.9: Corresponding tan delta curves at 10 Hz of the same hybrids as in Figure 3.8. Black squares mark glass transition temperature.

From the multiple frequecy traces taken during the DMA runs we were able to calculate the activation energy (E_a) for the glass transition temperature. Shown in Figure 3.10, the glass transition temperature for five different frequencies were plotted and the slope was used to determine the activation energy. The perkin elmer PMMA calibration sample has an E_a of 400 kJ/mol. The cast PMMA sample has a value of 124 kJ/mol (open circles in Figure 3.10). This is on the low end of activation energies for polymer glass transition temepartures. As silica is increased in the hybrids, the E_a's increase to higher values. The glass transition temperature can also be seen to shift to higher temperatures (towards the perkin elmer sample) as silica content is increased. All of the thermal and mechanical data is tabulated in Table 3.2.

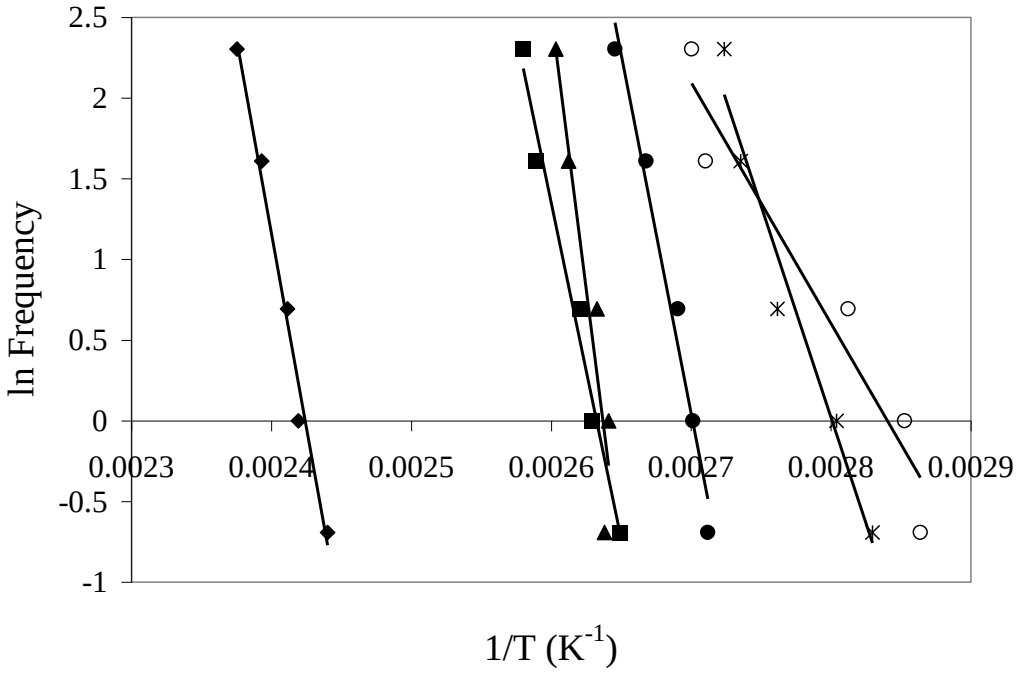

Figure 3.10: Activation Energy of glass transition region for PMMA-SiO_2 hybrids. Perkin Elmer (♦), Cast PMMA (○), 5 % SiO_2 (X), 13 % SiO_2 (●), 17 % SiO_2 (▲) and 28 % SiO_2 (■).

Table 3.2: Thermal and mechanical data for PMMA-SiO_2 hybrids. The S19 (19% SiO_2) sample is given in the table but not shown on above graphs for clarity.

Sample	% SiO_2	E'_{25} (GPa)	E'_{140} (GPa)	T_g (°C)	E_a (kJ/mol)	$T_{50\%}$ (°C)
Cast	0	2.38	.000944	95	124	323
S5	5.4	1.95	.00125	95	218	338
S13	12.5	2.21	.00325	105	370	360
S17	16.9	2.53	.0110	109	476	375
S19	18.5	2.56	.0107	111	314	378
S28	27.8	2.59	.0356	113	346	388

Conclusion

Pre-hydrolyzed tetraethoxysilane was successfully combined with poly (methyl methacrylate) to form PMMA-SiO_2 polymer-inorganic hybrids. The SiO_2 showed a relatively random distribution throughout the PMMA matrix. No signs of hydrogen bonding between the incompletely condensed silanol groups and PMMA ester side groups were seen on the IR spectra. If any hydrogen bonding is present it did not occur in a significant enough amounts to cause a shift in the carbonyl as expected. We did see some broadening of the carbonyl peak that could result from a weak intermolecular interaction. Even without a clear chemical interaction, the SiO_2 added to the PMMA matrix caused an improvement in the thermal and mechanical properties measured. The useful range of operating temperature, taken as the glassy plateau from the DMA curve, was increased to higher temperatures than cast PMMA. As the silica content was increased the degradation pathway was shifted to higher temperatures. At low silica content the degradation appeared similar to the cast PMMA so silica loading above 5 weight percent is important in causing an improvement in the thermal degradation pathway. Wider, less symmetric tan delta curves for the 17 and 25 weight percent silica hybrids indicated some inhomogeneity in the sample from an unknown cause.

Chapter 4

PS-SiO_2 sol-gel prepared Inorganic-Organic Hybrids

Introduction

Many researchers have prepared polystyrene (PS)-SiO_2 hybrids from different starting materials[21, 73-75]. For instance, polystyrene has been mixed with 3-(trimethoxy silyl) propyl methacrylate, which is a silane coupling agent, before tetraethylorthosilicate (TEOS) was added[21, 75]. This produced hybrids with enhanced properties when compared with the pure polymer. Other workers have used different starting materials for the SiO_2 component to create hybrids, including functionalized alkoxy silanes[22, 76], base-catalyzed reactions with TEOS[73], and silica particles simply blended into polystyrene[77]. These papers showed how polystyrenes thermal and mechanical properties could be increased by an additive.

This study prepared polystyrene-silica hybrids using tetraethoxysilane (TEOS) as the inorganic precursor. The constituents were physically mixed together in a sol-gel process. The amount of silica was varied from 0 to 30 weight percent. AFM was used in tapping mode to concurrently obtain height and phase images of the surface. The effect of increasing amount of silica on the degree of phase separation was determined and related to the mechanical and thermal properties of the hybrids determined using DMA and TGA. The usefulness of AFM as a technique to fully determine the phase separation and surface topography is probed in this study.

Experimental

Polystyrene (230,000 g/mol) (PS) and tetraethylorthosilicate (TEOS) were obtained from Aldrich. Tetrahydrofuran (THF) was obtained from Omnisolv and chloroform ($CHCl_3$) from Fischer. All chemicals were used as received.

The silica precursor solution was prepared from a sol-gel hydrolysis/polycondensation reaction of TEOS. Fifteen mL of TEOS was mixed

with 4.85 mL of 0.01 M HCl and stirred for 40 minutes at room temperature. The PS/Silica hybrid materials were prepared using a sol-gel process. One gram of PS was dissolved in 5.0g each of THF and $CHCl_3$. The pre-hydrolyzed TEOS solution was added to the dissolved PS samples following the amounts in Table 4.1. This mixture was stirred for 1 hour and then cast in an aluminum weighing dish. After drying for 2-3 days at room temperature, the sample was then placed into an air oven at 65 °C for 6 days. The samples obtained had no cracks and ranged from transparent to opaque. A PS sample was prepared from the solvents and ethanol as a control to obtain the base properties for comparison with the hybrids.

To identify chemical structures in the hybrids, FTIR spectra were collected. The samples were dissolved in $CHCl_3$ and coated onto a KBr window. The spectra were obtained using a Nicolet 510P with 2 cm^{-1} resolution. The coated KBr windows were dried before running. The thermal and mechanical properties were characterized by TGA (TA Instruments) and DMA (Perkin Elmer Inc.). The TGA was run in air with a ramp rate of 10 °C/min to 600 °C. The DMA was run using sample dimensions of 10 mm x 10 mm x 0.3 mm with a ramp rate of 2 °C/min run to 170 °C using frequencies of 1.0 and 10.0 Hz. AFM (Nanoscope III) was run on fresh fracture surfaces in tapping mode. A scan rate of 1-2 Hz was employed. The scan size used was 1μm. Images were modified using Nanoscope software and were formatted using SPIP.

Table 4.1: Amounts used to prepare PS-Silica hybrids. Based on 1.0 g of PS.

Wt% Silica Calculated	g Silica Calculated	g pre-hydrolyzed solution*
5.0 %	0.05 g	0.46 g
10.0 %	0.10 g	0.92 g
15.0 %	0.15 g	1.38 g
20.0 %	0.20 g	1.84 g
25.0 %	0.25 g	2.30 g

*Based on pre-hydrolysis of 10.0 g of TEOS producing 2.05 g SiO_2.

PS Hybrids

Appearance

The polystyrene-silica hybrids are shown after casting in Figure 4.1. The hybrids show decreasing opacity as silica content is increased. The hybrids also showed discoloration at high silica loadings after they were dried in the oven. These particular samples also broke easily and did not leave a clean edge.

Figure 4.1: Appearance of PS-SiO_2 hybrids. Increasing silica content from left to right: 2.4%, 8.4%, and 30.9% silica.

Fourier Transform Infrared Spectroscopy

The Fourier transform infrared (FTIR) spectra for polystyrene and the PS-SIO_2 hybrids are shown in Figure 4.2. The cast polystyrene sample shows C-H stretches around 2900 cm^{-1} from the alkyl groups. The C-H stretch from the hydrogen atoms on the aromatic ring occur around 3100-3000 cm^{-1}. The aromatic ring attached to the carbon chain gives characteristic peaks that can be used for identification. The C ring bonds show peaks occurring at 1604 cm^{-1} from the stretch and 700 cm^{-1} from the out of plane bend. The peaks in the range 1000-1600 cm^{-1} occur from the many motions of atoms in the polystyrene chain and are of little use for identification. The hybrids prepared from pre-hydrolyzed TEOS and PS show all of the peaks mentioned above from the polystyrene as well as new peaks that arise from the formation of silica. The 1100 cm^{-1} region shows broader peaks growing in from the Si-O motions in silica. We see an O-H stretch at 3400 cm^{-1} that is from residual silianol groups from the polycondensation of TEOS.

The silanol group shows a peak at 927 cm^{-1} that helped in the identification. A shoulder is seen to grow in on the peak at 1604 cm^{-1}. The cause of the shoulder could not be determined but may arise from interactions between silanol and the styrene ring. The FTIR spectra confirmed the presence of both constituents in the hybrid as well as showing that the hydrolysis and polycondensation reaction of TEOS did not run to completion. No clear indication of any chemical interactions between the constituents was noted.

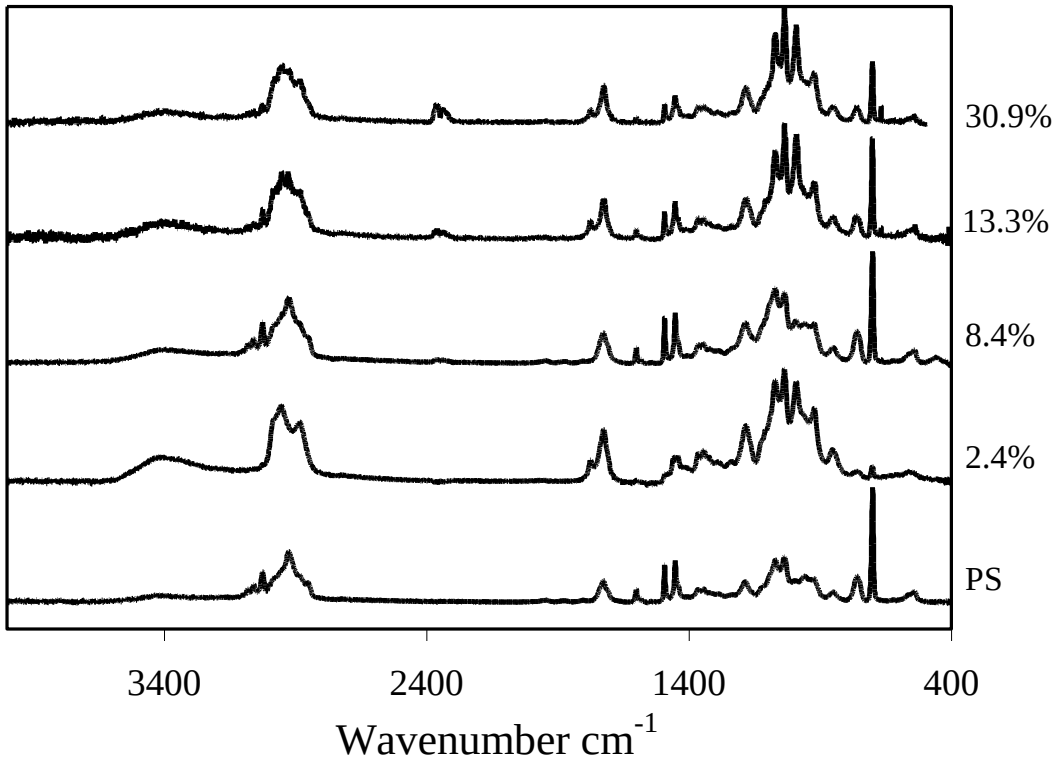

Figure 4.2: FTIR spectra of cast polystyrene and hybrids with varying silica content.

Thermogravimetric Analysis

TGA traces were run on all of the hybrids and cast polystyrene. These are all show in Figure 4.3 with their respective derivative plots shown in Figure 4.4. The weight loss below 320 °C is attributed to solvent evolution. The amount of

SiO_2 in each hybrid was determined by the weight left after the thermal run at 600 °C.

The curves are seen to shift to higher temperatures after solvent removal. The increasing SiO_2 content helps stabilize the polystyrene network. The thermal increase seen shows no additional improvement when silica weight percent is increased to 30. All silica amounts did show improvement over the cast polystyrene sample.

The corresponding derivative curves showed an increase in the polystyrene degradation pathway temperatures of the hybrids when compared to the cast polystyrene sample. The PS/SiO_2 hybrids peak temperatures all appeared in the same range. The interaction between the SiO_2 and polystyrene chain does increase the initial temperatures seen for degradation.

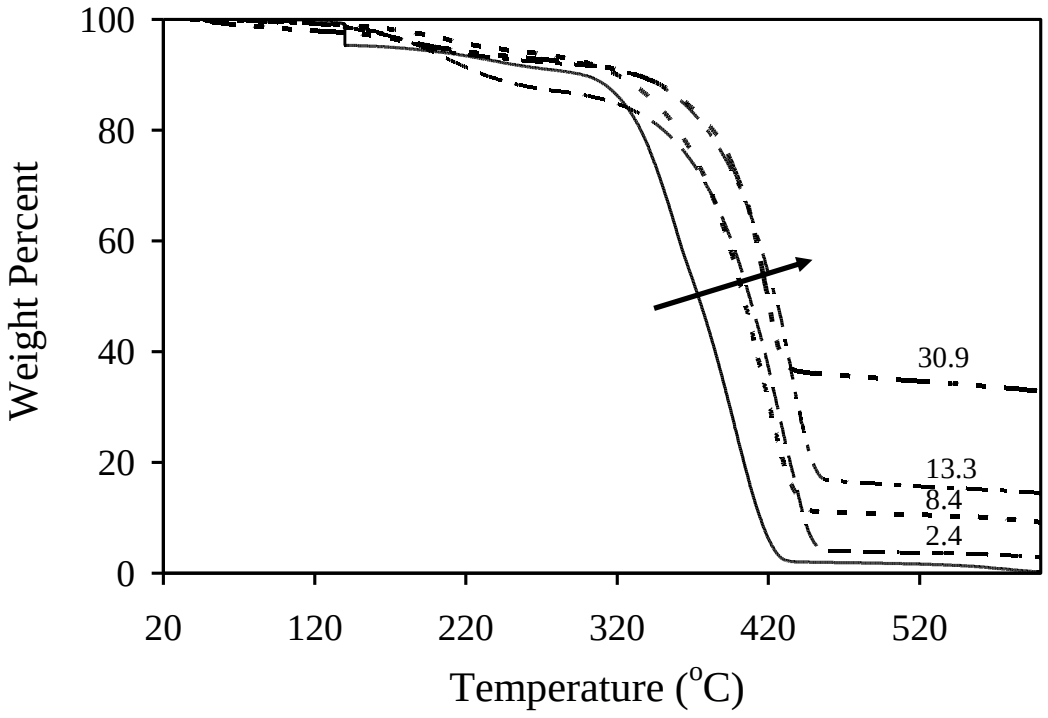

Figure 4.3: TGA traces for as received and cast polystyrene compared with the PS/Silica hybrids.

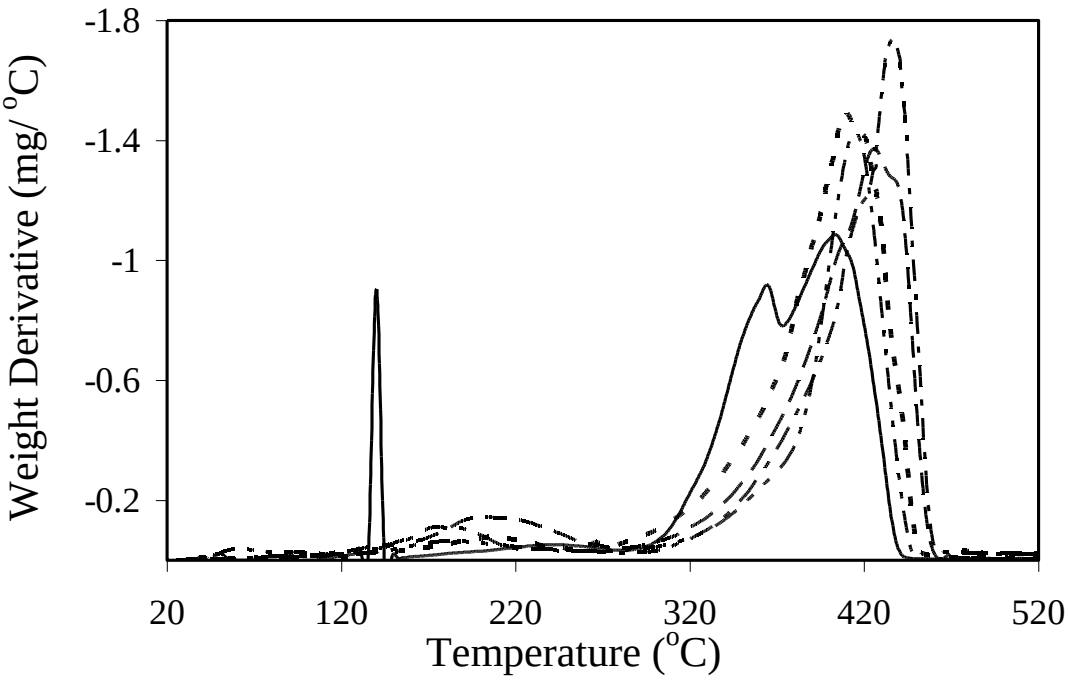

Figure 4.4: Corresponding derivative plots for the TGA traces given above.

Dynamic Mechanical Analysis

The storage modulus curves for the hybrids and cast polystyrene are shown in Figure 4.5. The polystyrene cast sample is the solid black line. The initial introduction of silica at low weight percent shows the same modulus value in the glass region with a decrease as silica content of 30.9% is achieved. The hybrids show an increase in modulus versus temperature after the glassy plateau. The 8.4% hybrid shows the greatest improvement and the addition of more silica causes the modulus to decrease. Normally when fillers are introduced an improvement in mechanical performance is seen. Given that no chemical interactions were noted from the infrared spectra, the polystyrene and silica are interacting on a physical level. The interfacial interaction between the polystyrene and silica would lead to the changes seen in the mechanical properties. Increasing the silica 13.3% and higher showed decreased modulus and poor mixing of constituents.

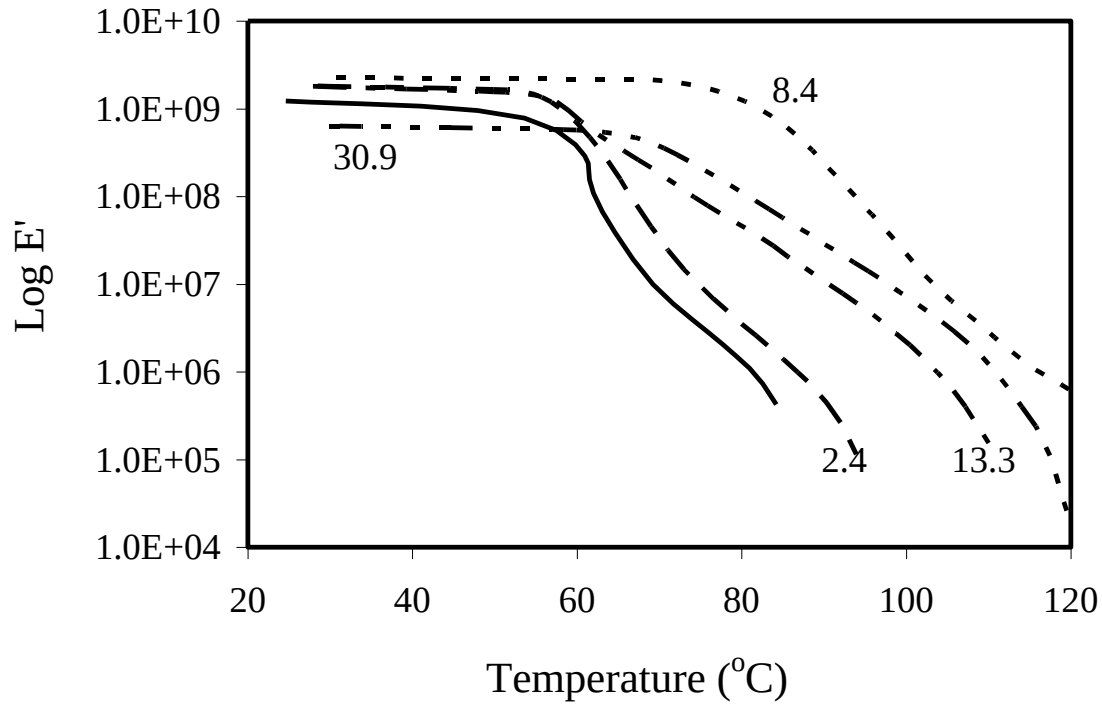

Figure 4.5: Modulus curves for hybrids and cast polystyrene sample.

The tan delta curves for the hybrids are given in Figure 4.6. The peak of the curve was taken as the glass transition temperature. The 2.4% hybrid showed a distinct peak higher than the cast polystyrene sample. The transition temperatures for the other hybrids were less clear. The hybrids did not go through a clear transition before material failure. The lack of a clear T_g could be indicative of the constituents mixing poorly. Since no T_g could be determined, an Arrhenius plot to determine the activation energy could not be made.

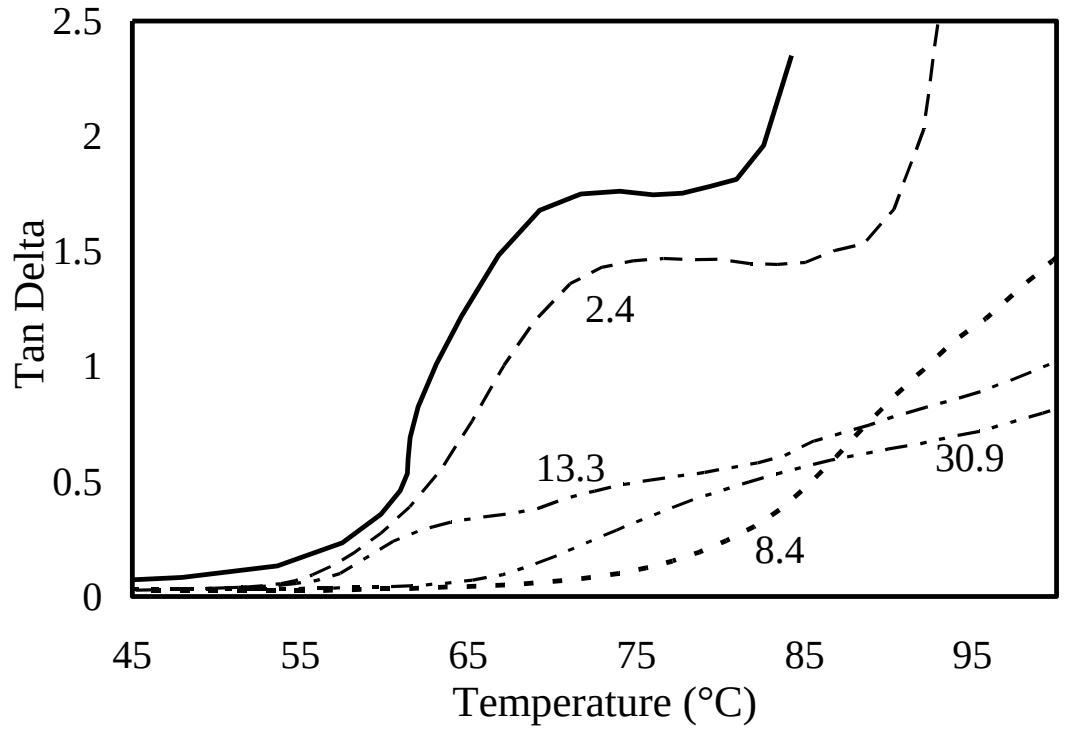

Figure 4.6: Tan delta curves for the hybrids and cast polystyrene.

Tapping Mode Atomic Force Microscopy

AFM images of the PS/SiO_2 hybrid fracture surfaces were acquired in tapping mode to give height and phase images. The morphology of the hybrid is shown in the height image. The polystyrene may deform slightly under the tip while the silica-rich areas should not. Using tapping mode minimizes the force interactions between the tip and sample and should lessen any issues of sample deformation or damage. This difference in hardness between the PS and SiO_2 allows a phase image to be taken concurrently with the height image. The distribution of the SiO_2 can be seen in the phase image where the height image does not differentiate between the two constituents.

The height images in Figure 4.7a-d show the effect of varying weight percents of silica on the morphology of the hybrids fracture surfaces. The hills and valleys show as light and dark respectively. The morphology goes from small granular features to larger granular features showing a cylindrical shape on the surfaces. The low silica content hybrid shows a fracture surface with random

grains and a low average roughness of 9nm. As the grain sizes increase with increasing SiO_2 content their shape shows greater roughness', going from 14 to 40 nm.

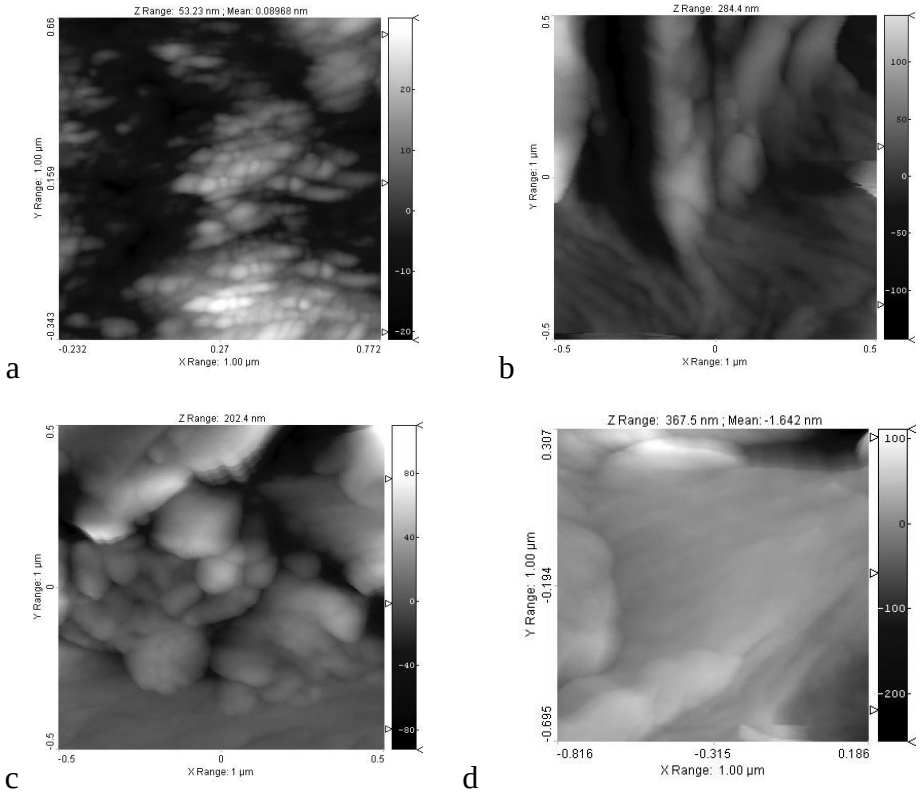

Figure 4.7: Height images of fracture surfaces. A) 2.4 % b) 8.4% c) 13.3 % d) 30.9%

The phase images shown in Figure 4.8a-d show light and dark areas that correspond to the different constituents present in the hybrids. The light areas are the silica and the dark areas are the polystyrene matrix. As the silica content increases more of it appears on the fracture surface. The silica is seen as particles at low weight percents and grows into more of a network at high weight percents. The phase changes that occur along topographical features with large height changes may not be due to silica.

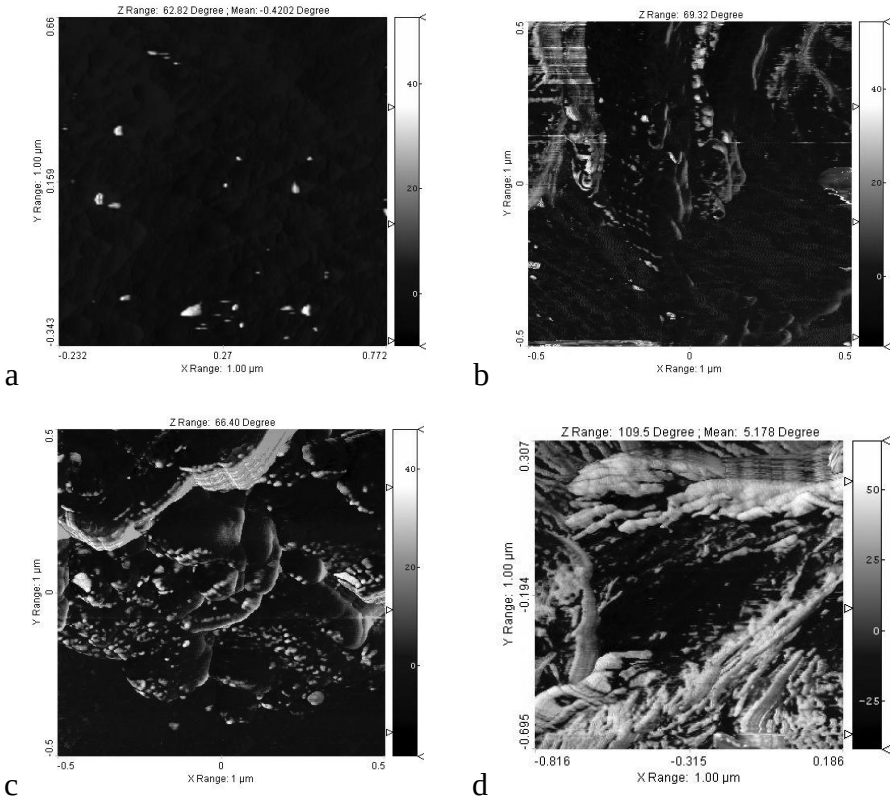

Figure 4.8: Phase images of the hybrids fracture images corresponding to the height images above. A) 2.4 % b) 8.4% c) 13.3 % d) 30.9%

Conclusion

PS-SIO_2 hybrids were prepared using a sol-gel chemistry methodology that is simple and straightforward. The hybrids showed no chemical interaction between the constituents so the resulting properties were relying on good physical interaction. The extent of phase separation between the constituents was determined by TM-AFM.

The TM-AFM images provided valuable insight into the silica formation along fracture edges. The agglomeration of silica at high weight percents interrupted the polystyrene matrix and allowed for easier break point which caused the mechanical response to decline. The thermal properties of the hybrids showed slower degradation pathways but the same onset temperature of degradation as the cast PS. The asymmetry of the tan delta peak made T_g determination impossible for all of the hybrids. The asymmetry could arise from the inhomogeneity of the

hybrids noted by the AFM phase images. All of the weight percents above 2.4% SiO_2 showed phase agglomeration.

While PS has π electrons available from the benzene ring that could potentially interact with the π electrons from the silanol group on SiO_2 that remained from the incomplete condensation and help distribute the two phases homogeneously, the stability of the benzene ring was seen to be a greater driving force. Incorporating weight percents of silica with better distribution could lead to PS-SiO_2 hybrids that show more improvement in their thermomechanical properties. To achieve this chemical modification of PS or SiO_2 may be needed. Overall, PS mixed in a sol-gel synthesis with pre-hydrolyzed TEOS did not produce hybrids with notable improvement. The SiO_2 could be used as filler at low weight percents in PS with little or no effect on the thermomechanical properties.

Chapter 5

PS-co-PMMA-SiO_2 sol-gel prepared inorganic-organic hybrids

Introduction

Creating copolymers provides a method of utilizing two different structural units to give a new material that shows properties characteristic of a single polymer. A copolymer results in better control of surface structure when compared with polymer blends[78]. The bulk properties of a copolymer will also differ from that of the blend or the individual polymers and can be manipulated by varying the concentration of the structural units[79]. The nearly limitless possible combination to create copolymers brings many new materials into areas such as biosensors, to adhesives, lubricants and coatings.

To further enhance the properties of polymers, sol-gel techniques are being used to combine an inorganic oxide with the organic polymer in a hybrid material. Tetraethoxysilane (TEOS), an organically modified inorganic material, is used in many studies to obtain a silica containing hybrid. The silica can be added and the physical interactions between constituents can be relied upon to enhance properties, or it can be modified to create chemical bonds with the polymer chain. Polystyrene (PS) has been combined with silica in various preparations[21-22, 73, 76] and Poly(methyl methacrylate) (PMMA) silica hybrids are one of the most studied systems[63, 67, 80-81]. The combination of PS-co-PMMA with silica to form hybrids has not been studied.

To realize improved properties the hybrid must not have macroscopic phase separation between the polymer and inorganic constituents. The silica hydrolyzed from TEOS under acidic conditions grows in a more linear manner than that obtained from basic catalyzed reactions and as a result may allow for a greater number of interactions with the polymer.[23-24] In this work to determine the silica distribution in the bulk of the material, tapping mode atomic force microscopy (TM-AFM) was employed to image fracture surfaces. TM-AFM has

been used on hybrid fracture and external surfaces of polymer-inorganic hybrids to show how materials with different mechanical properties are dispersed[29].

Preparation of a new polymer-inorganic hybrid consisting of polystyrene-co-poly (methyl methacrylate) and silica was achieved using a sol-gel process. The silica was prepared from the hydrolysis and polycondensation of tetraethoxysilane (TEOS). From previous studies, TEOS has been seen to interact favorably with polystyrene and poly (methyl methacrylate) so the introduction of TEOS into the copolymer should improve thermal and mechanical properties. Thermogravimetric analysis (TGA) and dynamic mechanical analysis (DMA) were used to measure these properties. The chemical environment of the silica in the polymer was studied with FTIR. TM-AFM was used to determine the hybrids morphology and to see the phase distribution.

Experimental

Polystyrene-co-poly (methyl methacrylate) (PS-co-PMMA) (22wt% Styrene) and tetraethylorthosilicate (TEOS) were obtained from Aldrich. Tetrahydrofuran (THF) was obtained from Omnisolv and chloroform ($CHCl_3$) from Fischer. All chemicals were used as received.

The PS-co-PMMA (1.0 g) was added to 10.0g of a 50/50 w/w mixture of THF/$CHCl_3$. The solution was stirred until fully dissolved at room temperature. The inorganic precursor solution was made by hydrolyzing 15.0 mL of TEOS with 4.85 mL of 0.01M HCl. This was stirred for 60 minutes at room temperature. In order to create the hybrids with varying silica weight percents varying amounts of the precursor solution were added using a 0.25 micron filter and then stirred for approximately 1 hour. The amounts added were calculated based on the yield of silica from the precursor preparation. The actual amount of silica present was determined by thermogravimetric analysis. The hybrid mixture was cast in an aluminum weighing dish and dried covered for 3 days at room temperature. The sample was then placed in an oven at 65 °C for 6-8 days. The samples obtained had no cracks when removed from the oven.

A separate sample of the PS-co-PMMA was prepared from 1.0g of the polymer dissolved in 10.0 g of the 50/50 w/w solvent mix. To this was added ethanol and water in amounts resulting from a typical hydrolysis reaction of TEOS. The copolymer was then cast and subjected to the same drying treatment as the hybrids.

FTIR spectroscopy was used to identify the chemical structure of the hybrids and copolymer. The samples were dissolved in chloroform and dropped onto a KBr window. The spectra were collected using a Nicolet 510P with 2 cm^{-1} resolution. The KBr windows were dried in an oven at 100 °C before running to help eliminate adsorbed water. The thermal and mechanical properties were characterized by TGA (TA Instruments) and DMA (Perkin Elmer). The TGA was run in air with a ramp rate of 10 °C/min to 600 °C and then the temperature TGA was held at 600 °C until the weight stopped changing. The DMA was run using sample dimensions of approximately 10 mm x 10 mm x 0.3 mm. A ramp rate of 2 °C/min to 170 °C using frequencies of 0.5, 1.0, 2.0, 5.0 and 10.0 Hz was employed. Tapping mode AFM (Nanoscope III) images were obtained on the external and fracture surfaces of the hybrids. The scan rate was kept below 2 Hz. The tips (Vistaprobes) were <10 nm in radius with a spring constant of 40 N/m and a resonant frequency of 300 kHz. The scan areas were 1 x 1 μm, 2 x 2 μm or 5 x 5 μm.

PS-co-PMMA Hybrids

Appearance

The PS-co-PMMA-SiO_2 hybrids are shown below in Figure 5.1. The hybrids with low silica content appear clear and turn more opaque as silica content is increased. The highest weight percent hybrid shows a different surface morphology that can be seen with the naked eye. This hybrid is also no longer opaque enough to see through.

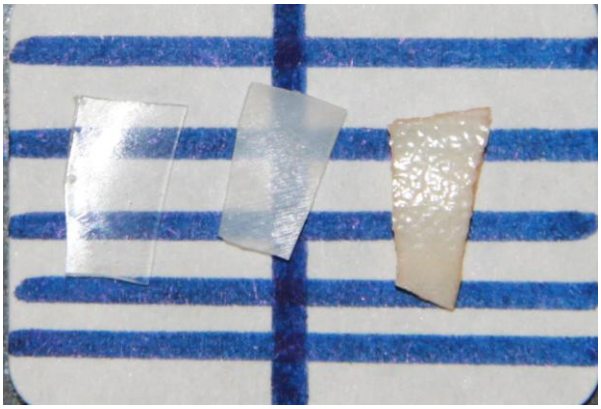

Figure 5.1: Appearance of PS-co-PMMA-SiO_2 hybrids. From left to right SiO_2 content is 0.129%, 9.15%, and 30.4%.

Fourier Transform Infrared Spectroscopy

The copolymer is a random arrangement of PS and PMMA monomers and the appearance of peaks characteristic to both monomers are present in the infrared spectra. Figure 5.2 shows the spectra of the copolymer and the hybrids prepared using it. The C-H stretches show peaks around 2900 cm^{-1}. The carbonyl from the PMMA portion shows up very prominently at 1730 cm^{-1}. The range between 500-1500 cm^{-1} contains many vibrations and stretches from both monomer units that are difficult to assign to a specific motion.

As pre-hydrolyzed TEOS is added to the copolymer the peak centered around 1000-1100 cm^{-1} is seen to grow, which is characteristic of Si-O motions from SiO_2. In the 9.15% and 30.4% SiO_2 hybrids there is an O-H stretch at 3400 cm^{-1} that is believed to be from silanol since a Si-O-H stretch is seen at 930 cm^{-1}. The 2.0% SiO_2 hybrid sample does not show much change in the frequency range relating to SiO_2. Since the weight percent is low the SiO_2 may be lost in the copolymer background. No clear shifts in the hybrid spectra from the copolymer spectra were seen which makes assigning any chemical interactions difficult. It is possible that the hybrids with silanol present will interact with the carbonyl. From the PS-SiO_2 study in Chapter 4 no favorable chemical interaction between the PS portion of the copolymer and silanol or SiO_2 is expected.

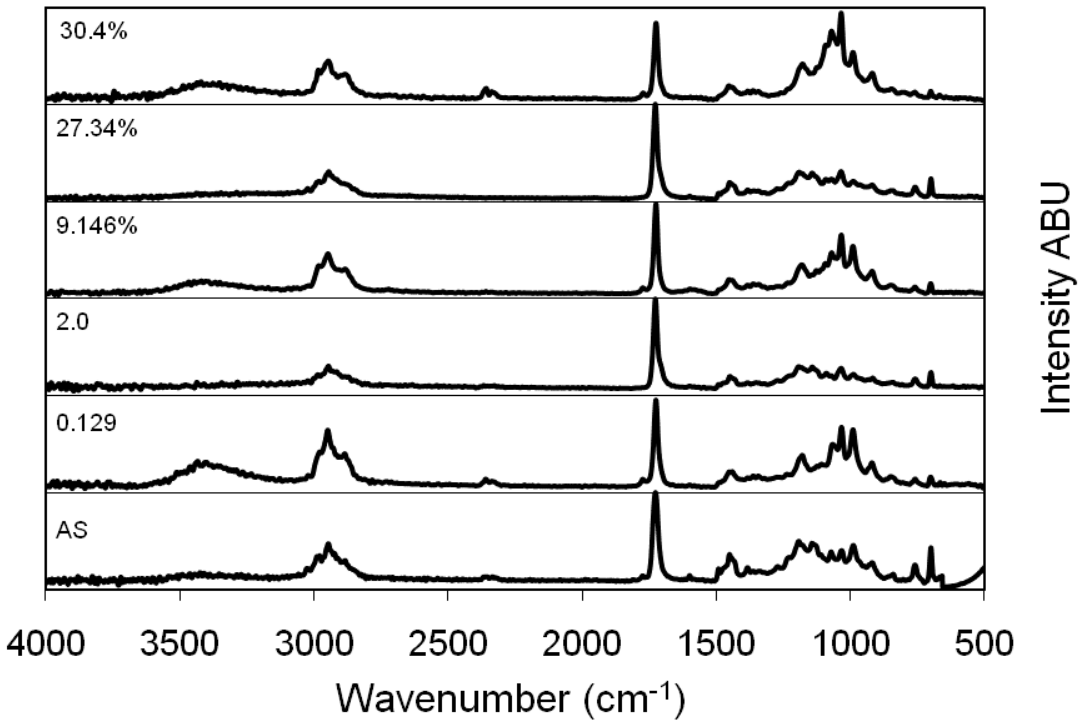

Figure 5.2: FTIR spectra of the prepared hybrids and copolymer were run on a KBr window. The weight percent of silica determined from TGA is shown on the traces.

Thermogravimetric Analysis

The TGA data in Figure 5.3 shows that the addition of silica to PS-co-PMMA produces a shift in the decomposition temperature onset and an increase in the 50% weight loss temperature of about 50 °C for the highest silica content. The amount of silica was determined from the mass remaining at 600 °C. The weight decrease seen before the decomposition of the polymer is from the loss of retained solvent and hydrolysis byproducts. The corresponding derivative curves shown in Figure 5.4 more clearly illustrate the thermal shifts mentioned above.

From the derivative curves the onset temperature can be clearly determined. The hybrids show the same onset temperature as the cast copolymer sample. The shift in the degradation pathway temperatures is not improved greatly until a weight percent of 30.4 SiO_2 is achieved. Weight percents between 9 and 30 may also cause an improvement in the degradation pathway temperatures but were

not prepared in this study. The degradation pathway for the copolymer and the hybrids occur over a broad temperature range. The mechanistic pathway of this copolymer has not been studied.

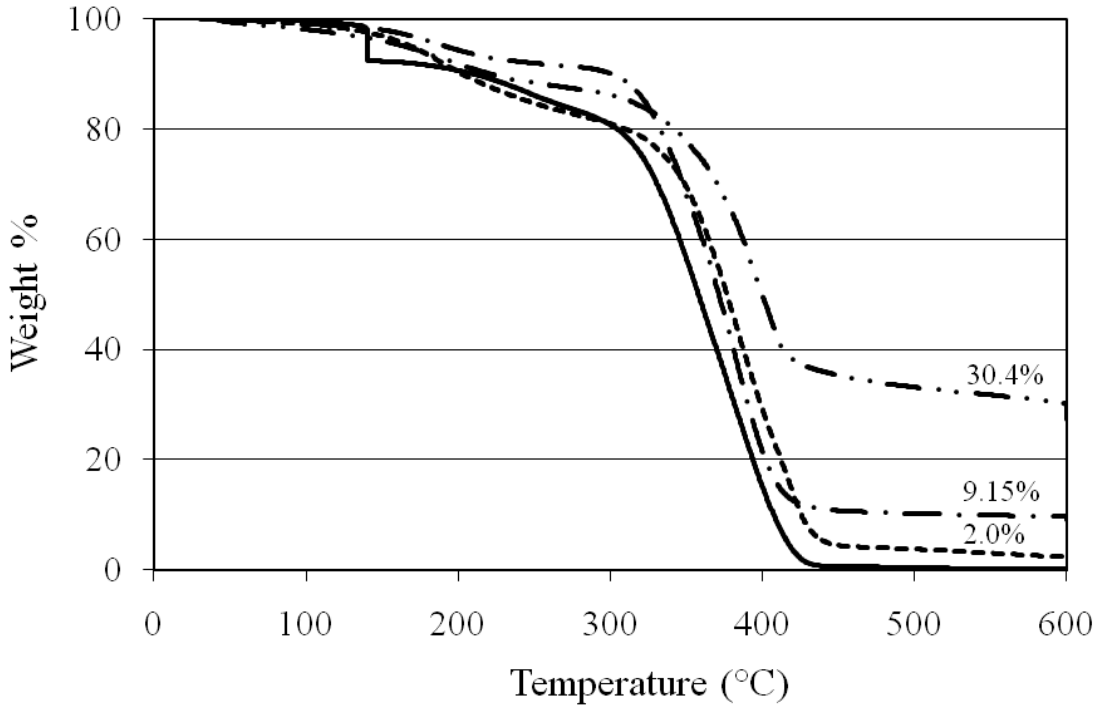

Figure 5.3: TGA traces of hybrids and copolymer. Silica content taken as weight percent left at 600 °C.

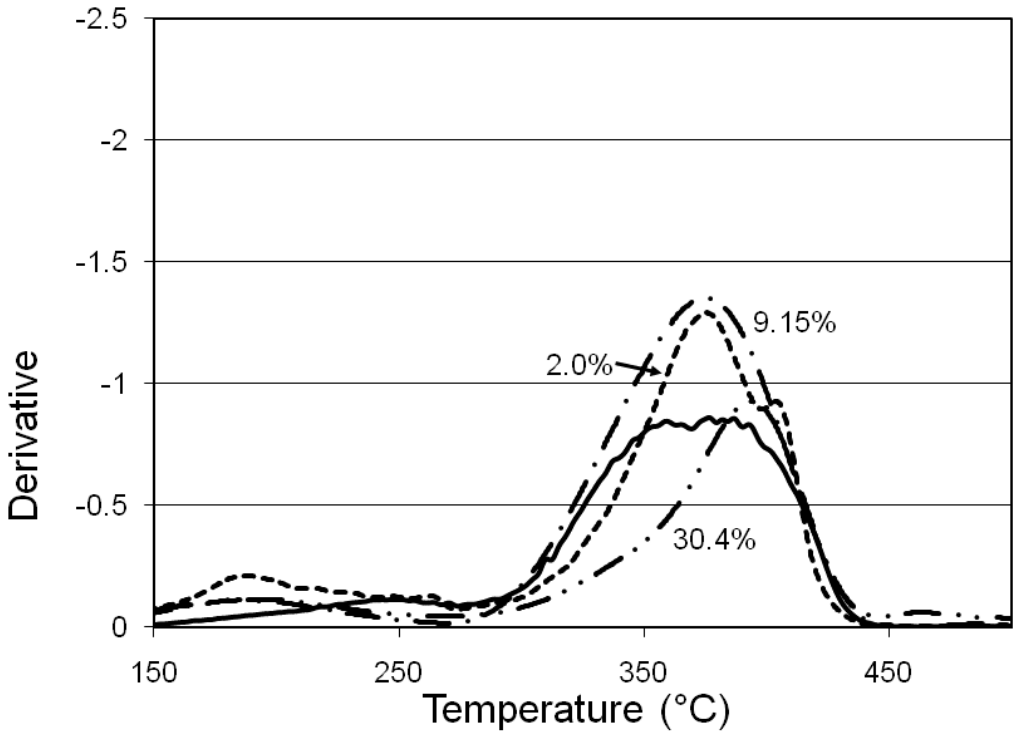

Figure 5.4: Corresponding derivative curves for TGA traces shown in Figure 2.

Dynamic Mechanical Analysis

Dynamic mechanical analysis (DMA) was performed on the hybrids and a comparable cast copolymer sample. Figure 5.5 shows the resulting traces. As expected, the modulus at room temperature shows little change with silica content[45]. The glassy plateau is extended to higher temperatures with increasing silica content. A more pronounced change is seen in the glass transition range and rubber modulus. The addition of silica increases these to higher temperatures. The increase in temperature in the transition range is the same for multiple silica weight percents, i.e. the 9% and 30%.

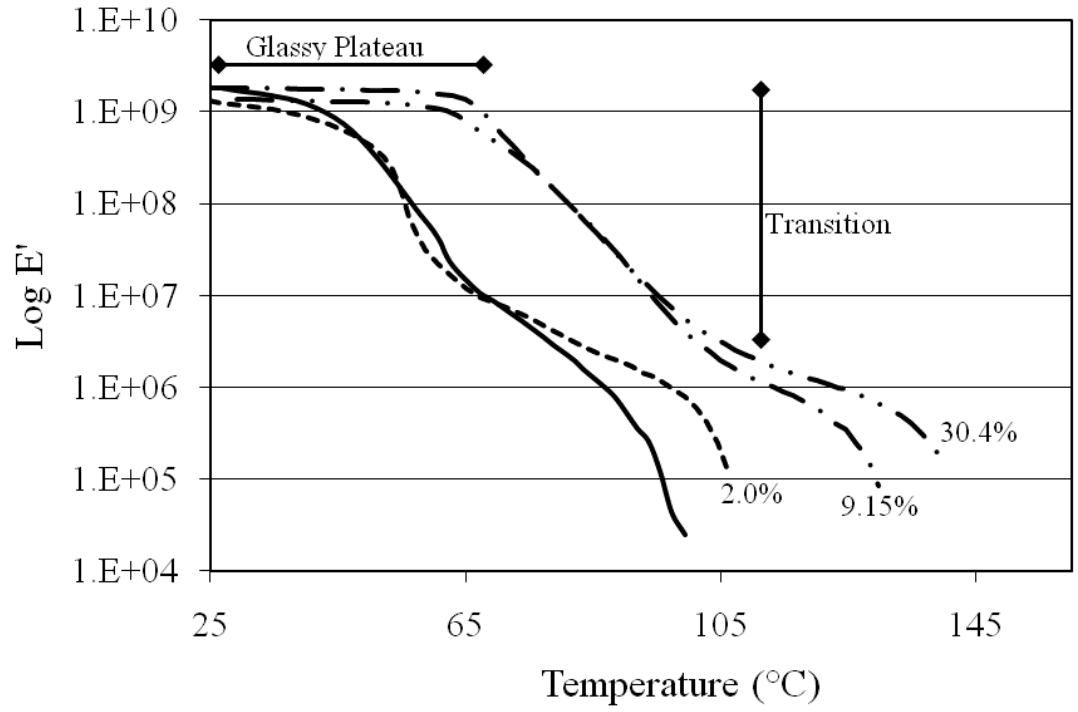

Figure 5.5: DMA traces for PS-co-PMMA hybrids showing increase in transition range and rubbery plateau along arrow with increasing silica content.

The corresponding tan delta curves are shown in Figure 5.6. The peak of the curve is taken as the glass transition temperature of the hybrid. The cast copolymer is shown as the solid black line. One transition is noted before the copolymer fails at higher temperatures on the as received sample. This shows that the styrene and methyl methacrylate components polymerized to the copolymer are arranged in a random manner that does not allow for phase separation, otherwise two distinct glass transition temperatures would be present. The addition of silica to the hybrids causes the curves to shift to higher temperatures. The hybrid with the 9.15 silica weight percent shows two peaks which could mean the silica interacted with portions of the copolymer causing the components (PS and PMMA) to separate into individual glass transition temperatures.

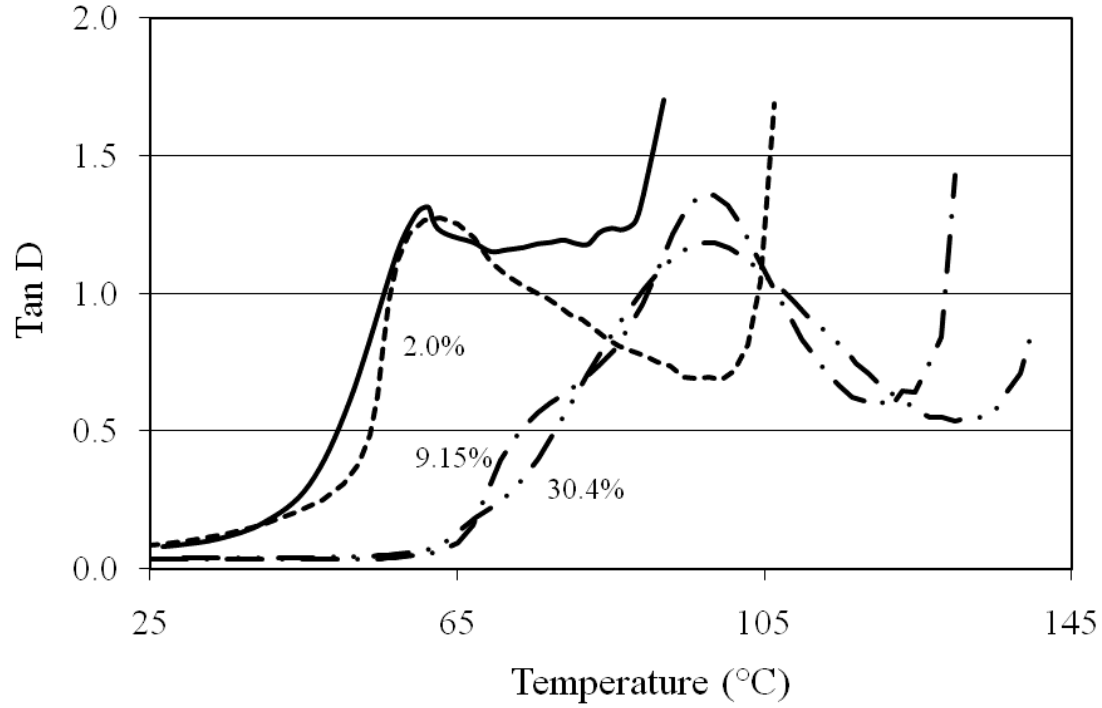

Figure 5.6: Tan Delta curves for hybrids. Peak taken as T_g value.

The activation energy (E_a) for the glass transition was determined from the Arrhenius plot shown in Figure 5.7. The cast sample appears on the right hand side of the Figure and shows definite scatter in the data points. The cast PS-co-PMMA film's scatter could be due to residual solvent causing a larger free volume that allows for more random copolymer movements when approaching the T_g temperature. The PS-co-PMMS SiO_2 hybrid curves all show data points that follow the trendline. The addition of SiO_2 does seem to stabilize the T_g as different frequencies are measured. The activation energy plots show that the hybrids have similar values to the cast PS-co-PMMA.

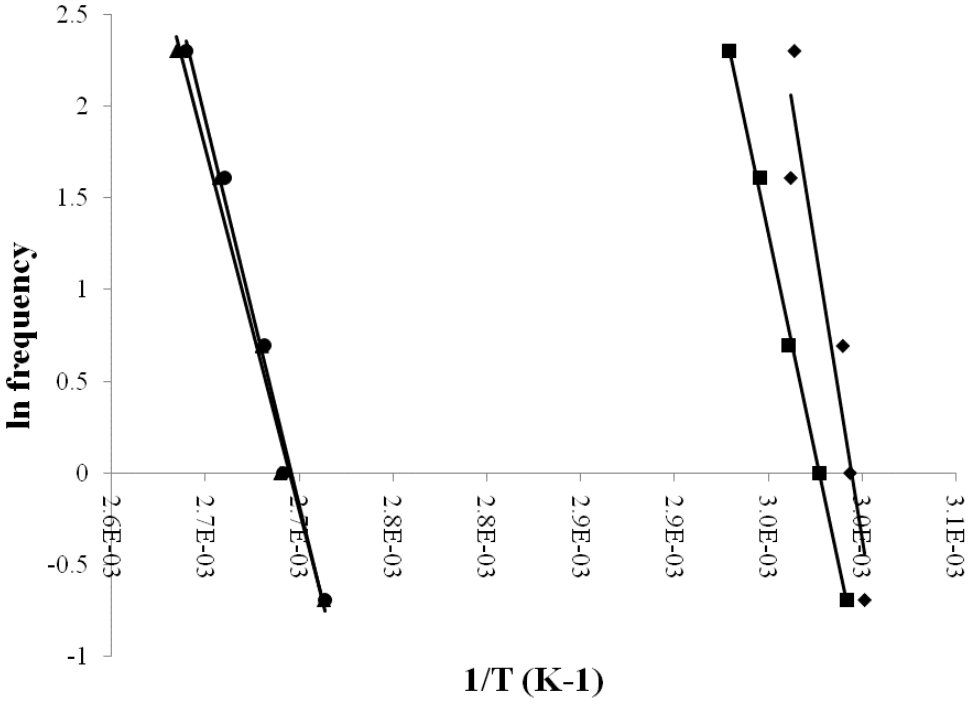

Figure 5.7: Arrhenius plots to determine the activation energy of the glass transition temperature for PS-co-PMMA-SiO_2 hybrids.

Tapping Mode Atomic Force Microscopy

The PS-co-PMMA hybrids contain constituents which possess different mechanical properties. The TM-AFM images shown in Figure 5.8 and 5.9 give the topography and phase of the surface and fracture respectively. The change in the height image reflects the piezoelectric response necessary to maintain fixed oscillation amplitude. The changes in the phase image reflect the oscillation delay relative to the excitation signal[82]. Taken concurrently, the height and phase allow the nanophase separation to be described relative to the topography and mechanical properties.

The surface images in Figure 5.8 show no phase separation at low silica content (a). More phase separation is seen as the silica content is increased (b-d) and the RMS values are reported in Table 5.1. The topography variations show a good correspondence to the phase changes. The average roughness's for all hybrids stay lower than 4 nm. The changes in topography due to silica content show island like formations growing in without much change to the z range.

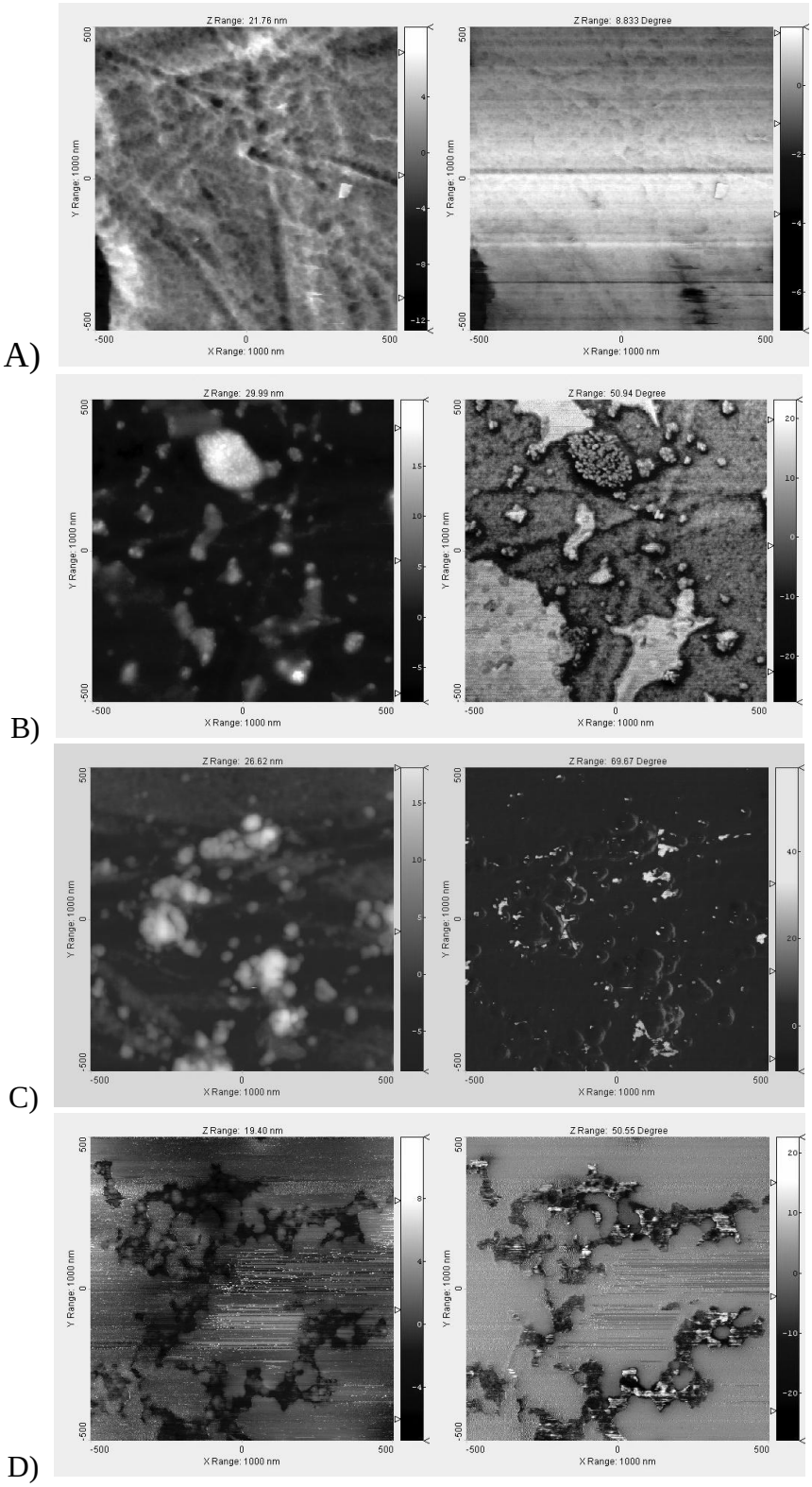

Figure 5.8: Height and Phase images of the surface of copolymer hybrids. A) 0.13% silica, B) 2.0% silica, C) 9.15% silica, and D) 30.4% silica.

Table 5.1: Roughness values and phase difference of ps-co-pmma/silica hybrid surfaces and fractures.

Sample	RMS (nm)	Phase (Degree)
0.13% surface	2.02	8.83
2.0% surface	3.73	50.94
9.15% surface	3.72	69.67
30.4% surface	1.78	50.55
0.13% fracture	6.03	107.7
2.0 % fracture	57.58	76.92
9.15% fracture	17.43	31.34
27.34% fracture	4.81	83.27

The fracture surfaces shown in Figure 5.9 show a random topography for the 0.13% hybrid with a more particle like appearance as the silica content is increased. The silica is seen to be distributed randomly throughout the phase images with no clear relationship to the topography noted. The high phase seen in the 0.13% hybrid shows phase change along topographical changes, which may not be due to the constituents. The silica content does seem to be the cause behind the changes in topography seen along the fractures. The height in the topography changes randomly and seems to depend on the scan site, which causes the roughness to fluctuate randomly.

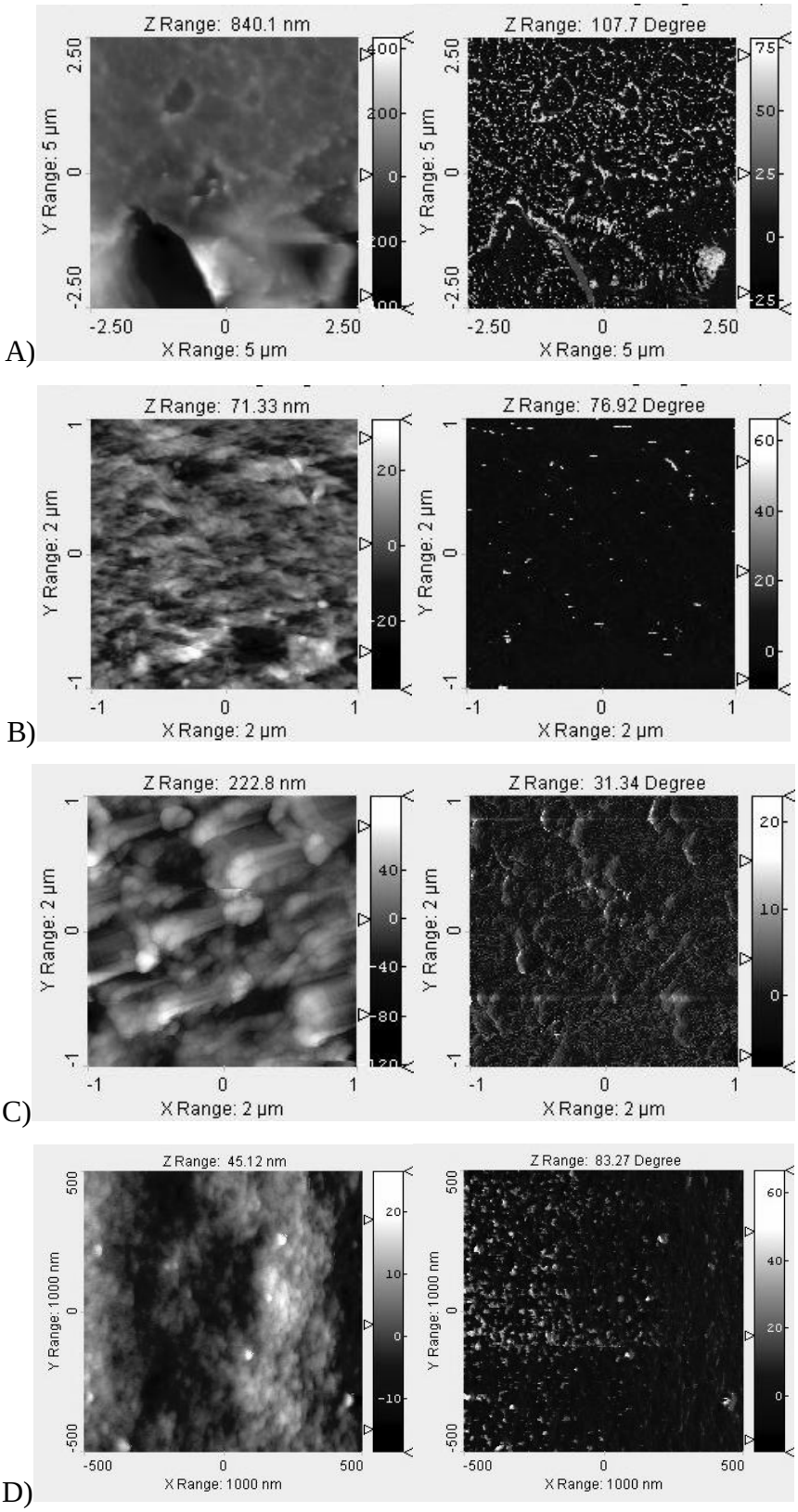

Figure 5.9: Height and Phase images of the fractures of ps-co-pmma/silica hybrids. A) 0.13% silica, B) 2.0% silica, C) 9.15% silica, D) 27.3% silica.

Conclusion

A PS-co-PMMA copolymer was successfully combined with pre-hydrolyzed TEOS to create new polymer-inorganic hybrids with varied silica content from 0 – 30 weight percent. The silica was seen on both the surface and throughout the fracture. The roughness of the external surface remained approximately constant with silica content. The SiO_2 appeared to phase separate at the external surface but did not on the internal fracture surfaces. The silica also causes morphological changes on the fracture surface going to a more particle like appearance. The glassy modulus changed little with added silica but moved to higher temperatures and the transition region and rubber plateau widened. These effects did not vary significantly from the samples with little silica to those with a large amount. The reason for this may be linked to the degree of phase separation seen on the external surface and the lack of significant random phase separation along the fracture surface.

Chapter 6

Tri-block copolymer PS-PI-PS-SiO_2 sol-gel prepared inorganic-organic hybrids

Introduction

Polymer-inorganic materials provide a means to combine two unlike materials into a new composite that retains properties from both constituents. The hybrid interface and size of the inorganic material in the organic polymer matrix affects the mechanical properties. Controlling the structure, and in turn the length scale, can lead to better control over the mechanical properties. Utilizing two polymers that are dissimilar to create a block copolymer can give you control over the structure.

The combination of polystyrene with polyisoprene into a tri-block copolymer creates a thermoplastic elastomer that has already found use as a pressure sensitive adhesive sealant. This tri-block combines the polystyrene glassy domains with a bridging polyisoprene rubbery domain.

This tri-block copolymer should allow for the incorporation of pre-hydrolyzed TEOS into a network domain. The only drawback with this particular block copolymer is that from our previous work with polystyrene (Chapter 5) we saw that the pre-hydrolyzed silica did not improve the mechanical or thermal properties in an appreciable manner. The pre-hydrolyzed TEOS could entangle with the rubbery block, causing a higher modulus value, or the self arrangement of the block copolymer could cause the silica particles to grow in the free volume spaces.

This study looked at PS-PI-PS combined with pre-hydrolyzed TEOS to create inorganic-organic hybrids. The amount of pre-hydrolyzed TEOS was varied to give us a range of weight percents to characterize. The SiO_2 should lead to discrete particle formation in the tri-block copolymer or incorporation in one of the blocks. Since the constituents are being combined in a sol-gel chemistry step to

create a Class 1 hybrid (only physical interactions) the SiO_2 could also entangle with one of the block to improve the thermal and mechanical properties.

Methodology

The tri-block copolymer polystyrene-polyisoprene-polystyrene (PS-PI-PS) (22wt% Styrene) and tetraethylorthosilicate (TEOS) were obtained from Aldrich. Tetrahydrofuran (THF) was obtained from Omnisolv and chloroform ($CHCl_3$) from Fischer. All chemicals were used as received.

The PS-PI-PS was weighed out to 1.0g and then dissolved in 5.0g each of THF and $CHCl_3$. The pre-hydrolyzed TEOS solution was prepared from 15.0mL of TEOS and 4.85 mL of 0.01M HCl. This mixture was stirred at room temperature for 1 hour. Various amounts of the pre-hydrolyzed solution were added to our dissolved tri-block copolymer through a 0.2 micron filter. The resultant hybrid solution was stirred for 1hour before casting into an aluminum weigh dish. This dish was allowed to sit covered for 3 days at room temperature. The hybrid was placed in an oven at 65 °C for 4 days. The shorter drying time was used since this polymer was stretchy and allowed for easier solvent removal.

A separate PS-PI-PS sample with no pre-hydrolyzed TEOS was prepared as above for comparison with our hybrids. To this was added ethanol and water in amounts resulting from a typical hydrolysis reaction of TEOS. The tri-block copolymer was then cast and subjected to the same drying treatment as the hybrids.

FTIR spectroscopy was used to identify the chemical structure of the hybrids and copolymer. The samples were dissolved in chloroform and dropped onto a KBr window. The spectra were collected using a Nicolet 510P with 2 cm^{-1} resolution. The KBr windows were dried in an oven at 100 °C before running to help eliminate adsorbed water. The thermal and mechanical properties were characterized by TGA (TA Instruments) and DMA (Perkin Elmer). The TGA was run in air with a ramp rate of 10 °C/min to 600 °C and then the temperature TGA was held at 600 °C until the weight stopped changing. The DMA was run using sample dimensions of approximately 10 mm x 10 mm x 0.3 mm. A ramp rate of 2

°C/min to 170 °C using frequencies of 0.5, 1.0, 2.0, 5.0 and 10.0 Hz was employed.

A fracture surface for the PS-PI-PS-SiO_2 hybrids could not be obtained at room temperature. To overcome this problem the hybrids were dipped in liquid nitrogen and then fractured. This still caused a problem because the hybrids warmed up too quickly when removed from the liquid nitrogen. Since no fracture surface could be obtained, tapping mode atomic force microscopy was only run on the external surface using a Nanoscope III from Digital Instruments.

PS-PI-PS Hybrids

Appearance

The hybrids were noted to be very stretchy upon removal from the aluminum weigh pan. Also, there was powder left behind in the pan that appeared to be SiO_2 from the pre-hydrolysis of TEOS. The hybrids themselves were clear and showed bubbles at random points. The appearance of the hybrids is shown in Figure 6.1. As the SiO_2 was introduced and increased round formations are seen to form in the polymer matrix. The silica particle that caused these formations did not always remain with the sample, most fell out when the sample was removed from the aluminum weigh dish.

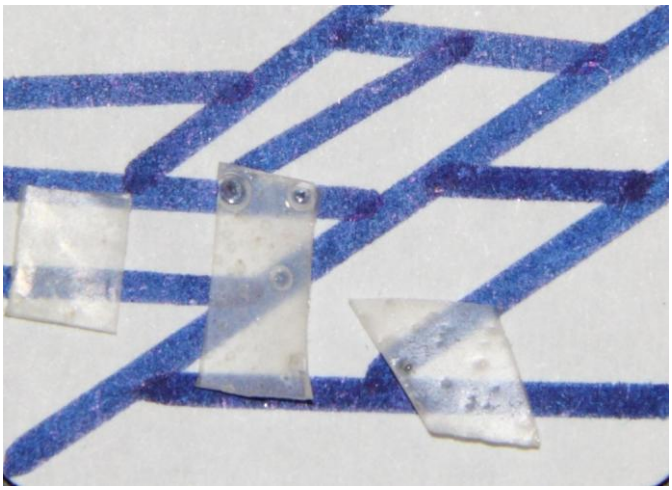

Figure 6.1: Appearance of PS-PI-PS-SiO_2 hybrids. From left to right SiO_2 amount increases.

Fourier Transform Infrared Analysis

The Fourier transform infrared spectra (FTIR) in Figure 6.2 show the tri-block copolymer as well as the hybrids. The peak at 698 cm^{-1} is indicative of the presence of an aromatic group that originates from the out of plane C-H stretch of the hydrogen attached to the benzene ring. The peak at 1450 cm^{-1} is from the carbon-carbon bonds stretch in the benzene ring. These stretches along with the C-H stretches appearing above 3000 cm^{-1} indicates the presence of the polystyrene block in this tri-block copolymer. The peaks slightly lower than 3000 cm^{-1} are from the alkane C-H stretches present on both polymers that make up the tri-block copolymer. The carbon-carbon double bond stretch from the polyisoprene shows peaks in the range 1600-1700 cm^{-1}. After identifying the peaks present from the PS-PI-PS backbone, the spectra that contain SiO_2 prepared from pre-hydrolyzed TEOS show a change in the peaks centered around 1100 cm^{-1}, which are indicative of a Si-O-Si stretch. There is a peak centered around3400 cm^{-1} that is present in all of the FTIR spectra taken that could be from incomplete hydrolysis or adsorbed water.

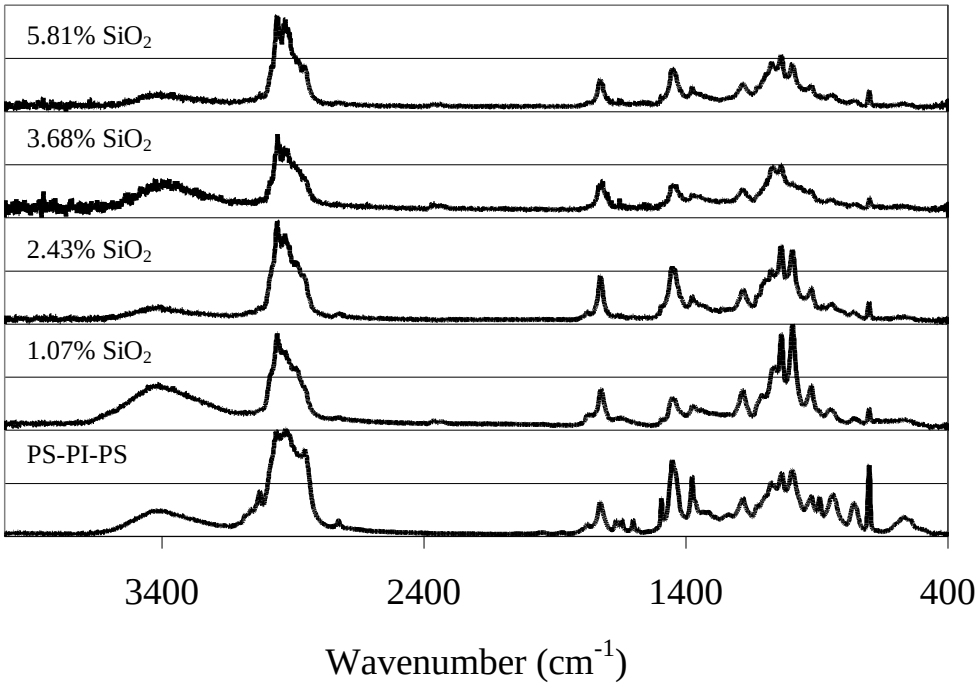

Figure 6.2: FTIR spectra for PS-PI-PS-SiO_2 hybrids.

Thermogravimetric Analysis

The preparation of the block copolymer polystyrene-polyisoprene-polystyrene (PS-PI-PS) following the methodology above did not have the desired effect. The PS-PI-PS was dissolved in 5.0g each of tetrahydrofuran (THF) and chloroform ($CHCl_3$). After that the pre-hydrolyzed TEOS solution was added in varying amounts to produce hybrids with different SiO_2 weight percents. Figure 2.20 shows the thermogravimetric analysis (TGA) curves obtained from the hybrids. The curves show that no solvent was retained (THF, $CHCl_3$, or ethanol) and that the remaining weight percents for the SiO_2 amount were much less than predicted by the amount of pre-hydrolyzed TEOS added. From the TGA data, it was determined that this block copolymer did not interact in a favorable manner to incorporate the silica.

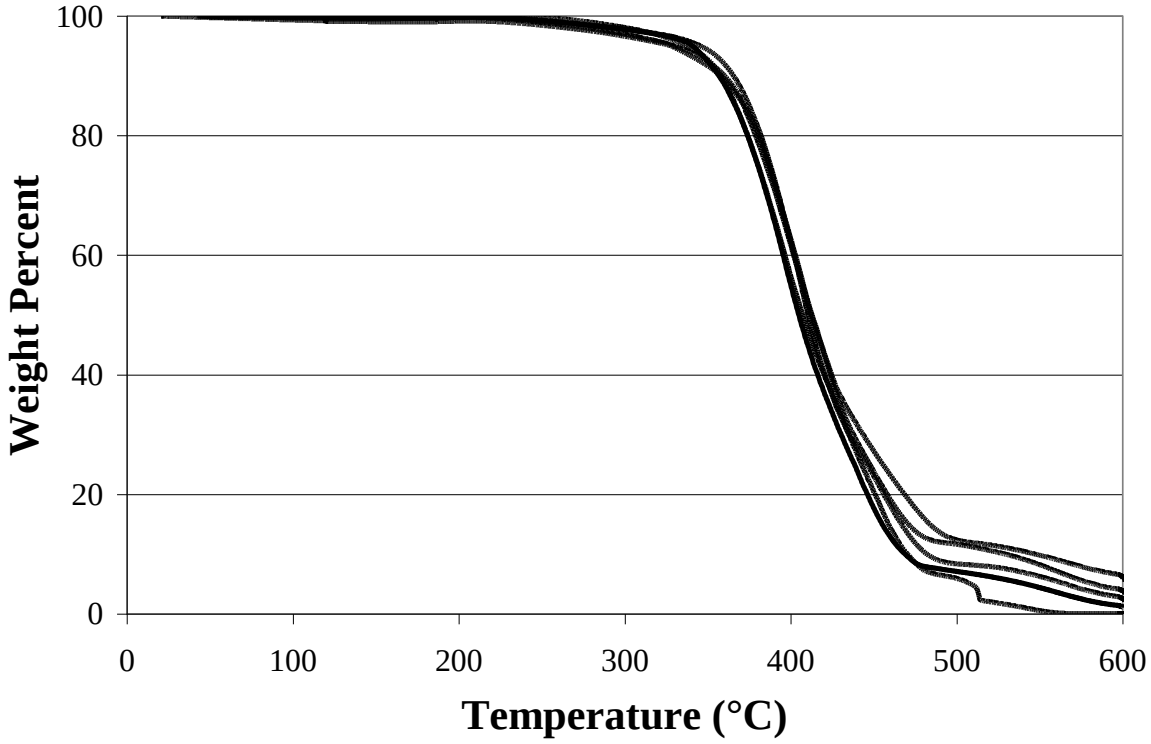

Figure 6.3: TGA traces for PS-PI-PS-SiO_2 hybrids.

Dynamic Mechanical Analysis

The hybrids were subjected to tensile tests using a dynamic mechanical analyzer. The results, in Figure 6.3, show mechanical properties that all appear the same. The traces show no correspondence with inorganic oxide content and gave values that correspond with the block copolymer with 0 weight percent silica. The limits of the DMA were reached with these samples around 120 °C.

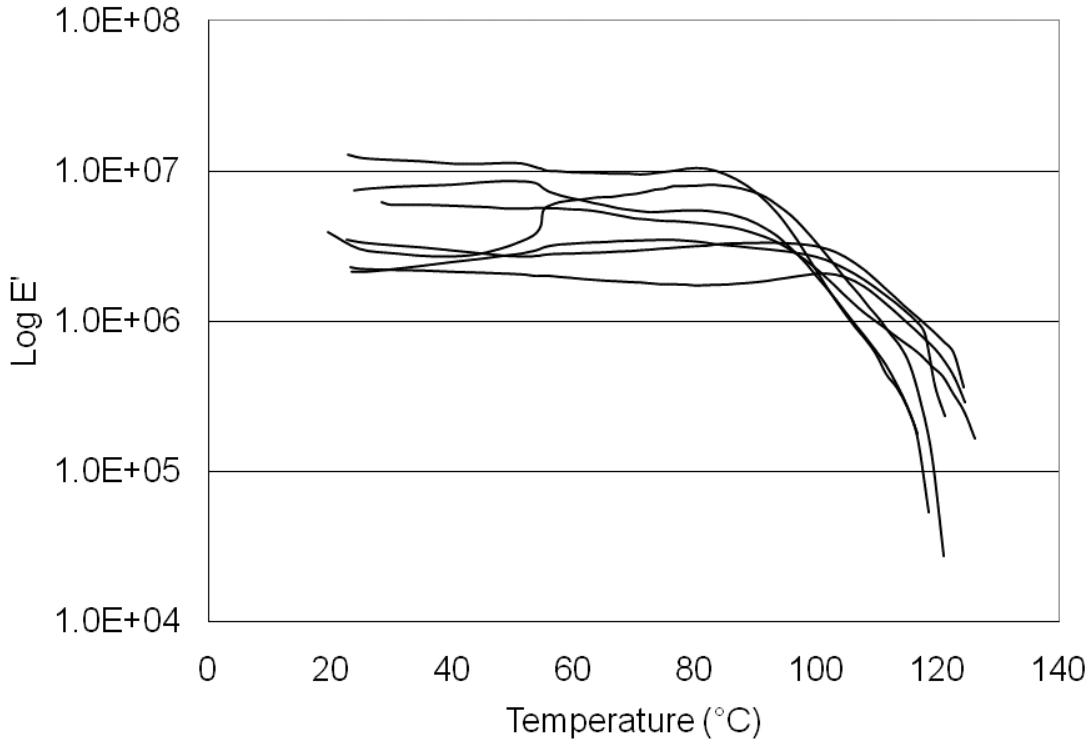

Figure 6.4: DMA traces for PS-PI-PS-SiO_2 hybrids.

Tapping Mode Atomic Force Microscopy

The PS-PI-PS tri-block copolymer's external surface was imaged as well as the hybrids that were prepared. As mentioned, no fracture surfaces were obtained for this stretchy polymer. The rubbery polyisoprene domain also made image acquisition difficult due to the tip-sample interactions. The PS-PI-PS with no inorganic material content shows a lamellar structure on the surface. This is clearly

seen in the phase image with the topography matching closely to the differences in phase. While a large topographical change could cause a difference in the phase image, the z height is around 18.30 nm for this sample and the correspondence between the two images is not an issue. The lamellar formation of the tri-block copolymer could be seen in the phase images of the prepared hybrids even though the topography changed drastically from the PS-PI-PS sample. The higher z range seen in the hybrid topographical images is a result of the indentations seen in the appearance of the hybrids. No identification of which phase was which in the PS-PI-PS could be determined from these images. No SiO_2 was seen as a phase change in the hybrid images. Any phase changes seen showed the lamellar formation of matched the edge of a large topographical change.

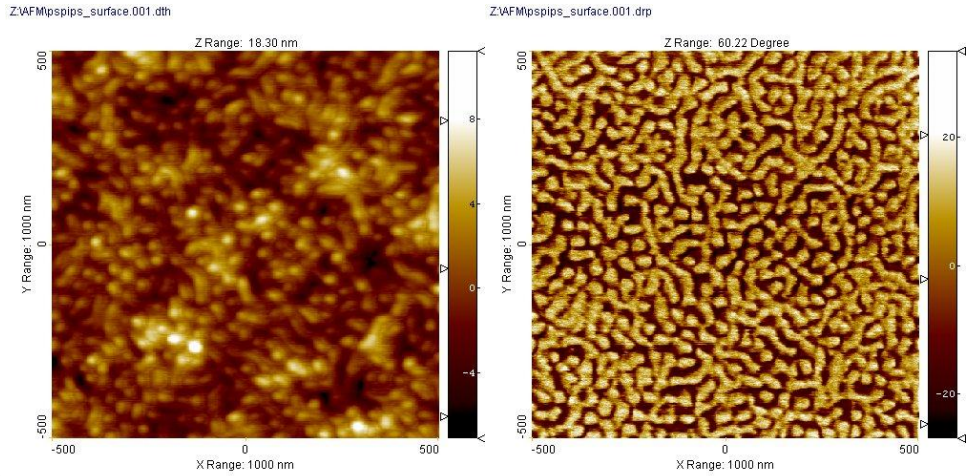

A

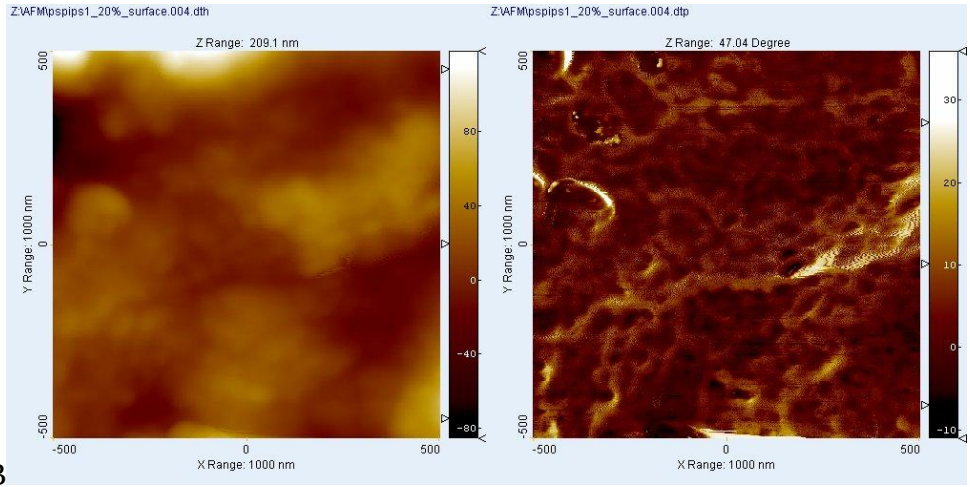

B

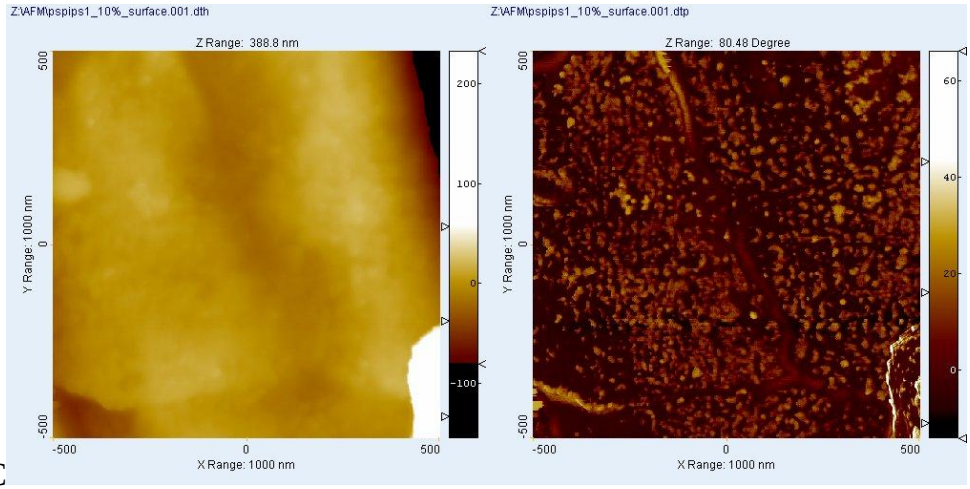

C

Figure 6.5: TM-AFM images of PS-PI-PS and hybrids prepared from PS-PI-PS and SiO_2. A) 0% SiO_2, B) 3.68% SiO_2, C) 5.81% SiO_2

Conclusion:

Utilizing PS-PI-PS as the polymer component in a polymer-SiO_2 hybrid prepared by physically mixing the constituents in a sol-gel process created hybrids that contained much lower amounts of SiO_2 than calculated. It was seen by the appearance of the hybrids that inorganic material was left in the aluminum weigh dish after removal of the hybrid. The large indents seen on the surface of the hybrid did lead to large scale changes in the topography. The mechanical response of the hybrids appeared random and showed values near a PS-PI-PS sample containing no SiO_2. This polymer matrix did however show a constant thermal response with no retention of the solvent mixture being seen. The SiO_2 that was retained was not integrated enough into the polymer matrix to cause any improvement to the thermal or mechanical properties. From the surface topography seen of the hybrids this polymer may find use as a template for the formation of inorganic particles with known dimension.

Chapter 7

Modeling mechanical and thermal properties of polymer-inorganic hybrids

Introduction

Composite materials with two phases, such as our polymer-inorganic hybrids, can show reinforcement of the mechanical properties when a harder phase (inorganic material) is mixed in with a polymer[83]. There are many theoretical models available to predict the elastic modulus and glass transition temperature. The hybrids prepared can be though of as homogeneous mixtures with the silica evenly and randomly distributed throughout. The dispersion of the phases can be determined with many techniques to check experimental data with our model fits such as SEM, TEM or AFM. We used tapping mode AFM to determine the silica distribution through the fracture. The usefulness of fitting models to polymer-inorganic hybrids to predict modulus and T_g would allow for the calculation of the weight percent inorganic component needed to obtain a given set of properties. Our polymer-inorganic hybrid systems provide a variety of chemistry and monomer arrangement against which to test the validity of the following models. If any of these models hold for our polymer-inorganic hybrids they could be applied to comparable systems where the polymer is glassy at room temperature and the chemistry allows fro possible hydrogen bonding or steric hinderance. This will allow for the preparation of hybrids based on a calculated silica weight percent to achieve a given modulus (E') or glass transition temperature (T_g).

Models in Literature

Modulus of Elasticity

The models used for the modulus calculation range from classical averaging schemes to complex schemes. The Voigt and Reuss[42] averages are classical averaging schemes that are simplistic and straightforward. The Voigt model has the constituents being subjected to the same strain. Figure 7.1 illustrates

the arrangement of the constituents, which are assumed to be in parallel for this model. This arrangement allows both the polymer and silica to experience and react to the same strain contributing to the measured stress. The viscoelastic response of the hybrid will then be dependent on the weighted average of the constituents moduli.

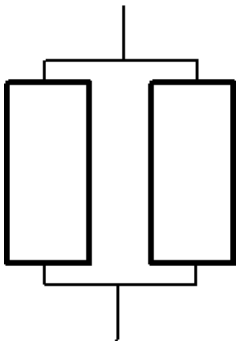

Figure 7.1: Voigt model showing components arranged in parallel.

The modulus is given by

$$E_c = E_f\phi + E_m(1-\phi) \qquad (1)$$

where E_c, E_f, and E_m are the Youngs modulus of the composite, filler and matrix respectively. The volume fraction of the filler is given as ϕ.

The Reuss model has the components arranged in series, which allows them to experience separate strains. Figure 7.2 shows the arrangement of the constituents. This arrangement allows for the lower modulus constituent, the polymer, to experience the strain independently from the higher modulus constituent, the silica. This allows the polymers mechanical properties to contribute more to the hybrids properties.

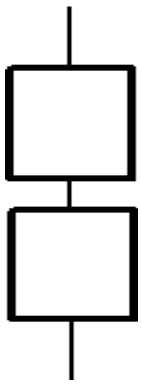

Figure 7.2: Reuss model showing components arranged in series.

The modulus is given by

$$\frac{1}{E_c} = \frac{\phi}{E_f} + \frac{(1-\phi)}{E_m} \tag{2}$$

where the subscripts carry the same meaning as in the Voigt model.

Hashin and Shtrickman[46, 84-85] developed a variational approach to the theory of elastic behavior in multiphase materials. This theory provides and upper and lower bounds for the effective elastic modulus of multiphase materials with arbitrary phase geometry. The model assumes the material is quasi-isotropic and quasi-homogeneous to try and provide bounds that are applicable to real materials. The modulus for the upper and lower bounds are given by

$$K_c^u = K_p + \frac{1-\phi}{\frac{1}{K_m - K_p} + \frac{3\phi}{3K_p + 4G_p}} \tag{3}$$

$$K_c^l = K_m + \frac{\phi}{\frac{1}{K_p - K_m} + \frac{3(1-\phi)}{3K_m + 4G_m}} \tag{4}$$

$$G_c^u = G_p + \frac{1-\phi}{\frac{1}{G_m - G_p} + \frac{6\phi(K_p + 2G_p)}{5G_p(3K_p + 4G_p)}} \tag{5}$$

$$G_c^l = G_m + \frac{\phi}{\frac{1}{G_p - G_m} + \frac{6(1-\phi)(K_m + 2G_m)}{5G_m(3K_m + 4G_m)}} \quad (6)$$

where the subscripts p and m refer to the filler and matrix respectively. The bulk modulus, K, and shear modulus, G, of the filler and matrix are calculated before being related to the Youngs modulus using

$$E = \frac{9KG}{3K + G} \quad (7)$$

The Hashin and Shtrikman fit provide more narrow bounds than either the Reuss or Voigt model does when calculating the modulus.

The Kerner equation provides a shear modulus calculation that takes into account a continuous and discontinuous phase between the constituents. This equation is said to fit systems best when the polymer is glassy and the filler is spherical. The Kerner equation is given by

$$\frac{G_c}{G_p} = \frac{G_f\phi_f / [(7-5\nu)G_p + (8-10\nu)G_f] + \phi_p / [15(1-\nu)]}{G_p\phi_f / [(7-5\nu)G_p + (8-10\nu)G_f] + \phi_p / [15(1-\nu)]} \quad (8)$$

where G is the shear modulus, ϕ is the volume fraction and ν is the poisson ratio of the polymer (usually between 0.35-0.40 for a glassy polymer). The subscripts c, p, and f are for the composite, polymer and silica respectively. To relate the Kerner equation's shear modulus to the Youngs the following relationship can be used

$$E = 2(1+\nu)G \quad (9)$$

The last model we will look at to calculate the modulus for our data set is the Guth-Smallwood equation. This equation is normally used to predict the modulus

of elastomers that are reinforced with silica or carbon black. The theory assumes the filler is dispersed in the polymer and uses the following equation

$$\frac{G_c}{G_p} = 1 + 2.5\phi_f + 14.1\phi_f^2 \qquad (10)$$

where G_c and G_p are the shear modulus of the composite and polymer respectively. The Youngs modulus can be calculated again by using equation 9.

Glass Transition Temperature

The glass transition temperature, T_g, of a polymer composite materials depends on the interactions present and the extent of mixing. If the attraction between the polymer and silica, in our case, is favorable an increase in T_g is expected. This improvement is due to a decrease in the overall free volume. The T_g is often seen to appear broader when fillers are introduced to the system. Not many models are available to calculate the T_g based on the components.

To calculate the glass transition temperature of a multiphase material using the Fox equation a homogeneous material on a molecular scale is assumed. The Fox equation is given by

$$\frac{1}{T_g} = \frac{\omega_1}{T_{g1}} + \frac{\omega_2}{T_{g2}} \qquad (11)$$

The T_g of the composite is calculated from the weight fractions of the constituents in the composite as well as their respective T_g's. Note that $\omega_1 + \omega_2 = 1$. This model assumes the phases are miscible. Since the polymer and SiO_2 have different densities, we used the volume fraction of SiO_2 in the above equations to calculate the glass transition temperatures.

Results and Discussion

The modulus was calculated for each hybrid system using the previously discussed models. Figures 7.3, 7.5, and 7.7 show the experimental data as well as the model predictions for PMMA, PS, and PS-co-PMMA respectively. The Voigt and Hashin & Shtrikman upper limit both show high modulus values with

increasing silica volume fraction. These fits have the filler contributing greatly to the composite modulus. The Reuss, Hashin & Shtrikman lower limit, Kerner, and Guth-Smallwood all predict lower modulus values for the hybrids. These fits have the polymer matrix contributing more to the composite modulus. For our hybrid systems, we would expect the models favoring a lower value to match more closely with the experimental values. The polymers used in this study are all considered glassy and when filler is added with no chemical interaction, the modulus at room temperature should be close to the unfilled polymer. This is due to a glassy polymer only having short range motions that the filler cannot interfere with as greatly as it could in a rubbery polymer. From the previous chapters we saw that PMMA showed a shift to higher modulus values with silica content, PS showed a constant modulus value that started to decrease with increasing silica and PS-co-PMMA showed a constant modulus value with increasing silica.

The glass transition was calculated for each of the hybrid systems using an additive model and the Fox equation. Figures 7.4, 7.6, and 7.8 show the experimental data as well as the model predictions for PMMA, PS, and PS-co-PMMA respectively. Increasing the silica content should cause the glass transition temperature to shift to higher values as it impedes long chain molecular motion in the polymer matrix. The PMMA data closely follow the Hashin & Shtrickman lower bounds and the Kerner model. The Kerner model matches better, calculating a slightly higher modulus for silica content. This shows that the silica is well distributed and interacting in a favorable manner. The silica is not however arranged in a manner that allows its response to the strain to be measurable in the hybrids. Given the improvement in modulus seen, the T_g should show an increase in temperature with silica weight percent. Figure 7.4 shows the experimental and calculated T_g values for PMMA-SiO_2 hybrids. The T_g shows a large increase in temperature at low volume fractions and slightly smaller intervals of increase in temperature at higher volume fractions. Both models over predicted the response of the hybrids T_g with the Fox model showing a better fit.

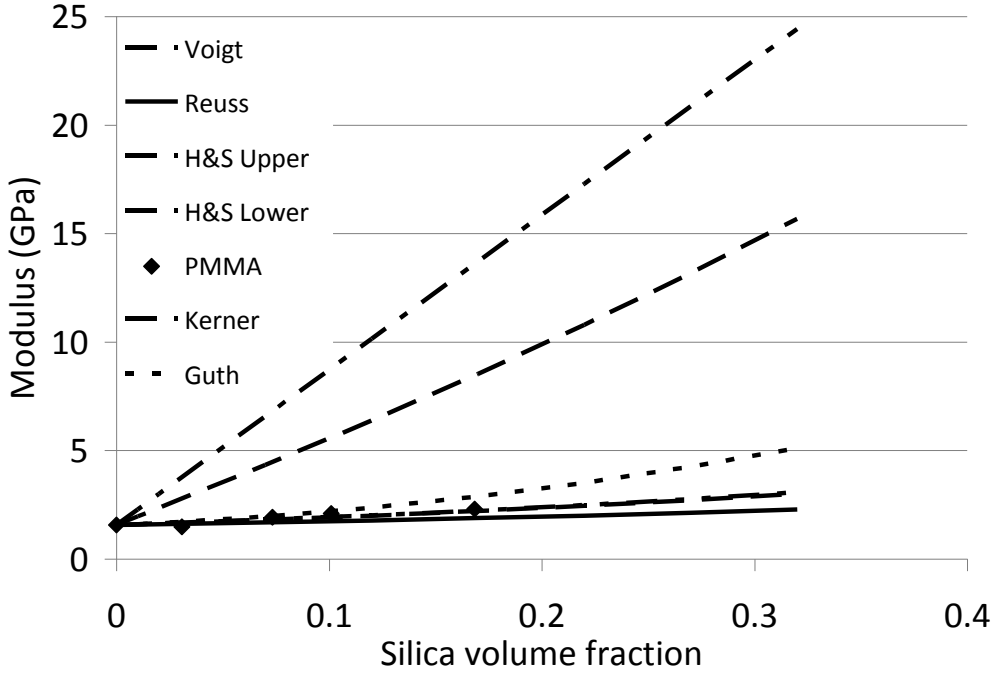

Figure 7.3: PMMA hybrid Modulus from experiment and models.

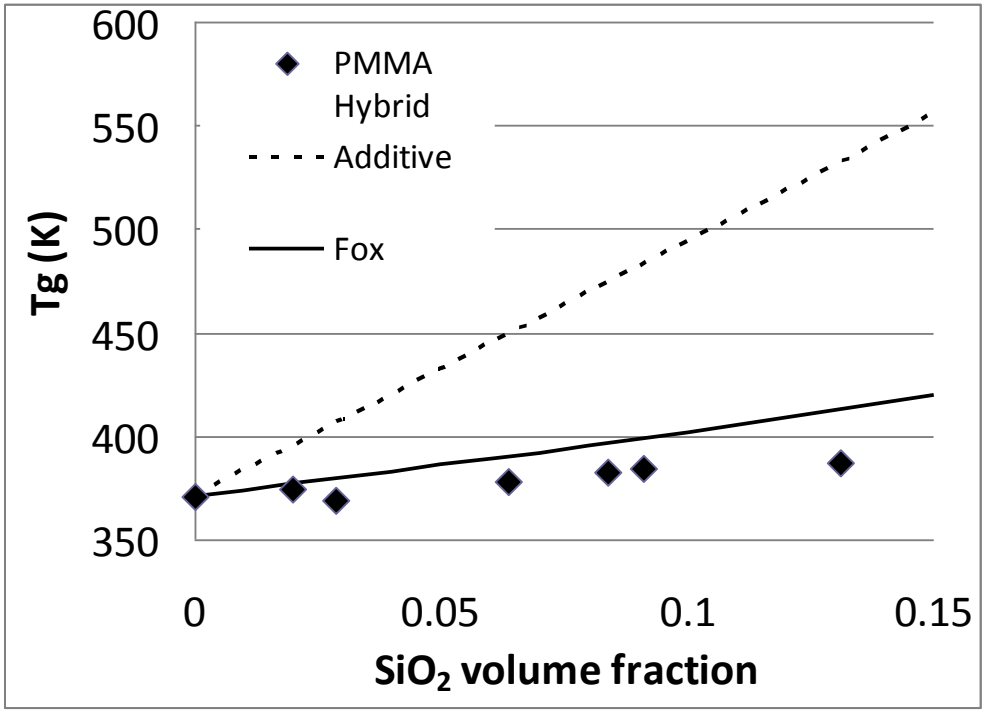

Figure 7.4: PMMA hybrid Tg from experiment and models.

The PS-SiO_2 hybrids modulus in Figure 7.5 shows a constant value with silica weight percent. It does decrease at the highest weight percent studied. The models all predict a higher modulus value with increasing silica content, which is not seen with our PS-SiO_2 hybrids. This lack of increase in the modulus shows that the filler is not well distributed and/or is not interacting in a favorable manner. A similar constant value for the T_g is expected. In Figure 7.6 the PS-Silica hybrids show no apparent increase with silica weight percent. The physical interaction between the PS and silica is not strong enough to interrupt and long range movement that the polystyrene undergoes.

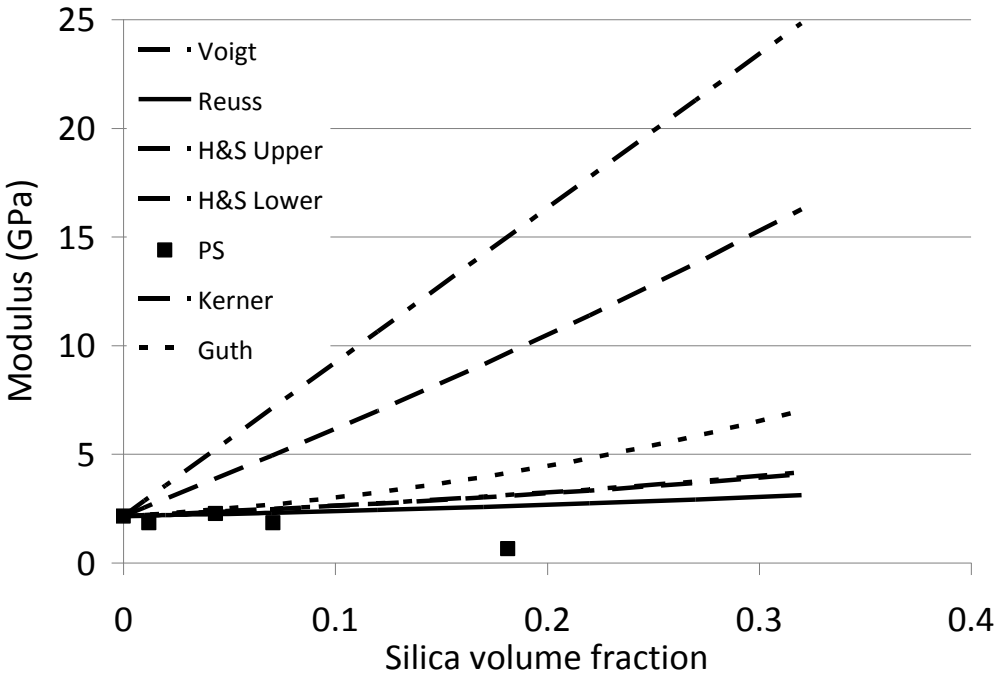

Figure 7.5: PS hybrid Modulus from experiment and models.

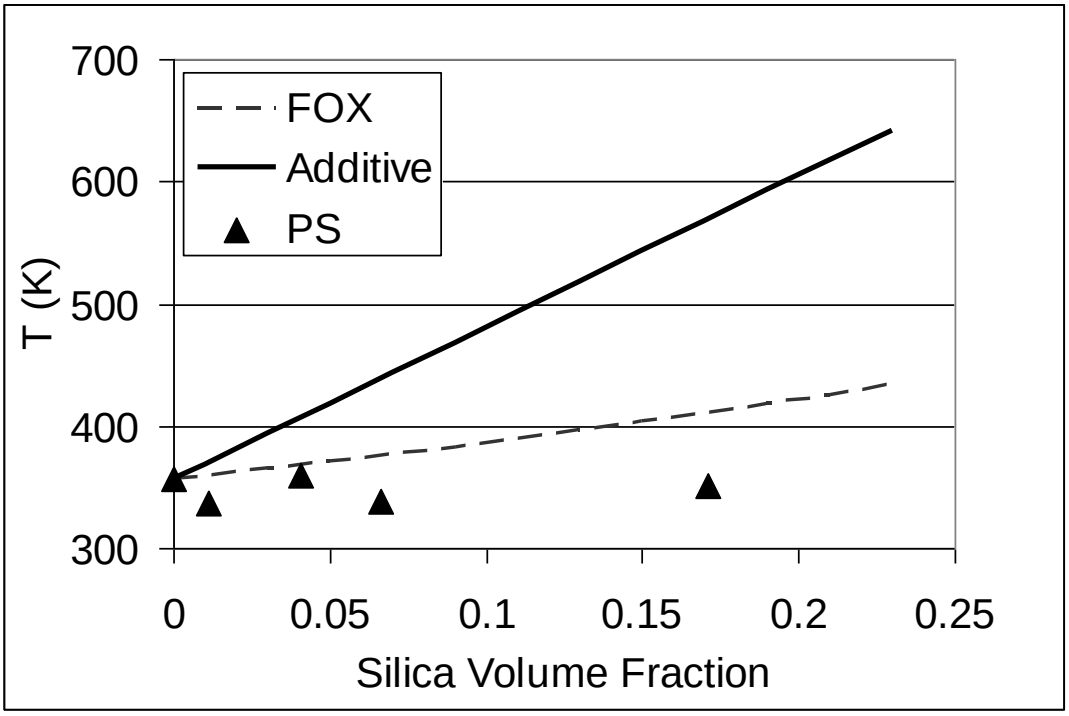

Figure 7.6: PS hybrid Tg from experiment and model.

The PS-co-PMMA-SiO_2 hybrids modulus in Figure 7.7 shows a constant value versus the silica content. Unlike the PS hybrids there is no drop to lower values as the silica weight percent is increased. The filler is not interacting favorably to cause the modulus to increase. The T_g of the hybrids show an increase in temperature with silica weight percent. There is some scatter of the data around the fits shown. It seems that the long range motion is inhibited enough by the silica to cause the increase in the T_g. The copolymer-silica hybrid shows a modulus response similar to the PS hybrids and a T_g response similar to the PMMA hybrids. The Fox model proved to be a good predictor of the T_g for the silica volume fractions studied here.

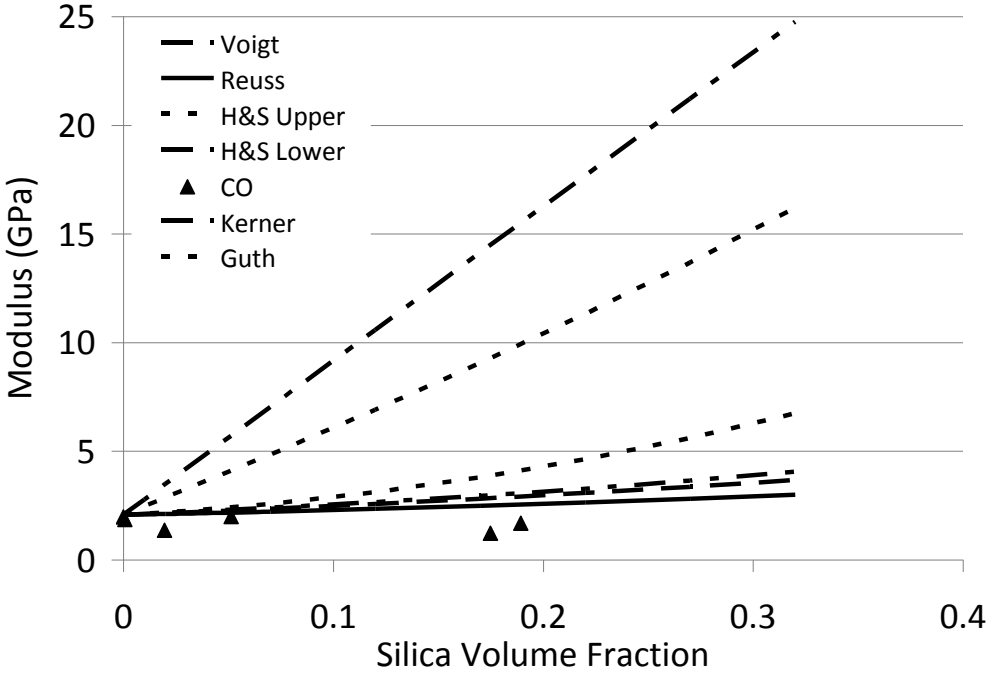

Figure 7.7: PS-co-PMMA hybrid Modulus from experiment and models.

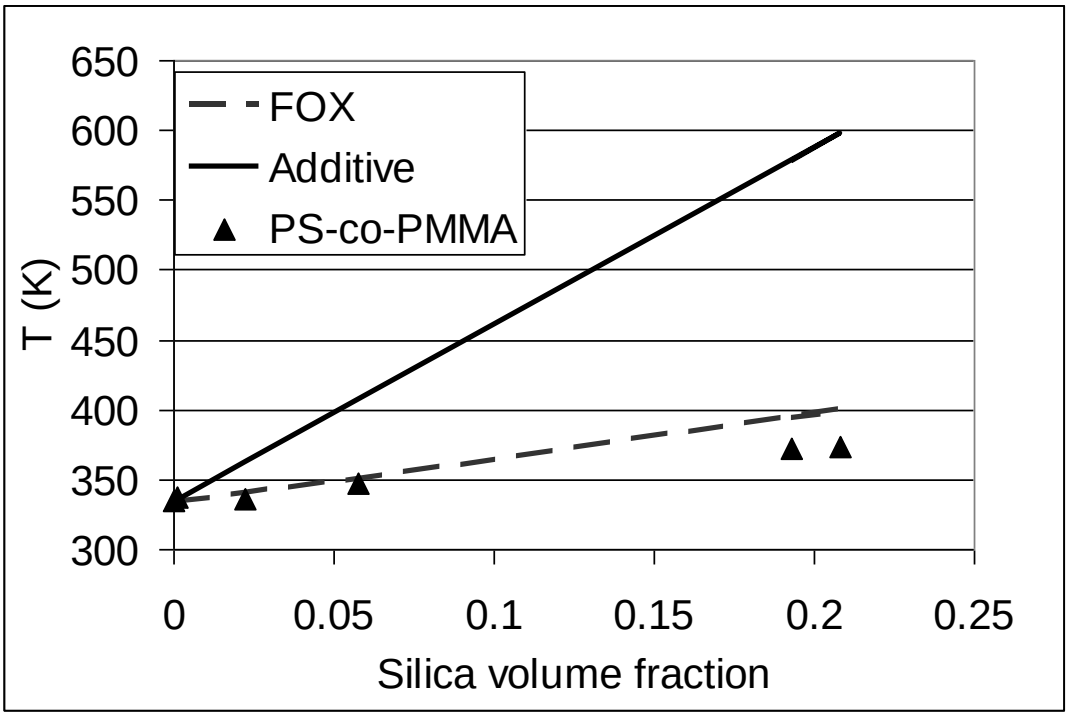

Figure 7.8: PS-co-PMMA hybrid T_g from experiment and models

Chapter 8
General Conclusions

The work presented in this dissertation describes the preparation and characterization of physically mixed polymer-SiO_2 hybrids to produce hybrids with improved mechanical and thermal properties. Improving the mechanical properties would give higher modulus, E′, values and improving the thermal properties would give higher glass transition values and decomposition temperature onset values. We utilized the following characterization techniques; thermogravimetric analysis (TGA), Fourier transform infra-red spectroscopy (FTIR), dynamic mechanical analysis (DMA), and atomic force microscopy (AFM). TGA, FTIR and DMA are employed in polymer studies to obtain their mechanical and thermal properties. AFM is used in tapping mode to provide information about the phase distribution of the constituents as well as obtain topographical images. AFM is used in place of SEM or TEM which show up in many polymer studies. A description of all of the techniques used was given in Chapter 2.

The preparation of the hybrids for each of the polymers studied starts from the hydrolysis and polycondensation of tetraethoxysilane (TEOS). This pre-hydrolyzed precursor solution was filtered and added to dissolved polymer samples to prepare the polymer-SiO_2 hybrid. This methodology was shown to work successfully for PMMA, PS, and PS-co-PMMA. Since these are all glassy polymers at room temperature it is reasonable to assume any glassy polymer at room temperature should be able to be combined with TEOS using our methodology. The individual hybrid preparation for each polymer system was described in their respective Chapter. To cure the hybrids different drying conditions were investigated and reviewed in Chapter 2 for cast PMMA. The samples were seen to degrade when the temperature was $\geq$ 100 °C or when heated under vacuum. The TGA traces of the cast samples showed solvent retention

leading us to choose the drying conditions that minimized this issue. The drying conditions for each polymer-SiO_2 system are detailed in their respective chapter.

The retention of organic products from the hydrolysis and polycondensation of TEOS showed a profound effect on the properties of the hybrids and in turn the cast polymers. The effect of ethanol added to a PMMA samples is seen to decrease the modulus by about a factor of 1.5 when compared with cast samples containing no ethanol. A decrease in the T_g was also seen for cast samples with ethanol. To achieve a correct view of how the silica content influences our polymer-inorganic hybrids all of the polymers used were prepared with ethanol added. When preparing any polymer-inorganic hybrid any product resulting from the preparation methodology must be accounted for in the polymer used to determine the baseline properties.

The individual polymer-SiO_2 hybrid systems were all characterized in Chapters 4, 5, and 6. The PMMA-SiO_2 hybrid system characterized in Chapter 4 showed improved thermal and mechanical properties. The modulus, E′, at 25 °C was modeled effectively with the Kerner equation and Hashin & Shtrikman lower bound equation in Chapter 7. These models both show a complex relationship between the continuous and discontinuous phases of a glassy polymer with filler distributed throughout. The silica was seen to be randomly distributed along the fracture in the AFM images. There was difficulty in assigning the phase to some images due to large height changes in the topography. The glass transition temperature moves to higher values with increasing silica but not in the linear manner calculated by the Fox equation. The T_g values measured were above the calculated values until high weight percents (~30%) of silica were encountered.

The PS-SiO_2 hybrid system characterized in Chapter 5 showed no improvement in thermal properties and a decrease in glassy modulus. None of the models for predicting the modulus or glass transition reviewed in Chapter 7 were close when compared with the experimental values. The decrease in the modulus values and lack of change in the T_g with increasing silica is due to the phase separation which is seen in the AFM images. The silica exhibits stronger intermolecular forces with itself than with the polystyrene leading to

agglomeration. In order to create a PS-SiO_2 hybrid with improved properties the surface of the silica or the PS chain would need to be modified to allow more favorable interactions between the constituents. The silica can be used as filler in PS to lessen the cost of materials because the mechanical and thermal properties did not change.

The PS-co-PMMA-SiO_2 hybrid system characterized in Chapter 6 showed improvement in the thermal properties and a steady glass transition temperature. The glassy modulus presented a constant value with increasing silica content that was no predicted by any of the models given in Chapter 7. The glass transition temperature showed scattered experimental data around the fox equation calculated values. This could be due to uneven mixing of the constituents or the SiO_2 interactions with the copolymer favoring one side group over the other. The AFM images showed the silica was randomly distributed throughout the fracture.

The information provided in this dissertation will help other investigators prepare polymer-inorganic hybrids utilizing a simple methodology that is applicable to a variety of polymers. We only studied SiO_2 as an inorganic oxide choice but the hydrolysis reaction used with TEOS could be transferred to many other organically modified inorganic starter materials such as titanium isopropoxide. The thermal and mechanical properties depended on the pendant group attached to the polymer backbone and could not be easily predicted by any of the models used in this study. When stronger intermolecular forces were possible between the side group and inorganic oxide the models in Chapter 7 gave calculated values closer to the experimental values. The phase distribution seen on the fracture surfaces taken by TM-AFM could be correlated to the changes in mechanical and thermal properties. If the distribution appeared random an improvement in modulus values was noted. Table 8.1 compares the different hybrid systems at the same silica weight percent. The PMMA showed the best response to silica being integrated. The PS remained fairly constant, decreasing at higher weight percents and the copolymer system showed improvement in the glass transition range and minimal change in the mechanical response.

Table 8.1: Comparison of polymer films with various silica content. E′ is given in GPa.

	0% Silica		~10% Silica		~30% Silica	
Sample	E' @ 25	T_g @ 10Hz	E' @ 25	T_g @ 10Hz	E' @ 25	T_g @ 10Hz
PMMA	1.565	97.15	1.923	104.83	2.296	114.4
PS	1.24	83.26	1.832	64.7	.6412	77.62
CO	2.00	64.2	1.84	105.6	1.40	106.4

Bibliography

1. U. Schubert, Husing, N., Lorenz, A., *Chem. Mater.*, 1995, **7**, 2010-2027.
2. J. Wen, Wilkes, G. L., *Chem. Mater.*, 1996, **8**, 1667-1681.
3. G. Schottner, *Chem. Mater.*, 2001, **13**, 3422-3435.
4. F. Bauer, Flyunt, R., Czihal, K., Buchmeiser, M.R., Langguth, H., Mehnert, R., *Macromol. Mater. Eng.*, 2006, **291**, 493-498.
5. V. A. Soloukhin, Posthumus, W., Brokken-Zijp, J.C.M., Loos, J., de With, G., *Polymer*, 2002, **43**, 6169-6181.
6. H. Nakazumi, Amano, S., Sakai, K., *Proceedings of SPIE-The International Society for Optical Engineering*, 1994, **2288**, 356-363.
7. H. Y. Chang, Lin, C.W., *Journal of Membrane Science*, 2003, **218**, 295-306.
8. Y. Su, Liu, Y., Sun, Y., Lai, J., Guiver, M.D., Gao, Y., *Journal of Power Sources*, 2006, **155**, 111-117.
9. Y. Su, Wei, T., Hsu, C., Liu, Y., *Desalination*, 2006, **200**, 656-657.
10. A. Jain, Toombes, G.E.S., Hall, L.M., Mahajan, S., Garcia, C.B.W., Probst, W., Gruner, S., Wiesner, U., *Angew. Chem. Int. Ed.*, 2005, **44**, 1226-1229.
11. J. Cho, Ju, H., Park, Y., Hong, J., *Macromolecular Materials and Engineering*, 2006, **291**, 1155-1163.
12. T. Kashiwagi, Morgan, A.B., Antonucci, J.M., VanLandingham, M.R., Harris, Jr. R.H., Awad, W.H., Shields, J.R. , *Journal of Applied Polymer Science*, 2002, **89**, 2072-2078.
13. C. H. Lee, Min, K.A., Park, H.B., Hong, Y.T., Jung, B.O., Lee, Y.M., *Journal of Membrane Science*, 2007, **303**, 258-266.
14. K. G. Neoh, Tan, K.K., Goh, P.L., Huang, S.W., Kang, E.T., Tan, K.L., *Polymer*, 1999, **40**, 887-893.
15. Y. Liu, Hsu, C., Su, Y., Lai, J., *Biomacromolecules*, 2005, **6**, 368-373.
16. A. Saxenz, Tripathi, B.P., Shahi, V.K., *J. Phys. Chem. B*, 2007, **111**, 12454-12461.
17. X. J. Xiang, Qian, J.W., Yang, W.Y., Fang, M.H., Qian, X.Q., *Journal of Applied Polymer Science*, 2006, **100**, 4333-4337.
18. S. Yano, Iwata, K., Kurita, K., *Mater. Sci. Eng.*, 1998, **C6**, 75-90.
19. C. Sanchez, Soler-Illia, G.J., Ribot, F., Grosso, D., *Comptes Rendus Chimie*, 2010, **6**, 1131-1151.
20. C. J. T. Landry, Coltrain, B.K., Brady, B.K., *Polymer*, 1992, **33**, 1486.
21. J. Jang, Park, H., *Journal of Applied Polymer Science*, 2001, **85**, 2074-2083.
22. G.-H. Hsiue, Kuo, W.-J., Huang, Y.-P., Jeng, R-.J., *Polymer*, 2000, **41**, 2813-2825.
23. A. M. Buckley, Greenblatt, M., *J. Chem. Educ.*, 1994, **71**, 599-602.
24. C. R. Silva, Airoldi, C., *J. Colloid and Interface Science*, 1997, **195**, 381-387.
25. Y. Wei, Jin, D., Brennan, D.J., Rivera, D.N., Zhuang, Q., DiNardo, N.J., Qiu, K., *Chem. Mater.*, 1998, **10**, 769-772.

26. J. Striova, Higgins, D.A., Collinson, M.M., *Langmuir*, 2005, **21**, 6137-6141.
27. W. Liu, Wu, L., Tian, X., Zheng, J., Cui, P., He, S., Zhu, C., *Polym. Bull.*, 2010, **65**, 133-143.
28. S. N. Magonov, Reneker, D.H., *Annu. Rev. Mater. Sci.*, 1997, **27**, 175-222.
29. T. Shindou, Katayama, S., Yamada, N., Kamiya, K., *J. of Sol-Gel Sci. and Tech.*, 2003, **27**, 15-21.
30. S. Yano, *Polym.*, 1994, **35**, 5565-5570.
31. P. Banet, Griesmar, P., Serfaty, S., Vidal, F., Jaouen, V., Huerou, J.-Y., *J. Phys. Chem. B.*, 2009, **113**, 14914-14919.
32. Z. J. Hou, Liu, L.Y., Xu, L., Xu, Z.L., Wang, W.C., Li, F.M., Ye, M.X., *Chem. Mater.*, 1999, **11**, 3177-3180.
33. Y.-G. Hsu, Tu, L.-C., Lin, K.-H., *J. Polym. Res.*, 2001, **8**, 37-47.
34. Y. A. Attia, ed., *Sol-Gel Processing and Applications*, Plenum Press, New York, 1994.
35. R. Aelion, Loebel, A., Eirich, F., *J. Am. Chem. Soc.*, 1950, **72**, 5705-5712.
36. M. G. Voronkov, Khimich, E.N., Khimich, N.N., *Russ. J. Appl. Chem.*, 2008, **80**, 732-735.
37. D. Fischer, Psospiech, D., Scheler, U., Navarro, R., Messori, M., Fabbri, P., *Macromol. Symp.*, 2008, **265**, 134-143.
38. H. Zou, Wu, S., Shen, J., *Chem. Rev. (Washington, DC, U. S.)*, 2008, **108**, 3893-3957.
39. J.-M. Yeh, Huang, Kuan-Yeh, Dai, Chung-Feng, Chand, B.G., Weng, Chang-Jian, *J. Appl. Polym. Sci.*, 2008, **110**, 2108-2114.
40. B. Didier, Mercier, R., Alberola, N. D., Bas, C., *J. Polym. Sci., Part B: Polym. Phys.*, 2008, **46**, 1891-1902.
41. S. Chen, Dong, P., Yang, G., Yang, J., *Ind. Eng. Chem. Res.*, 1996, **35**, 4487-4493.
42. L. H. Sperling, *Introduction to Physical Polymer Science*, Third edn., John Wiley & Sons, Hoboken, NJ, 2001.
43. R. M. Silverstein, Bassler, G.C., Morrill, T.C., *Spectroscopic Identification of Organic Compounds*, 3rd edn., 1974.
44. I. Schmitz, Schreiner, M., Grasserbauer, M., *Applied Surface Science*, 1997, **115**, 190-198.
45. E. Verploegen, Dworken, B.T., Faught, M., Kamperman, M., Zhang, Y., Wiesner, U., *Macromol. Rapid Commun.*, 2007, **28**, 572-578.
46. C. P. Wong, Bollampally, R. S. , *J. Appl. Polym. Sci.*, 1999, **74**, 3396-3403.
47. S. Bistac, Schultz, J., *Int. J. Adhes. Adhes.*, 1997, **17**, 197-201.
48. M. L. Zhang, March, N. H. ,Peeters, A. ,Van Alsenoy, C. ,Van Doren, V. E., *J. Appl. Phys.*, 2001, **89**, 3627-3630.
49. P. P. Simon, Ploehn, H.J., *J. Rheol.*, 2000, **44**, 169-183.
50. S. Jacobsen, Fritz, H.G., *Polym. Eng. Sci.*, 1999, **39**, 1303-1310.
51. P. J. Flory, *J. Chem. Phys.*, 1950, **18**, 108-111.
52. M. P. Scott, Rahman, M., Brazel, C.S., *Eur. Polym. J.*, 2003, **39**, 1947-1953.
53. K. Ute, Miyatake, N., Hatada, K.,, *Polymer*, 1995, **36**, 1415-1419.

54. T. G. Fox, *Bull. Am. Phys. Soc.*, 1956, **1**, 123.
55. M. Takayanagi, *Am. Chem. Soc., Div. Org. Coat., Plast. Chem., Prepr.*, 1963, **23**, 75-82.
56. J. R. Fried, *Polymer Science & Technology*, Second edn., Prentice Hall Professional Technical Reference, Upper Saddle River, 2003.
57. Q. Liu, Zheng, J., Fang, D., *Spectrosc. Lett.*, 2004, **37**, 225-233.
58. S. Sakka, Kamiya, K., *J. Non-Cryst. Solids.*, 1982, **48**, 31-46.
59. J. Sun, Akdogan, E. K., Klein, L. C., Safari, A., *J. noncrys. sol.*, 2007, **353**, 2807-2812.
60. S. Ludwigs, Steiner, U., Kulak, A., Lam, R., Meldrum, F. C., *Adv. Mater.*, 2006, **18**, 2270-2273.
61. F. Zhang, Lee, D., Pinnavaia, T. J., *Polym. Chem.*, 2010.
62. T. C. Chang, Wang, Y.T., Hong, Y.S., Chiu, Y.S., *J. Poly. Sci. Part A: Poly. Chem.*, 2000, **38**, 1972-1980.
63. F. Yang, Nelson, G. L., *J. Appl. Poly. Sci.*, 2004, **91**, 3844-3850.
64. C. A. Avila-Herrera, Gomez-Guzman, O., Almaral-Sanchez, J. L., Yanez-Limon, J. M., Munoz-Saldana, J., Ramirez-Bon, R., *J. noncrys. sol.*, 2006, **352**, 3561-3566.
65. Z. H. Huang and K. Y. Qiu, *Polymer Bulletin*, 1995, **35**, 607-613.
66. S. Ahmad, S. Ahmad and S. Agnihotry, *Bulletin of Materials Science*, 2007, **30**, 31-35.
67. M. A. Zulfikar, A. Wahab Mohammad and N. Hilal, *Desalination*, 2006, **192**, 262-270.
68. H. P. Fu, Hong, R.Y., Zhang, Y.J., Li, H. Z., Xu, B., Zheng, Y., Wei, D. G., *Polym. Adv. Technol.*, 2009, **20**, 84-91.
69. Y.-H. Hu, Chen, C.-Y., *Polym. Degrad. Stab.*, 2003, **82**, 81-88.
70. J. D. Peterson, Vyazovkin, S., Wight, C.A., *Macromol. Rapid Commun.*, 1999, **20**, 480-483.
71. T. Hirata, Kashiwagi, T., Brown, J.E., *Macromol.*, 1985, **18**, 1410-1418.
72. T. Hirata, Kashiwagi, T., Brown, J.E., *Polym. Preprints*, 1984, **25**, 176-177.
73. R. Tamaki, Naka, K., Chujo, Y., *Polymer Bulletin*, 1997, **39**, 303-310.
74. R. Tamaki, Chujo, Y., *Chem. Mater.*, 1999, **11**, 1719-1726.
75. Y. Wei, Yang, D., Tang, L., *Journal of Materials Research*, 1993, **8**, 1143-1152.
76. R. Tamaki, Samura, K., Chujo, Y., *Chem. Commun.*, 1998, **10**, 1131-1132.
77. M. A. Ver Meer, Narasimhan, B., Shanks, B.H., Mallapragada, S.K., *Applied Materials and Interfaces*, 2010, **2**, 41-47.
78. W. C. Johnson, Wang, J., Chen, Z., *J. Phys. Chem. B*, 2005, **109**, 6280-6286.
79. C. H. Park, Kim, J.H., Ree, M., Sohn, B-H., Jung, J.C., Zin, W-C., *Polymer*, 2004, **45**, 4507-4513.
80. Z. H. Huang, Qiu, K. Y., *polymer*, 1997, **38**, 521-526.
81. M. Ivankovia, Brnradic, I., Ivankovic, H., Huskic, M., Gajovic, A., *polymer*, 2009, **50**, 2544-2550.
82. P. Leclere, Lazzaroni, R., *Antec*, 2006, 1682.

83. J. L. Almaral-Sanchez, Lopez-Gomez, M., Ramirez-Bon, R., Muoz-Saldana, J., *J. of Mater.*, 2006.
84. Z. Hashin, Shtrikman, S., *J. Mech. Phys. Solids*, 1963, **11**, 127-140.
85. Z. Hashin, *J. Appl. Mech.*, 1983, **50**, 481.

Appendix

Thermogravimetric Analysis

TA Instruments

Sample Preparations: Polymer and hybrid samples cut into small pieces (0.5mmx0.5mm approx.) and placed in aluminum sample pan. Distribute sample evenly in pan weight to 10-15 mg. Load pan into instrument.

Normal Run:

Ramp 10 °C/min to 600.0 °C

If wt% < 0.01 hold 15 minutes

Isothermal Run:

Ramp 10 °C/min to 140.0 °C

Isothermal hold 40 min

Ramp 10 °C/min to 600.0 °C

If wt% < 0.01 hold 15 minutes

All polymers and hybrids can be run with no adjustments to either program or sample preparation needed. Isothermal run used when solvent present in sample.

Differential Scanning Calorimetry

TA Instruments

Sample Preparations: Polymer and hybrid samples cut into very small particles (try to get as close to powder as possible) and placed into aluminum sample pan. Place pan lid on and seal shut. Sample needs to be evenly distributed in pan and load approximately 10 mg. Load pan into instrument.

Program:

°C/min to T*

*Temperature run to determined from thermogravimetric run. Use temperature 10-20 °C less than degradation onset.

All polymers and hybrids with no solvent present can be run using DSC. Offgasing of samples with any residual solvent builds up in system and can cause pan lids to burst.

Fourier Transform Infra-red Spectroscopy

Sample Preparation: Cut small piece of polymer or hybrid and redissolve in chloroform. Dropped onto a KBr window that has already been scanned as the background. This was dried at 100 °C then run on the IR. Depending on signal strength, more drops were added and dried.

Program:

Scan 400 cm^{-1} to 4000 cm^{-1}
Resolution 2 cm^{-1}
Averaged 40 scans

A carbon dioxide peak shows up in the scans due to the system background fluctuations. Need to use different polymer/solvent ratio to get good signal. Try dilute and add more drops as needed.

Dynamic Mechanical Analysis

Perkin Elmer
Cast samples of polymers and hybrids were cut into rectangular samples with nominal dimensions of 40 mm x 10 mm. The thicknesses obtained from the amount of sample cast into an aluminum weigh dish was around 0.3 mm. The thickness was determined using an optical scope. The samples running dimensions were 10 mm x width mm x thickness mm.

Hard Polymers/Hybrids

2 °C/min ramp to 170 °C

Run in tension mode

Select 0.5, 1.0, 2.0, 5.0, and 10.0 Hertz

DMS Tension Setting:

L Amplitude (um) 5

Minimum Tension/Compression Force (mN) 100

Tension/Compression Force Gain 1.5

Force Amplitude Default Value (mN) 70

Soft Polymers/Hybrids

2 °C/min ramp to 170 °C

Run in tension mode

Select 0.5, 1.0, 2.0, 5.0, and 10.0 Hertz

DMS Tension Setting:

L Amplitude (um) 10

Minimum Tension/Compression Force (mN) 100

Tension/Compression Force Gain 1.0

Force Amplitude Default Value (mN) 1000

Atomic Force Microscopy – Tapping Mode

Veeco Nanoscope III – Multimode

Freshly fractured piece of polymer/hybrid were clamped to a table. The fractured end was sliced off and mounted on an AFM sample puck. Program:

Scanned 1 micron to 5 micron sample sizes

512 pixels

Fracture surfaces are very uneven and approach must be done cautiously.